

TOMAWAC

Validation Manual

Version v8p5
December 1, 2023



Contents

1	Introduction	7
1.1	A word of caution	7
1.2	Validation layout	7
2	Presentation	9
2.1	General	9
2.2	Capabilities	9
2.2.1	Application domain of the model TOMAWAC	9
2.2.2	Wave interactions with other physical factors	10
2.2.3	The physical processes modelled in TOMAWAC	11
3	3D coupling	13
3.1	Purpose	13
3.2	Description of the problem	13
3.3	Geometry and Mesh	13
3.3.1	Wave conditions	13
3.4	Results	15
4	Coupling Wind	19
4.1	Purpose	19
4.2	Description of the cases	19
4.3	Results	19
4.4	Coupling TELEMAC-2D and TOMAWAC with a wind and a hotstart	20
5	Manche	24
5.1	Purpose	24
5.2	Description of the problem	24
5.3	Results and Comments	25

6	Next_Comput	29
6.1	Purpose	29
6.2	Description of the problem	29
6.3	Results	30
6.4	Hot start while reading a tide	30
6.5	Hot start while reading a wind varying in time	30
7	Porous	33
7.1	Purpose	33
7.2	Description of the problem	33
7.3	Physical parameters	33
7.4	Geometry and Mesh	33
7.5	Initial and Boundary Conditions	34
7.6	Numerical parameters	34
7.7	Results	34
8	Rip	35
8.1	Results	35
9	Spheric	38
9.1	Purpose	38
9.2	Description of the problem	38
9.3	Results	39
10	Triplets	41
10.1	Purpose	41
10.2	Description of the problem	41
11	Veget	43
11.1	Purpose	43
11.2	Description of the problem	43
11.3	Physical parameters	43
11.4	Geometry and Mesh	43
11.5	Initial and Boundary Conditions	44
11.6	Numerical parameters	44
11.7	Results	44

12	Angular Spread	45
12.1	Purpose	45
12.2	Description of the problem	45
12.3	Results	45
13	Bottom friction	48
13.1	Purpose	48
13.2	Description of the problem	48
13.3	Geometry and mesh	48
13.4	Numerical parameters	49
13.5	Initial and Boundary Conditions	49
13.6	Results	49
14	Calais	50
14.1	Purpose	50
14.2	Description of the problem	50
14.3	Results and Comments	50
15	Dean	55
15.1	Purpose	55
15.2	Description of the problem	55
15.3	Reference	55
15.4	Physical parameters	55
15.5	Geometry and Mesh	55
15.6	Initial and Boundary Conditions	56
15.7	Numerical parameters	56
15.8	Results	56
16	Deferl_bj78	58
16.1	Purpose	58
16.2	Description of the problem	58
16.3	Physical parameters	59
16.4	Geometry and Mesh	59
16.4.1	Initial and Boundary Conditions	59
16.5	Numerical parameters	59
16.6	Results	60
16.6.1	Conclusion	60

17 Fetch Limited	62
17.1 Purpose	62
17.2 Reference experiments	63
17.3 Geometry of the domain and bathymetry	63
17.3.1 Mesh	64
17.3.2 Spectro-angular discretization	64
17.4 Initial and Boundary conditions	64
17.4.1 Numerical parameters	64
17.5 Results - infinite depth	65
17.5.1 Wave growth depending on the fetch for different wind velocities	65
17.5.2 Non-dimensionnal variances and peak frequencies	66
17.5.3 Variance spectrum for a constant wind	67
17.5.4 Finite depth TOMAWAC results	69
17.6 Conclusion	70
17.6.1 Infinite Depth	70
17.6.2 Finite depth	70
17.6.3 Some Tests	70
18 Impose spectra	75
18.1 Description of the problem	75
18.2 Numerical parameters	76
18.3 Results	77
19 Opposing current	79
19.1 Purpose	79
19.2 Description of the problem	79
19.3 Reference	79
19.4 Physical parameters	79
19.5 Geometry and Mesh	79
19.6 Initial and Boundary Conditions	80
19.7 Numerical parameters	81
19.8 Results	81
20 Reflection	82
20.1 Purpose	82
20.2 Description of the problem	82
20.3 Geometry and Mesh	82
20.4 Initial and Boundary Conditions	82
20.5 Results	82
20.6 Test of rotated boundary	83

21	Shoal: Submerged elliptical mound	85
21.1	Purpose	85
21.2	Reference experiments	85
21.3	Test-case description	86
21.3.1	Geometry of the domain and bathymetry	86
21.3.2	Meshes	86
21.3.3	Initial and Boundary conditions	87
21.4	Numerical parameters	88
21.5	TOMAWAC Results	88
21.6	Conclusion	93
22	Turning wind	94
22.1	Purpose	94
22.2	Description of the problem	94
22.3	Physical parameters	94
22.4	Geometry and Mesh	94
22.5	Initial and Boundary Conditions	94
22.6	Numerical parameters	95
22.7	Results	95
23	Whirl current	97
23.1	Purpose	97
23.2	Description of the problem	97
23.3	Initial and Boundary Conditions	98
23.4	Geometry and Mesh	99
23.5	Numerical parameters	100
23.6	Results	100
23.7	Conclusion	103
	Bibliography	104

1. Introduction

1.1 A word of caution

This document contains information about the quality of a complex modelling tool. Its purpose is to assist the user in assessing the reliability and accuracy of computational results, and to provide guidelines with respect to the applicability and judicious employment of this tool. This document does not, however, provide mathematical proof of the correctness of results for a specific application. The reader is referred to the License Agreement for pertinent legal terms and conditions associated with the use of the software.

The contents of this validation document attest to the fact that computational modelling of complex physical systems requires great care and inherently involves a number of uncertain factors. In order to obtain useful and accurate results for a particular application, the use of high-quality modelling tools is necessary but not sufficient. Ultimately, the quality of the computational results that can be achieved will depend upon the adequacy of available data as well as a suitable choice of model and modelling parameters.

1.2 Validation layout

This validation is presented hereafter using a *validation sheet form*, each sheet detailing the physical concepts involved, the physical and numerical parameters used and comparing both numerical and reference solutions. Then, each sheet displays the following informations:

- **Purpose & Problem description :** These first two parts give reader short details about the test case, the physical phenomena involved and specify how the numerical solution will be validated;
- **Reference :** This part gives the reference solution we are comparing to and explicits the analytical solution when available;
- **Physical parameters :** This part specifies the geometry, details all the physical parameters used to describe both porous media (soil model in particularly) and solute characteristics (dispersion/diffusion coefficients, soil \equiv pollutant interactions...);
- **Geometry and Mesh :** This part describes the mesh used in the TOMAWAC computation;
- **Initial and boundary conditions :** this part details both initial and boundary conditions used to simulate the case ;

- **Numerical parameters** : this part is used to specify the numerical parameters used (adaptive time step, mass-lumping when necessary...);
- **Results** : we comment in this part the numerical results against the reference ones, giving understanding keys and making assumptions when necessary.

2. Presentation

2.1 General

TOMAWAC is a scientific software which models the changes, both in the time and in the spatial domain, of the power spectrum of wind-driven waves and wave agitation for applications in the oceanic domain, in the intracontinental seas as well as in the coastal zone. The model uses the finite elements formalism for discretizing the sea domain; it is based on the computational subroutines of the TELEMAC system as developed by the EDF R&D's Laboratoire National d'Hydraulique et Environnement (LNHE). TOMAWAC is one of the models making up the TELEMAC system. The acronym TOMAWAC being adopted for naming the software was derived from the following English denomination:

TELEMAC-based Operational Model Addressing Wave Action Computation

TOMAWAC can be used for three types of applications:

- Wave climate forecasting a few days ahead, from wind field forecasts. This real time type of application is rather directed to weather-forecasting institutes such as Météo-France, whose one mission consists in predicting continuously the weather developments and, as the case may be, publishing storm warnings.
- Hindcasting of exceptional events having severely damaged maritime structures and for which field records are either incomplete or unavailable.
- Study of wave climatology and maritime or coastal site features, through the application of various, medium or extreme, weather conditions in order to obtain the conditions necessary to carry out projects and studies (harbour constructions, morphodynamic coastal evolutions, ...).

2.2 Capabilities

2.2.1 Application domain of the model TOMAWAC

TOMAWAC is designed to be applied from the ocean domain up to the coastal zone. The limits of the application range can be determined by the value of the relative depth d/L , wherein d denotes the water height (in metres) and L denotes the wave length (in metres) corresponding to the peak spectral frequency for irregular waves.

The application domain of TOMAWAC includes:

- **the oceanic domain**, characterized by large water depths, i.e. by relative water depths of over 0.5. The dominant physical processes are: wind driven waves, whitecapping dissipation and non-linear quadruplet interactions.
- **the continental seas and the medium depths**, characterized by a relative water depth ranging from 0.05 to 0.5. In addition to the above processes, the bottom friction, the shoaling (wave growth due to a bottom rise) and the effects of refraction due to the bathymetry and/or to the currents are to be taken into account.
- **The coastal domain**, including shoals or near-shore areas (relative water depth lower than 0.05). For these shallow water areas, such physical processes as bottom friction, bathymetric breaking, non-linear triad interactions between waves should be included. Furthermore, it could be useful to take into account the effects related to unsteady sea level and currents due to the tide and/or to the weather-dependent surges.

Through a so-called finite element spatial discretization, one computational grid may include mesh cells among which the ratio of the largest sizes to the smallest ones may reach or even exceed 100. That is why TOMAWAC can be applied to a sea domain that is featured by highly variable relative water depths; in particular, the coastal areas can be finely represented.

The application domain of TOMAWAC does not include the harbour areas and, more generally, all those cases in which the effects of reflection on structures and/or diffraction may not be ignored.

A first version of a diffraction model is available in TOMAWAC and is able to represent some diffraction effects. The model presents still some limits. It is highly recommended to use phase-resolving models when a detailed simulation of diffraction effects is required (e.g. harbor agitation).

2.2.2 Wave interactions with other physical factors

Several factors are involved in the wave physics and interact to various extents with the waves changing their characteristics. The following main factors should be mentioned:

- bathymetry and sea bottom geometry (bottom friction, refraction, surf-breaking, non-linear effects of interactions with the bottom, sand rippling...)
- atmospheric circulation (wind and pressure effects)
- tide pattern (variation of currents and water heights),
- three-dimensional oceanic circulation currents,
- over/underelevations caused by exceptional weather events, resulting in sea levels variations up to several meters (storm, surges).

The fine modelling of the interactions between these various physical factors and the waves is generally rather complex and several research projects are currently focused on it. Within the application domain as defined in the previous paragraph, TOMAWAC models the following interactions:

- **wave-bathymetry interaction**: the submarine relief data input into TOMAWAC are constant in time, but the sea level can change in time. In addition to the effects of the sea level variations in time, TOMAWAC allows to take into account refraction, shoaling, bottom friction and bathymetric breaking. TOMAWAC simulations can take into account some diffraction effects.

- **wave-atmosphere interaction:** this interaction is the driving phenomenon in the wave generation, takes part in energy dissipation processes (whitecapping, wave propagation against the wind...) and is involved in the energy transfer. To represent the unsteady behaviour of this interaction, TOMAWAC requires 10 m wind fields (specification of the couple of horizontal velocity components) with a time step matched to the weather conditions being modelled. These wind fields can be provided either by a meteorological model or from satellite measurements.
- **wave-current interaction:** the sea currents (as generated either by the tide or by oceanic circulations) may significantly affect the waves according to their intensity. They modify the refractive wave propagation direction, they reduce or increase the wave height according to their propagation direction in relation to the waves and may influence the wave periods if exhibiting a marked unsteady behaviour. In TOMAWAC, the current field is provided by the couple of horizontal components of its average (or depth-integrated) velocity at the nodes of the computational grid. TOMAWAC allows to model the frequency changes caused either by the Doppler effect or by the unsteady currents, as well as by an heterogeneous current field.

2.2.3 The physical processes modelled in TOMAWAC

Those interactions being taken into account by TOMAWAC have been reviewed and a number of physical events or processes have been mentioned in the previous paragraph. These processes modify the total wave energy as well as the directional spectrum distribution of that energy (i.e. the shape of the directional spectrum of energy). So far, the numerical modelling of these various processes, although some of them are now very well known, is not yet mature and keep on providing many investigation subjects. Considering the brief review of physical interactions given in the previous paragraph, the following physical processes are taken into account and digitally modelled in TOMAWAC:

—> **Energy source/dissipation processes:**

- wind driven interactions with atmosphere. Those interactions imply the modelling of the wind energy input into the waves. It is the prevailing source term for the wave energy directional spectrum. The way that spectrum evolves primarily depends on wind velocity, direction, time of action and fetch (distance over which the wind is active). It must be pointed out that the energy which is dissipated when the wind attenuates the waves is not taken into account in TOMAWAC.
- whitecapping dissipation or wave breaking, due to an excessive wave steepness during wave generation and propagation.
- bottom friction-induced dissipation, mainly occurring in shallow water (bottom grain size distribution, ripples, percolation...)
- dissipation through bathymetric breaking. As the waves come near the coast, they swell due to shoaling until they break when they become too steep.
- dissipation through wave blocking due to strong opposing currents.

—> **Non-linear energy transfer conservative processes:**

- non-linear resonant quadruplet interactions, which is the exchange process prevailing at great depths.
- non-linear triad interactions, which become the prevailing process at small depths.

—> Wave propagation-related processes:

- wave propagation due to the wave group velocity and, in case, to the velocity of the medium in which it propagates (sea currents).
- depth-induced refraction which, at small depths, modifies the directions of the wave-ray and then implies an energy transfer over the propagation directions.
- shoaling: wave height variation process as the water depth decreases, due to the reduced wavelength and variation of energy propagation velocity.
- current-induced refraction which also causes a deviation of the wave-ray and an energy transfer over the propagation directions.
- interactions with unsteady currents, inducing frequency transfers (e.g. as regards tidal seas).
- diffraction by a coastal structure (breakwater, pier, etc...) or a shoal, resulting in an energy transfer towards the shadow areas beyond the obstacles blocking the wave propagation. The current version of the diffraction model implemented in TOMAWAC is able to represent qualitatively some diffraction effects.

It should be remembered that, due to the hypothesis adopted in paragraph 2.2.1 about the TOMAWAC application domain, the reflection (partial or total) from a structure or a pronounced depth irregularity is not addressed by the model.

3. 3D coupling

3.1 Purpose

This test case has been created to test the coupling between TOMAWAC and TELEMAC-3. Four different coupling are tested here:

- In the first one that we will call the classical one, the forces due to waves are constant along the depth of water. This coupling is very close to the coupling that is made with telemac2d.
- In the second coupling that we will call 3D coupling, all the quantities are dependant of the depth. This coupling is closer to what happen in reality. For more detail about the second coupling the reader can read [31].
- The third coupling is like the first one but TOMAWAC and TELEMAC-3 are defined on different domains and meshes using TEL2TOM technique (see [7] for a detailed description). The mesh of TOMAWAC is twice coarser and a little bit larger.
- The forth coupling is a 3D coupling where TOMAWAC and TELEMAC-3 are defined on different domains and meshes.

3.2 Description of the problem

We took the geometry from the classical test case 'littoral', a coupling case between TOMAWAC and TELEMAC-2 and GAIA

3.3 Geometry and Mesh

The beach is 1000 m long, 200 m wide with a regular mesh with elements size of the order $\Delta x = 20$ m and $\Delta y = 5$ m. The beach slope ($Y=200$ m) is 5%. The water depth along the open boundary ($Y=0$) is $h=10$ m. We use a triangular regular grid. The mesh is as shown on Figure 3.1

3.3.1 Wave conditions

Incoming waves (waves height , period and directions) are imposed offshore at $y = 0$, such that $H_s = 1$ m, $T_p = 8$ s. The Jonswap spectrum is used. The waves direction is 30 deg relative to the y-axis.

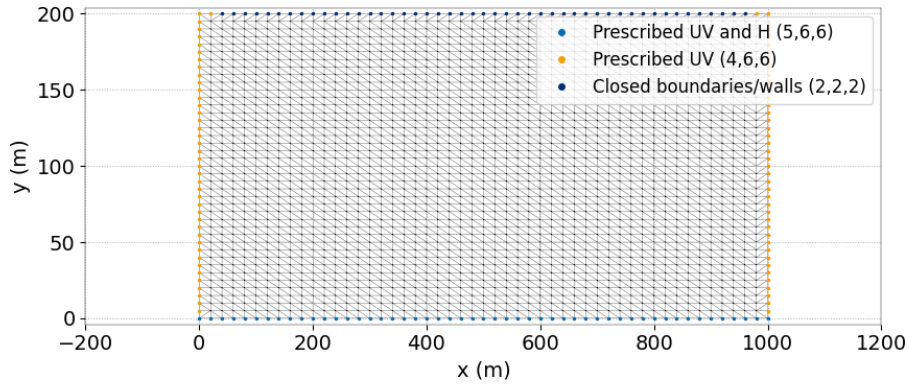


Figure 3.1: 2D mesh of the domain in the two first coupling.

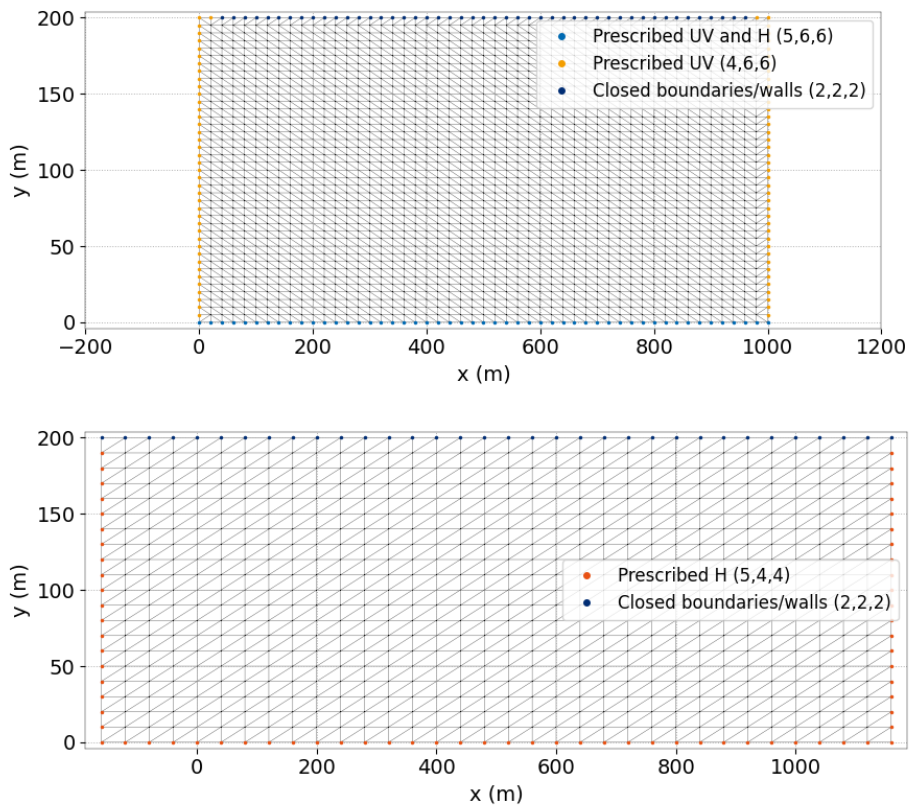


Figure 3.2: 2D mesh of the domain in the two last coupling. TELEMAC-3 up and TOMAWAC bottom

⇒ Offshore (Y=0): Offshore wave imposed/no littoral current/no set up

Tomawac: The wave height is imposed on the offshore boundary (5 4 4) ($H_s=1m$), for a wave period ($T_p=8s$).

Telemac2D: The current and free surface are imposed to 0 along the offshore boundary (5 5 5).

3.4 Results

The results are presented Figures 3.4 (Velocity U on a vertical plan) 3.5 (velocity on the bottom) 3.3(Wave heighth Hm0) with the classical coupling.

On Figures 3.6, 3.7 and 3.8, we present the results of the 3D coupling.

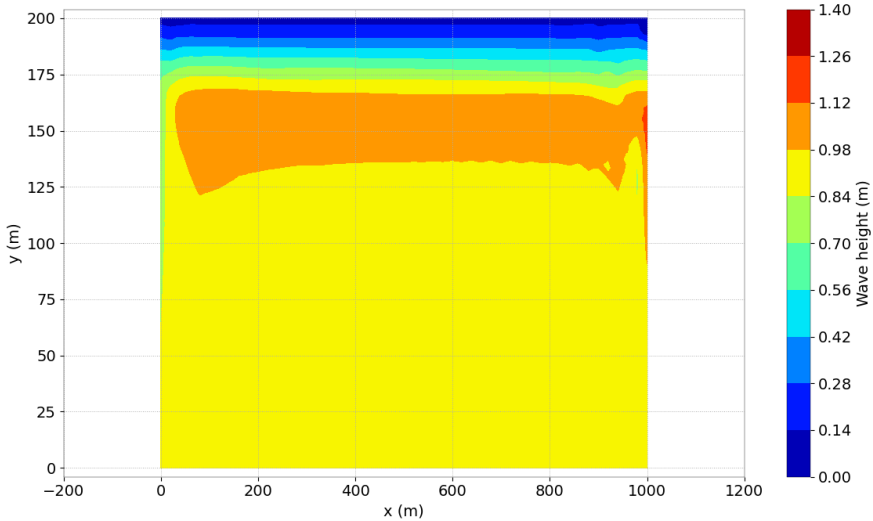


Figure 3.3: Wave Heighth calculated by TOMAWAC.

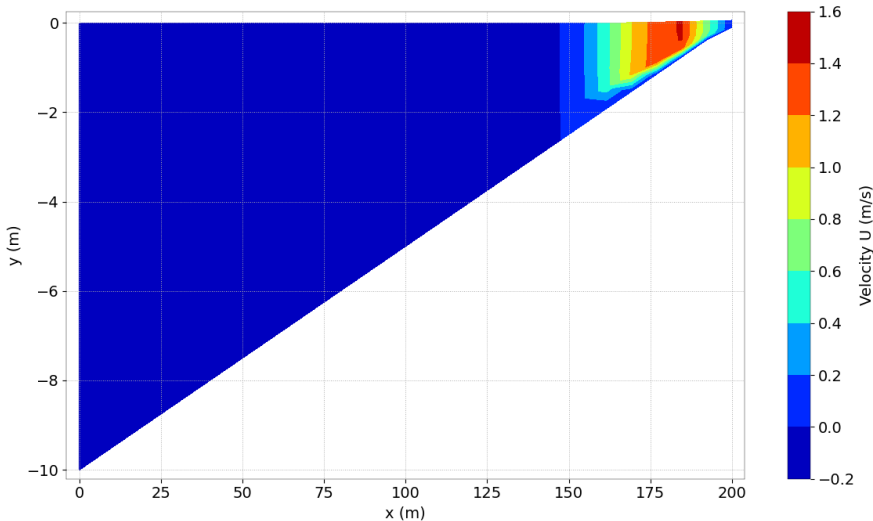


Figure 3.4: Celerity U on a vertical plan at x=500.

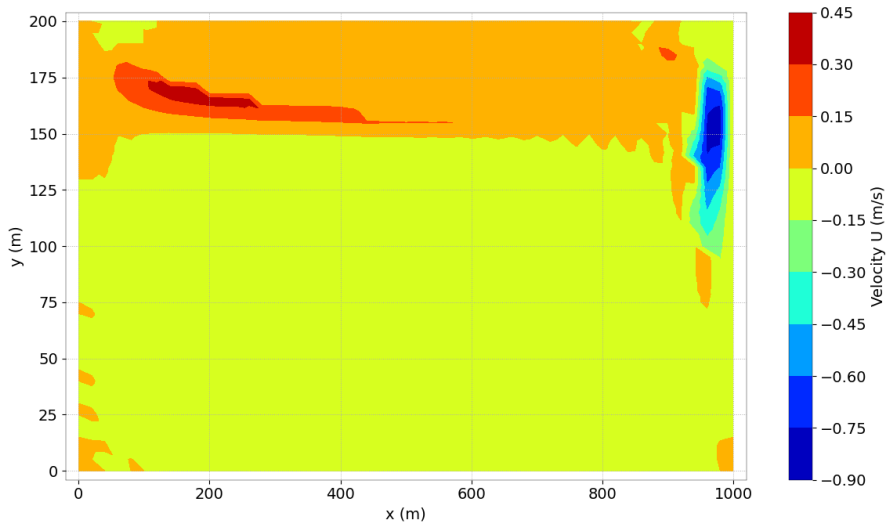


Figure 3.5: Celerity U on the bottom calculated by TELEMAC-3 d.

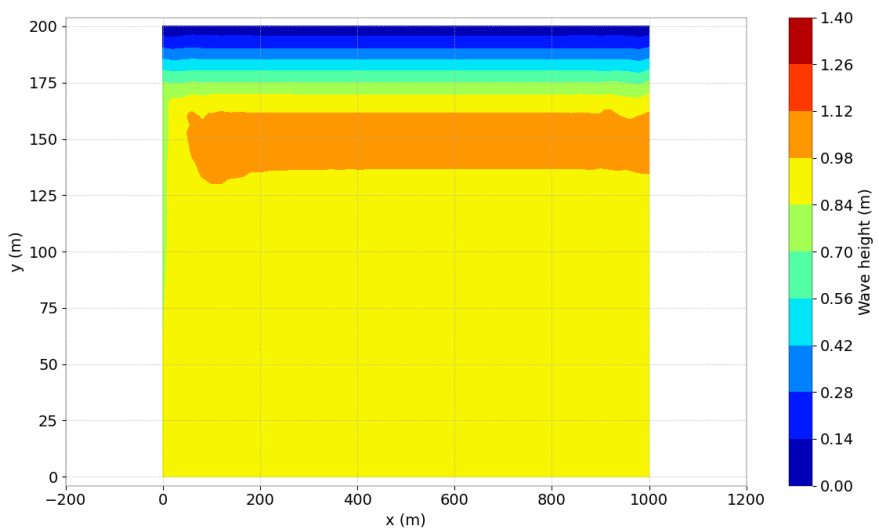


Figure 3.6: Wave Height calculated by TOMAWAC with the 3D coupling.

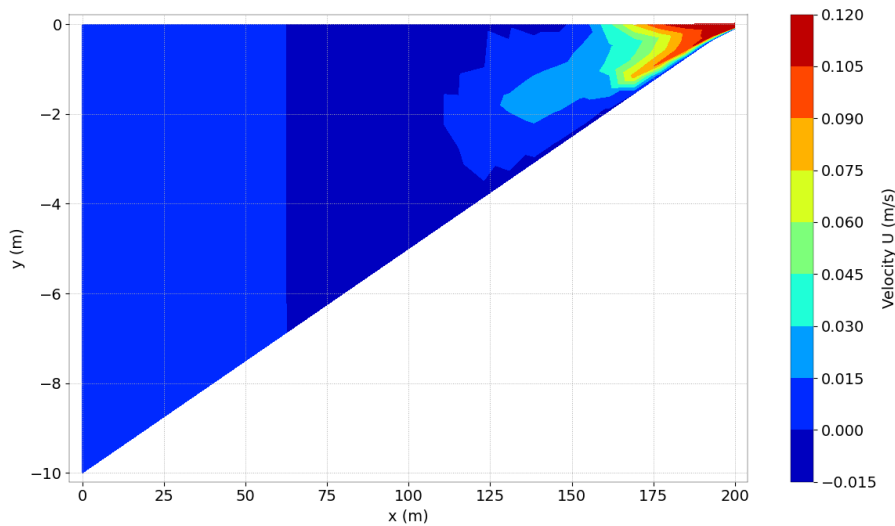


Figure 3.7: Celerity U on a vertical plan at $x=500$.

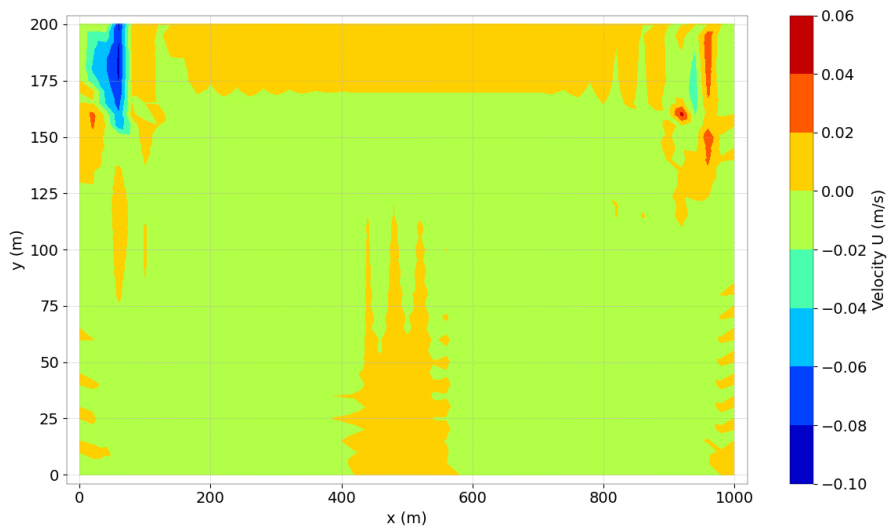


Figure 3.8: Celerity U on the bottom calculated by TELEMAC-3 d with the 3D coupling.

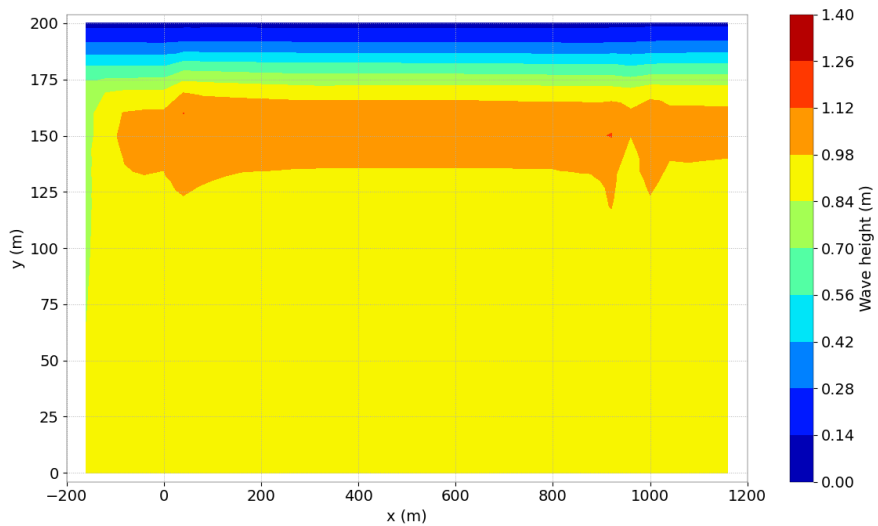


Figure 3.9: Wave Height calculated by TOMAWAC with a classical coupling on different meshes

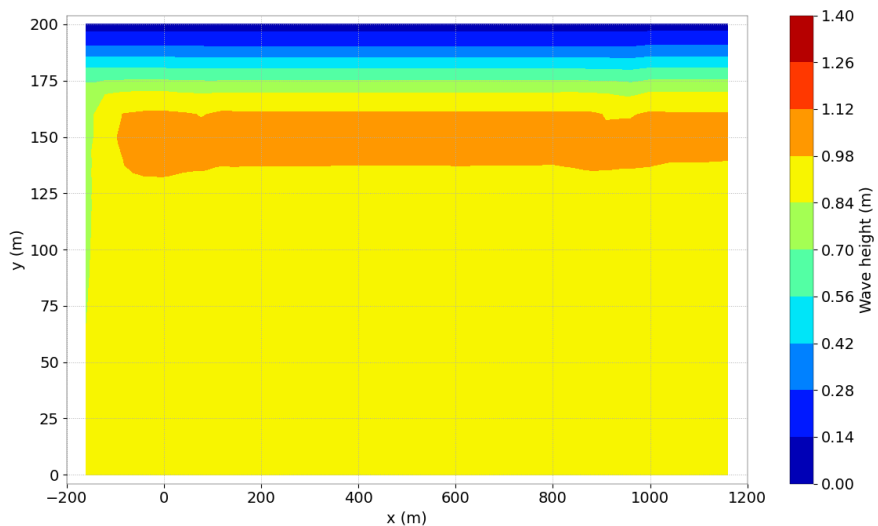


Figure 3.10: Wave Height calculated by TOMAWAC with a real coupling coupling on different meshes

4. Coupling Wind

4.1 Purpose

This case has been created to ensure that in case of a coupling between TELEMAC-2 d or TELEMAC-3 d and TOMAWAC, the wind transmitted as a coupling variable is well taken into account.

4.2 Description of the cases

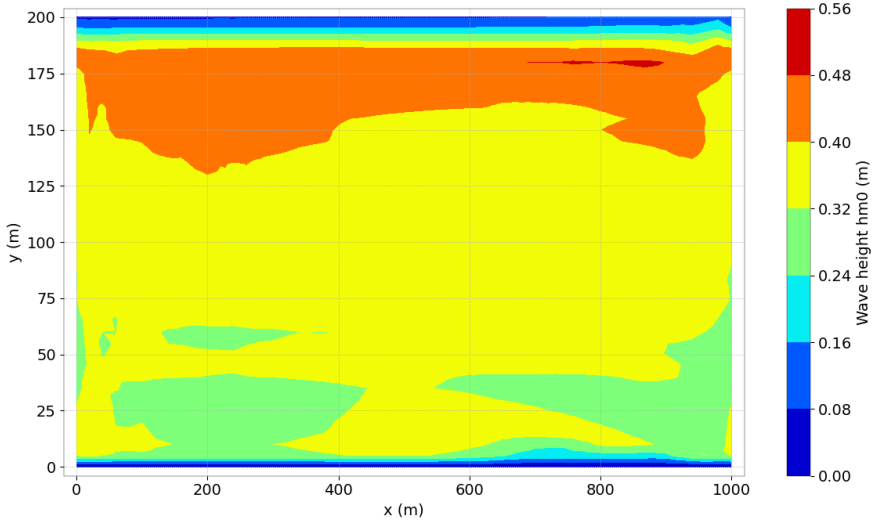
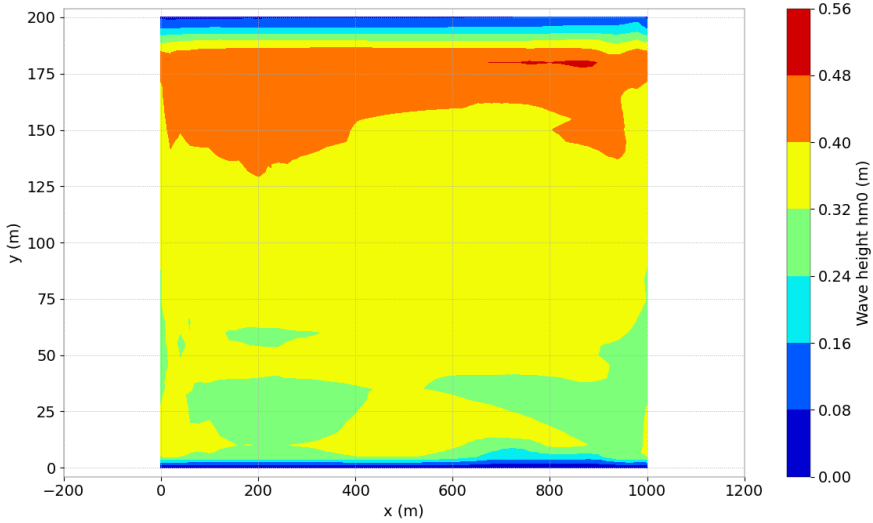
Several case of coupling are tested. The first one is inherited from case littoral but to simplify we erased the coupling with (gaia) (steering file *t2d_littoral.cas*). From this case, we also test the tel2tom technic. We remind here that this technic allows us to couple telemac2d and tomawac on different meshes and different domain. First we test the technic on the same mesh (steering file *t2d_same.cas*) and then on different meshes (steering file *t2d_different.cas*). In the case of different mesh tomawac is calculated on a coarser mesh but a little bit bigger.

In a second time, we are testing the coupling with wind in 3 dimension. Note that the wind is still in 2D since TOMAWAC uses a 2D wind. The first case is a 2D coupling in 3 dimension (steering file *t3d_littoral.cas*) and the second case is a real 3D coupling (steering file *t3d_3Dcoupling.cas*) In all case, we build the reference with a wind exchanged by file (written by TELEMAC-A nd read by TOMAWAC). Note that the reference can not be constructed anymore, since after the validation, the coupling with the use of a wind file in TOMAWAC is forbidden. Then we verify that the wind exchanged by coupling leads to a result equal to the result of the reference. Note that in the case of different mesh, the wind written on the mesh of TOMAWAC is written by another telemac2d steering file (*t2d_diffwind.cas*). In that case the boundary conditions are not the same as for littoral as it would necessitate a dedicated user fortran for that mesh and it is not the point of this test.

On a practical point of vue, since a wind read by TOMAWAC is interpolated on time step between 2 read, we had to construct our results with a coupling period of 1, so that the wind transmitted by coupling has the same actualisation.

4.3 Results

We present the results obtained for hm0 in all case, but the most important result is that there is no difference if the wind is exchanged by file or by coupling. This validates the developpements done for all the coupling.

Figure 4.1: $Hm0$ in classical 2D coupling.Figure 4.2: $Hm0$ with tel2tom and same mesh.

4.4 Coupling TELEMAC-2D and TOMAWAC with a wind and a hotstart

We give here an example of a coupling between TELEMAC-2D and TOMAWAC with a constant wind in space varying linearly in time. The aim is to ensure that the wind is the same on both side at every time step. After a hot start we also ensure that it is still the case (see Figure 4.6). A first run is done during 500s, then we do a hot start and simulate during 500s. The solution is then compared to a solution we call reference solution, i.e. a simulation done during 1000s without any hotstart (see Figure 4.7).

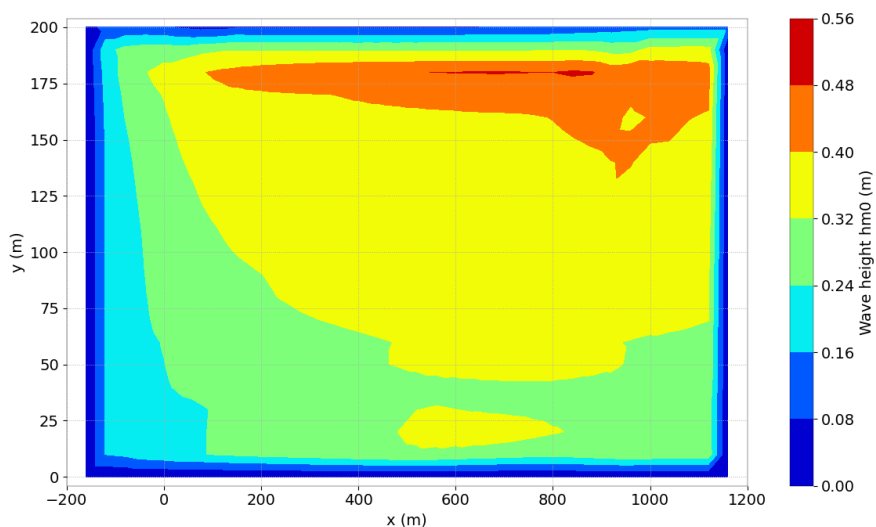


Figure 4.3: Hm0 with tel2tom and different mesh.

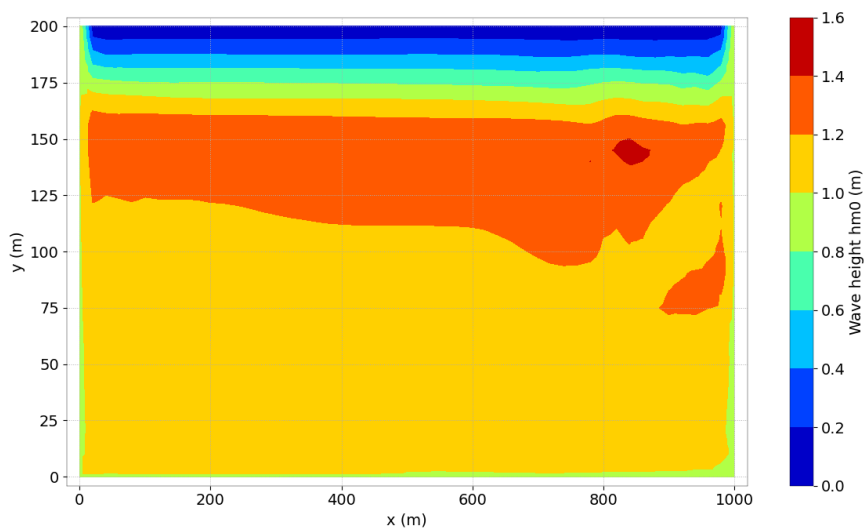


Figure 4.4: Hm0 in the case 3D littoral.

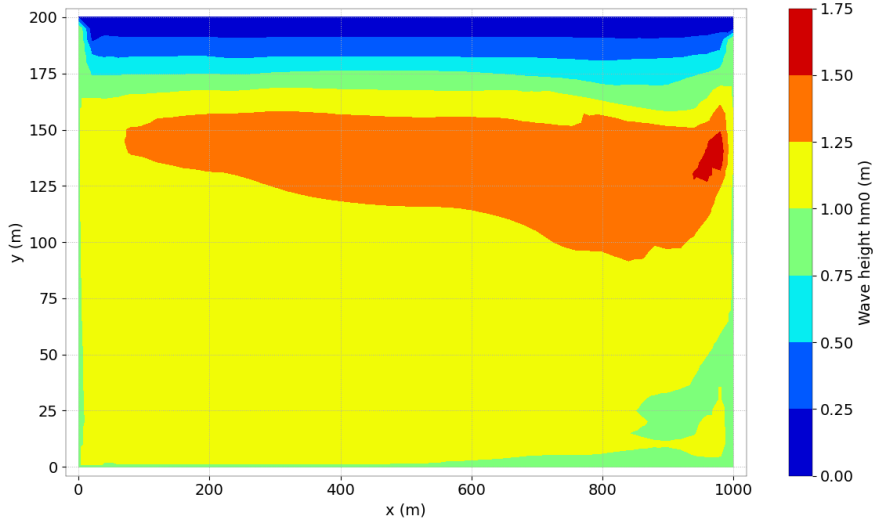


Figure 4.5: $Hm0$ in the case 3D coupling.

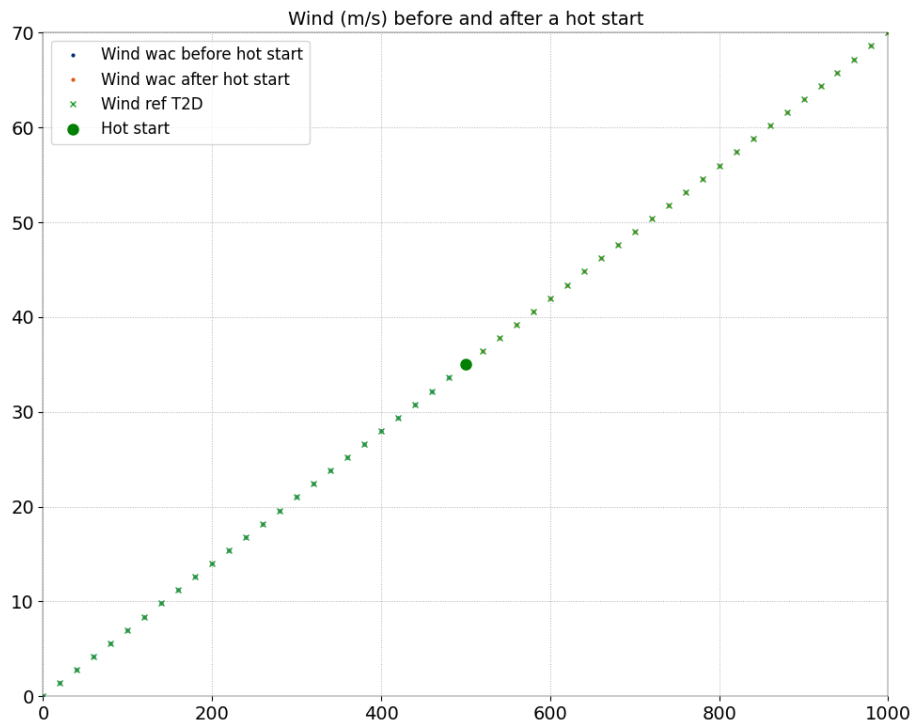


Figure 4.6: Wind in TOMAWAC before and after hotstart compared to the wind in the reference TELEMAC-2D result file

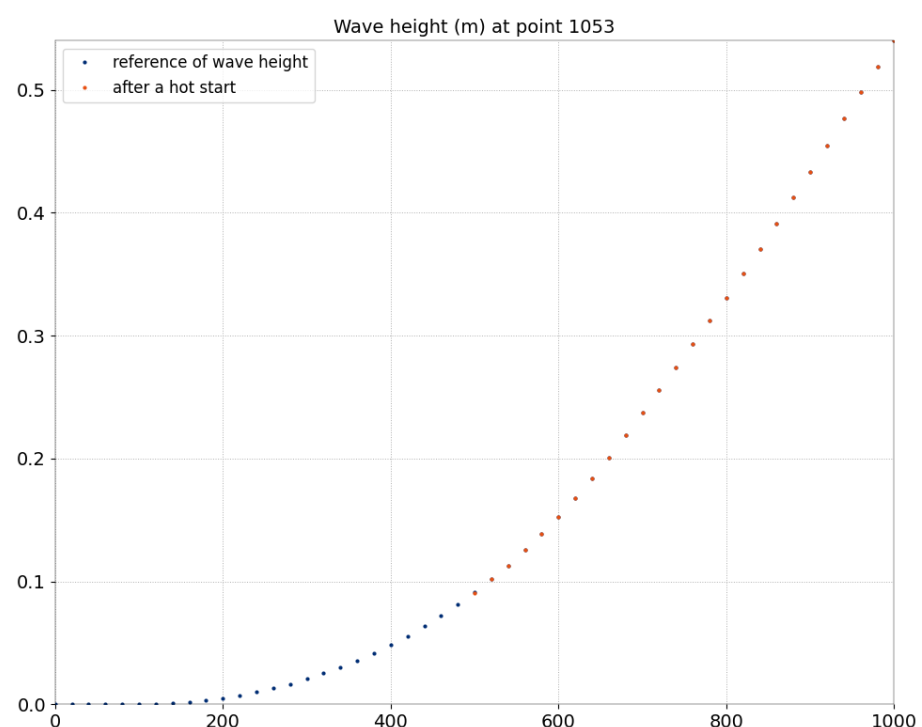


Figure 4.7: Comparison of the wave height between the hot start calculation and the reference calculated during 1000s

5. Manche

5.1 Purpose

This test case has been exhibited from an old version (V5P4), the reference case at this time was called r2d.V1P3. It has got mainly one interest, to compare results from old versions to the new version.

5.2 Description of the problem

We simulate the storm that occurred in 1990 in Manche. This test was a test described in the validation of TOMAWAC 1.0 [5]. Because of many changes in the code it had been abandoned. It now works with the new version but not in parallel because of the fortran user that sets the boundary.

We discretize with 25 frequencies and 12 directions. The minimal frequency is 0.04177248 and the frequential ratio 1.1. The mesh is shown on picture 5.1, as we are interested in storm in the Manche the mesh is finer around the manche. The time step is 300s and we simulate during 14 days.

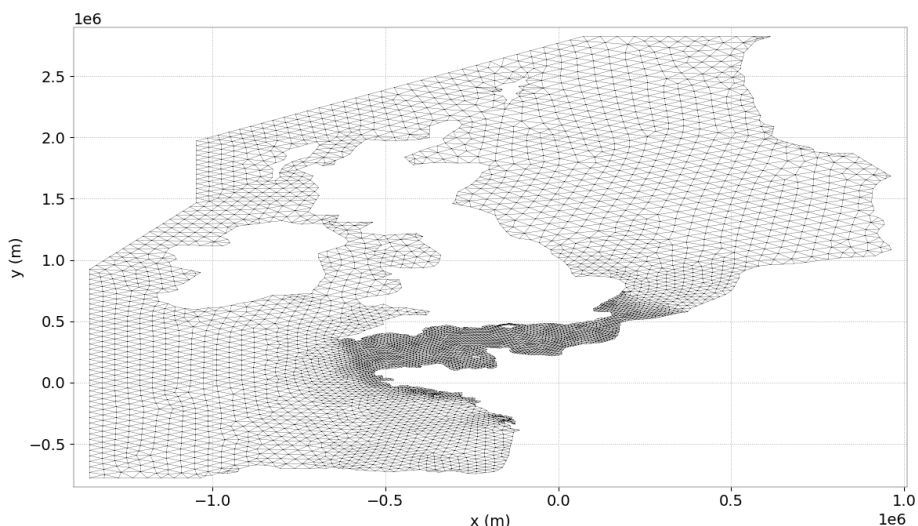


Figure 5.1: Mesh of the sea.

In fact we are going to work with spherical coordinate so the 'real' bathymetry will be the one showed on Figure 5.2. In the code if the bathymetry is more than -10 m, it is set to -10 m.

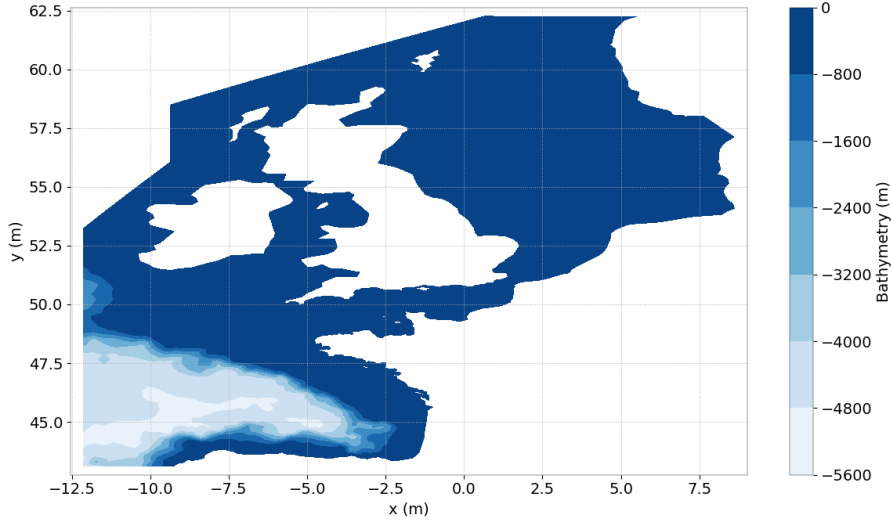


Figure 5.2: Real Bathymetry used in the code.

We take into account the wind through a file that gives the wind in all point of the mesh every 6 hours. On this point, in the original file the time was given with a deprecated format, so we took the wind from the results of the old simulation which was given in a new format (number of seconds after 0).

Nowadays time format is given through a number *YYYYMMDDHHMMNN*, and it used to be given by MDDHH. As we kept the fortran user to describe boundaries conditions one will read this format in the keyword *DATE DE DEBUT DU CALCUL = 1161500* for *1990 01 16 15:00:00*

5.3 Results and Comments

If one run the validation with old results, one will see a difference of 30% wave height result, it is only on a few points (see figure 5.3) and it does not spread on all the results, it can be explained by a bug corrected in characteristic method on boundaries some years ago.

When we observe global results, we would say that there are no difference between reference and new result (see 5.4 5.5 and 5.6). To run validation we have updated the reference, it is a result of the version 7.2

As the calculation is made in spherical coordinates but the initial mesh is done in cartesian coordinates. TOMAWAC calculates a conversion through Fortran user. The result is a little bit different if we take the conversion from the coordinate of the old version because of simple precision in the coordinate. That is the reason of the difference between last comparison when running validation.



Figure 5.3: In colour points where diff of wave height is more than 1 meter.

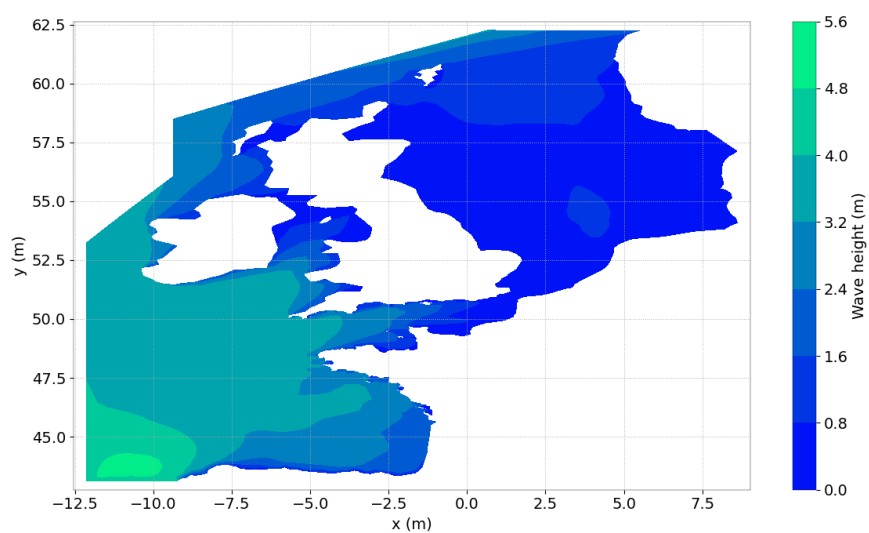


Figure 5.4: Wave height for last version.

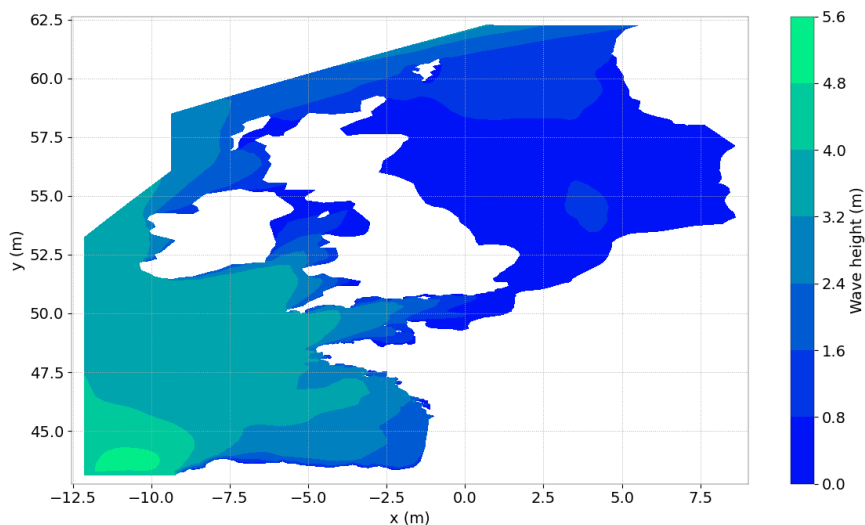


Figure 5.5: Wave height for coordinate changed outside the code.

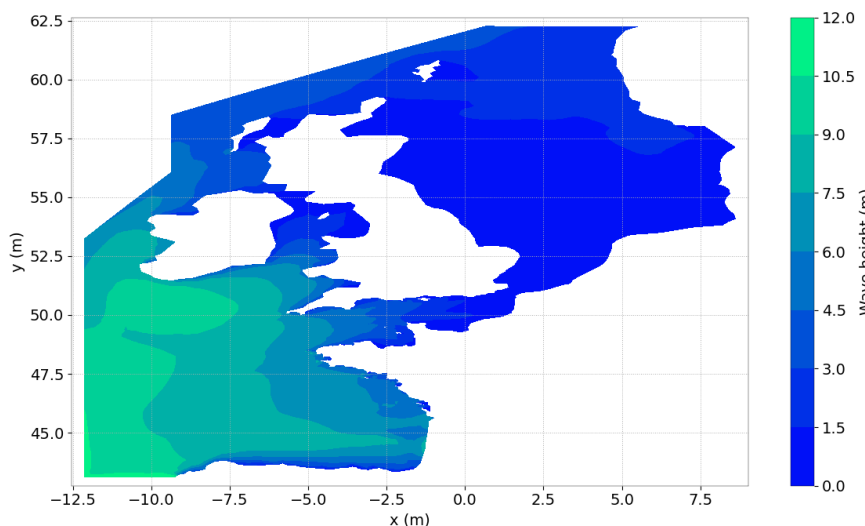


Figure 5.6: Wave height for V1P3 version.

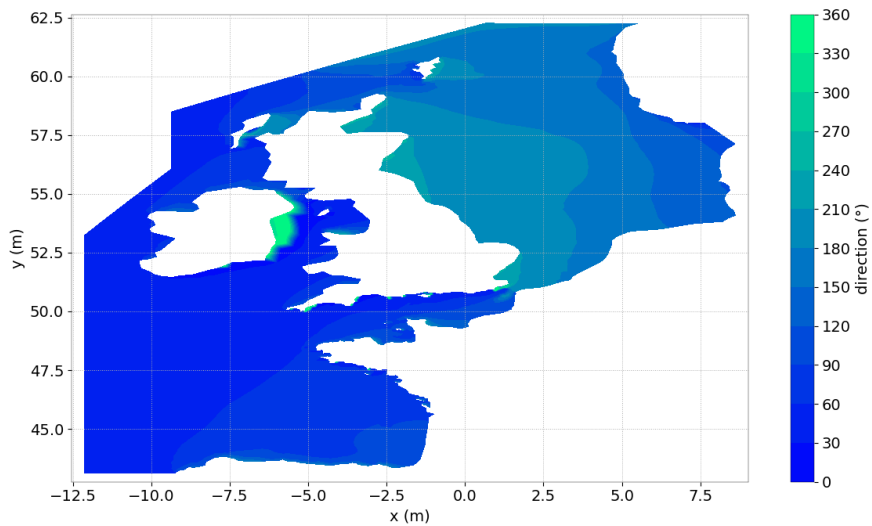


Figure 5.7: Mean Direction for last version.

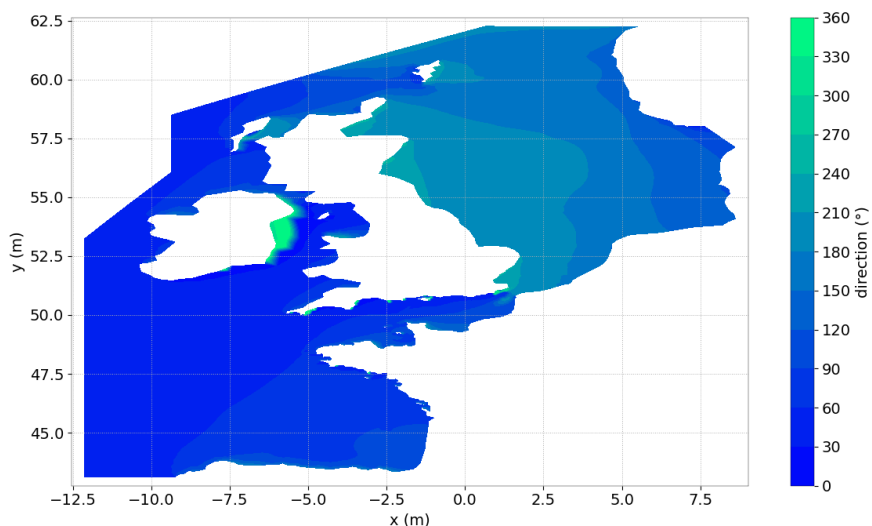


Figure 5.8: Mean direction for reference file.

6. Next_Comput

6.1 Purpose

The aim of this case is to test a computation that follows another one. We start from a calculated state at a time and we simulate some new time step.

6.2 Description of the problem

The simulation is the same as the shoal test case so one will read that test case for physical description. We start here from a shoal simulation until time 600s. The result of this previous simulation is inside the file indicated by the keyword *PREVIOUS COMPUTATION FILE (FICHIER DU CALCUL PRECEDENT in french)*. This file has been created by adding the keyword *GLOBAL RESULT FILE (FICHIER DES RESULTATS GLOBAUX in french)* in the shoal steering case. We simulate for 600 other seconds. We can compare the result to the one obtained by shoal test case with 1200 seconds of simulation.

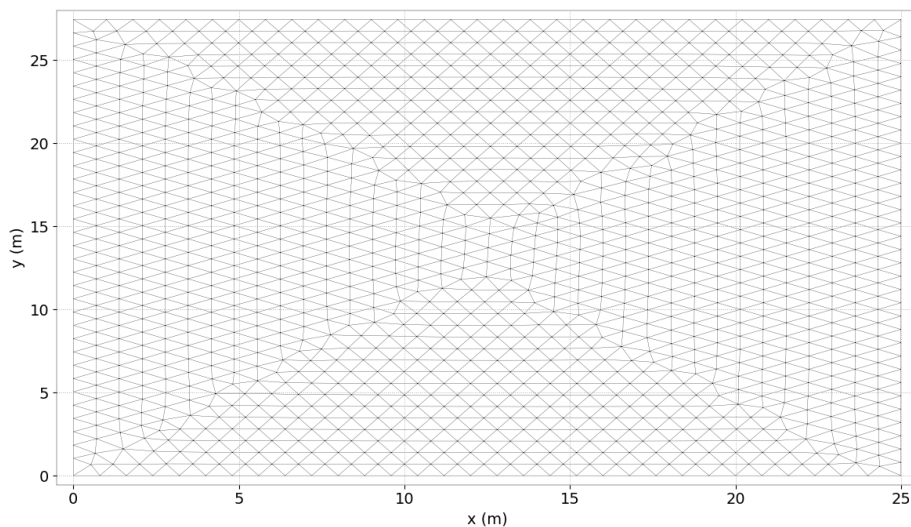


Figure 6.1: Mesh of the domain.

6.3 Results

After 600 s, the difference with the full shoal simulation is null. The reference file is the result of shoal with 12000s.

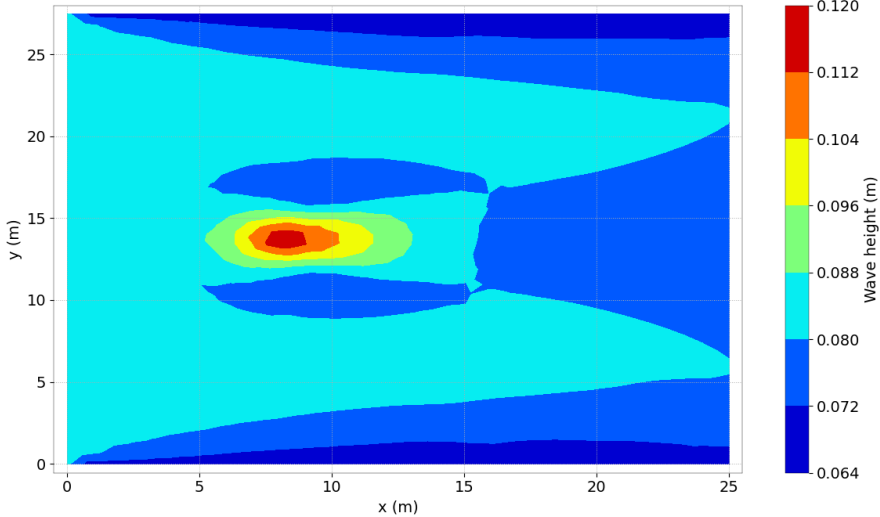


Figure 6.2: Wave height hm0.

6.4 Hot start while reading a tide

A second test is made to verify that when reading a tidal file with water depth and currents varying in time, those variables are still interpolated after the hot start see Figures 6.3 and 6.4.

6.5 Hot start while reading a wind varying in time

A third test is made to verify that when reading a wind varying in time in a file the wind is still interpolated between two points read see Figure 6.5, we can see the effect on the wave height on Figure 6.6 where the solution after a hot start is the same as the one of a calculation for the full time.

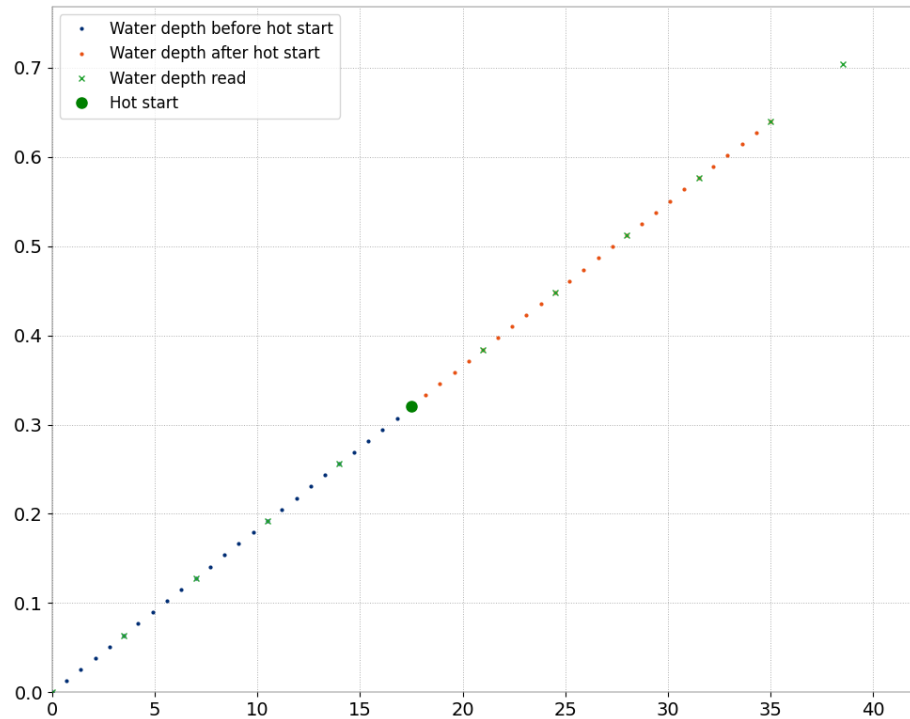


Figure 6.3: Current norm interpolated after the hot start

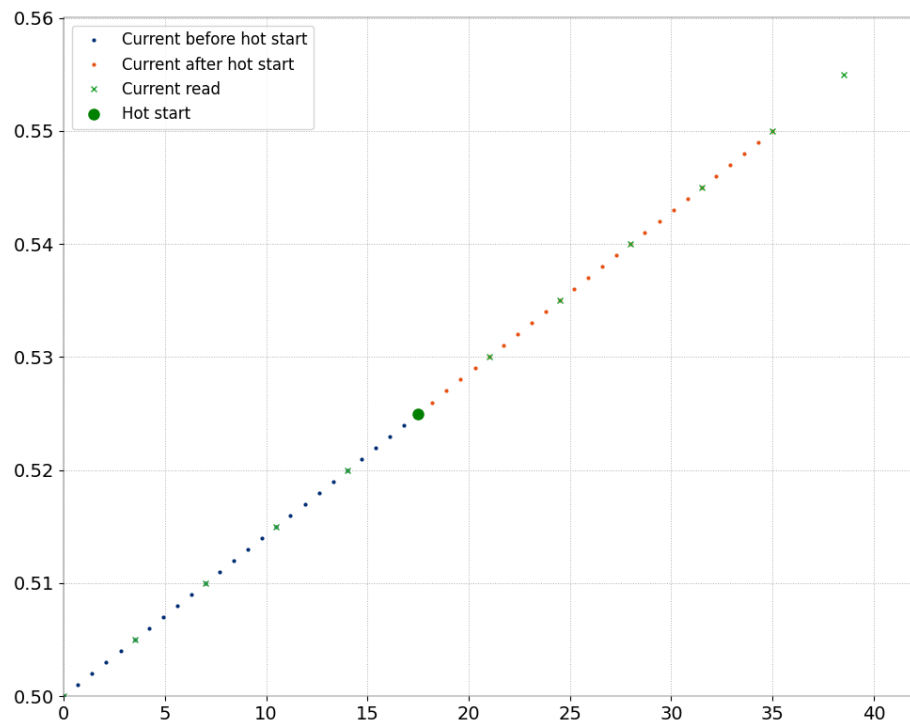


Figure 6.4: Water depth interpolated after the hot start

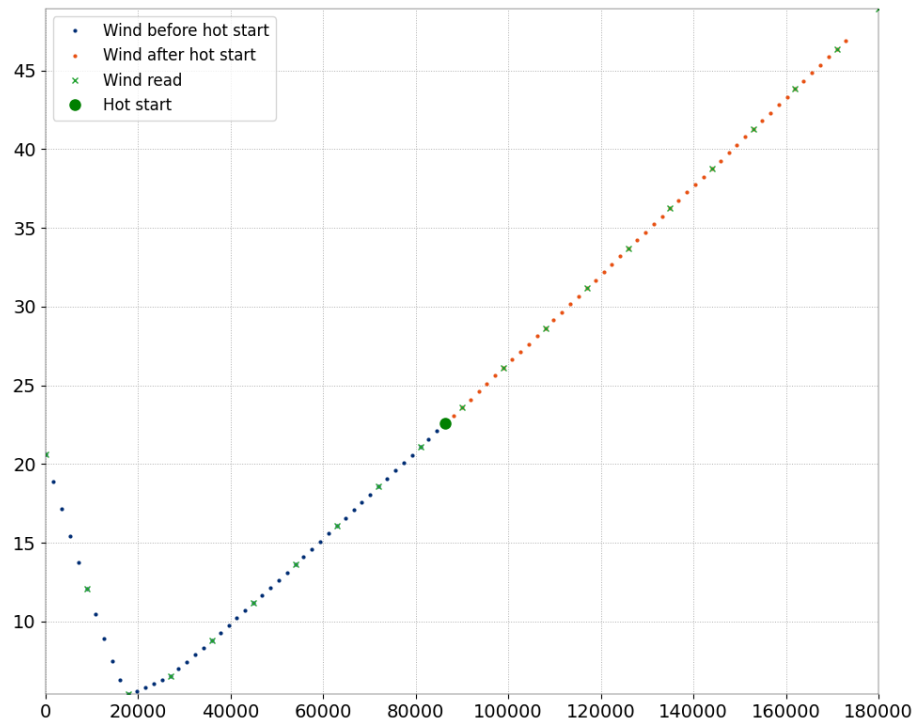


Figure 6.5: Wind norm interpolated after the hot start

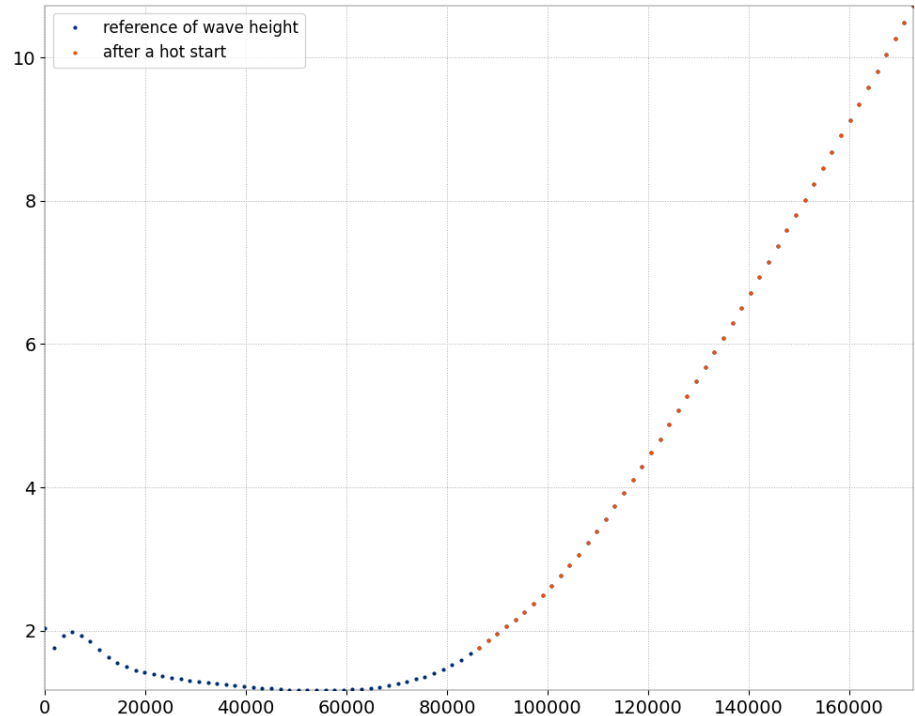


Figure 6.6: Wave height compared between a hot start and a reference calculated from the real start.

7. Porous

7.1 Purpose

This test case has been created to test the dissipation due to a porous media. That is only a test that checks non regression solution. In order to test the subroutine of the trunk the test has not any fortran user. This implies to have porous media in all the domain of calculation.

7.2 Description of the problem

We simulate the dissipation due to porous media in a square. The domain is a square defined by the points (0,0) and (100,100). Since we are using the domain set in *qporos*, The porous media is a square between points (40,39) and (50,61).

7.3 Physical parameters

Simulations were carried out with a water depth $h = 2.0$ m and a wave height of 0.56 m at the incident wave boundary. The media defined in *qporos* has a porosity rate of 0.8 a damping mass coefficient of 2.5, and a linear friction coefficient of 1.

7.4 Geometry and Mesh

The computational domain was composed of a flat (slope = 0.0) 2D grid with an aspect ratio of 1 (cross-shore direction):10 (along shore direction). The calculation grid size was set as 2.0 m in the wave propagation direction. There are 906 nodes and 1500 triangles.

The area where Porous media is taken into account is defined by the file *Zone.txt*'

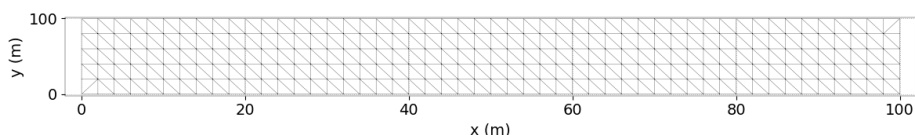


Figure 7.1: Mesh of the domain.

7.5 Initial and Boundary Conditions

The initial significative height is 0.015 m with an initial frequency of 1 Hz and an initial peak factor of 3.3 and a mean direction of 90° and a initial directionnal spread of 0. The boundary conditions are given by a jonswap spectrum with a boundary pic factor of 3.3Hz a significative height of 0.5656 m and a boundary frequency pic of 1 Hz.

7.6 Numerical parameters

The time step was of 1s and the duration of the computation of 1200 s. The spectro-angular mesh has 36 directions and 6 frequencies. The frequential ratio was of 1.01 and the minimum frequency of 0.9705 Hz.

7.7 Results

We can see on Figure 7.2 the impact of porous media compared to Figure 7.3

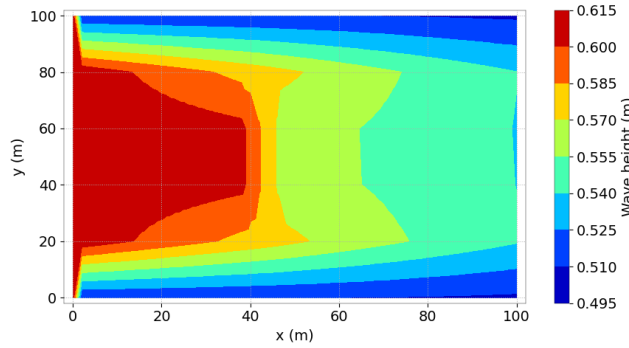


Figure 7.2: Wave height hm0 with porous media.

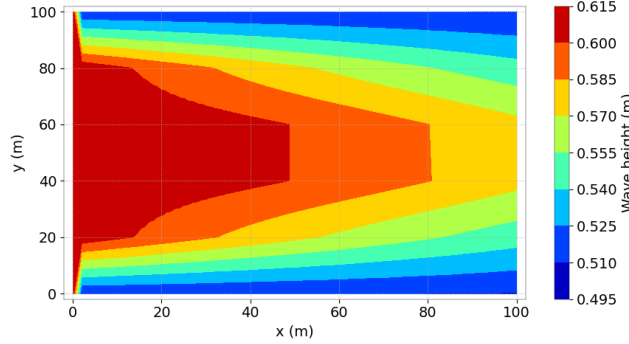


Figure 7.3: Wave height hm0 without porous media.

8. Rip

This case test rip current

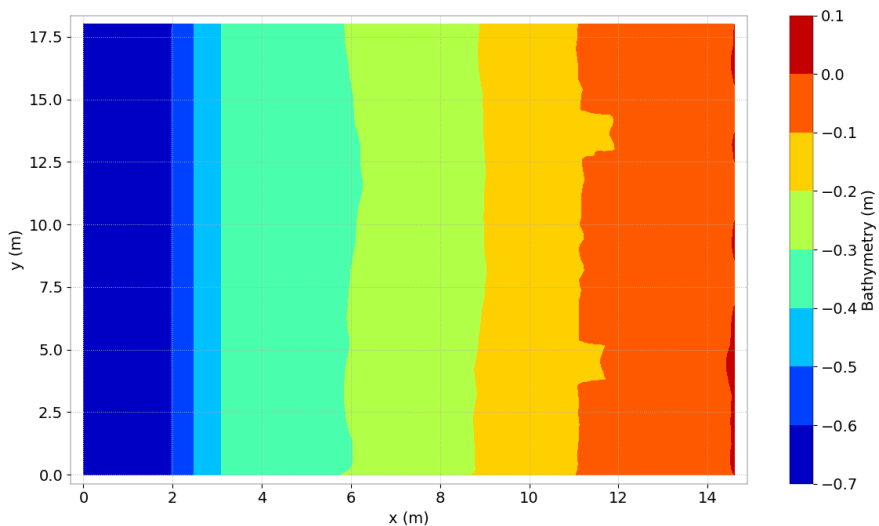


Figure 8.1: Bathymetry and mesh

8.1 Results

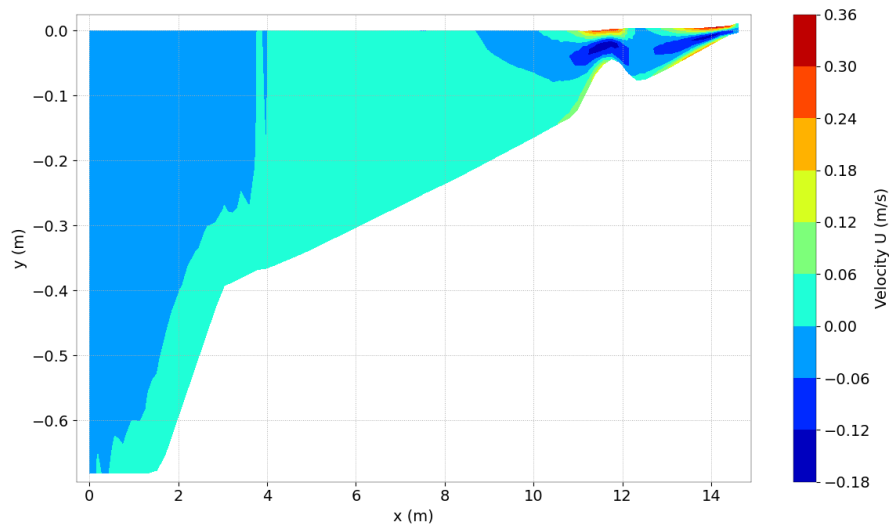


Figure 8.2: Celerity U on a vertical plan along $y=9$.

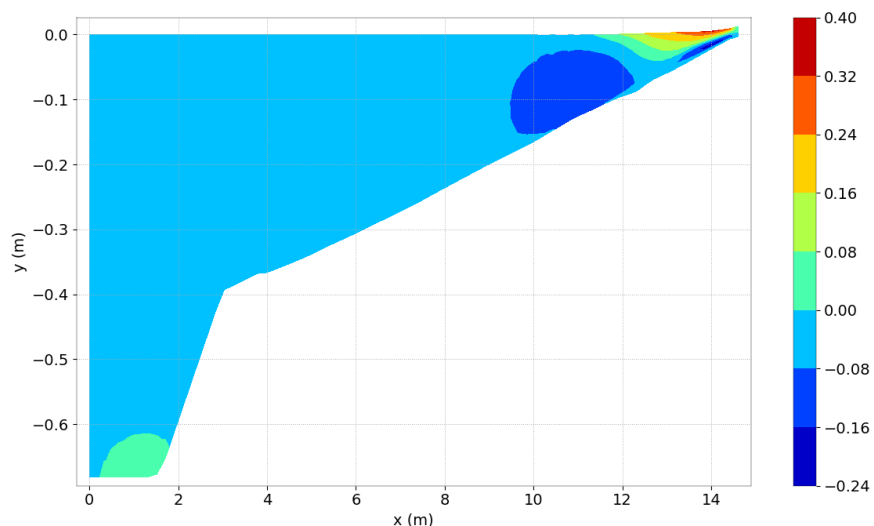


Figure 8.3: Celerity U on a vertical plan along $y=13.6$.

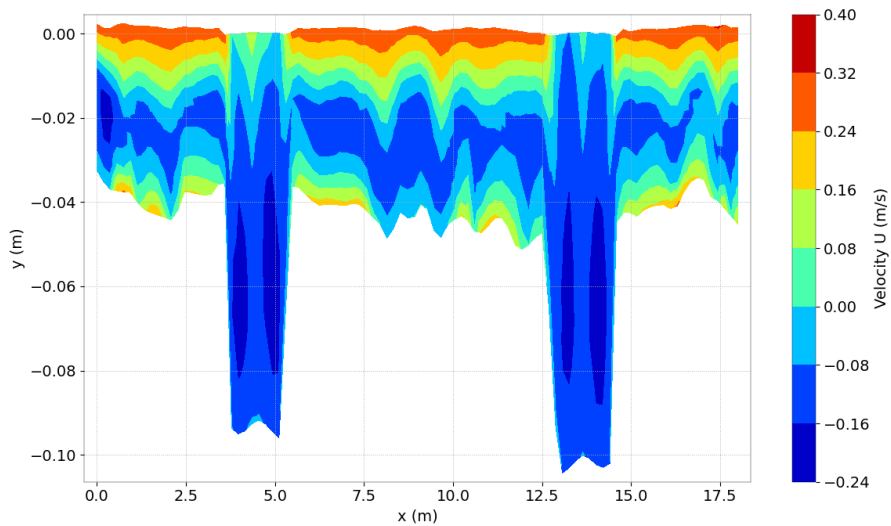


Figure 8.4: Celerity U on a vertical plan along $x=11.8$.

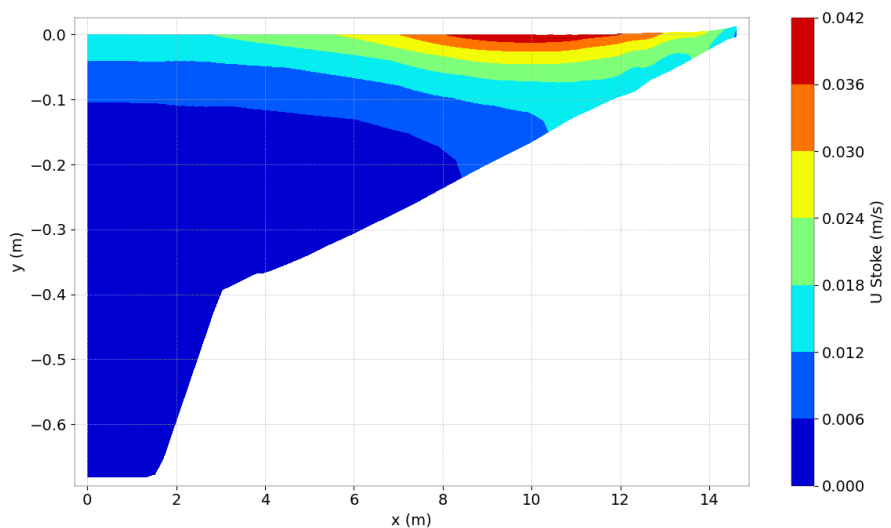


Figure 8.5: U_{STOKES} on a vertical plan along $y=13.6$.

9. Spheric

9.1 Purpose

This test case has been made to test spherical coordinate.

9.2 Description of the problem

The case look like channel sea but we intentionnaly put an infinite depth.

We discretize the spectrum with 31 frequencies and 36 directions. The minimal frequency is 0.04 and the frequential ratio 1.1.

The time step is 180s and we simulate during 50mn.

We take into account the wind through a file that gives the wind in all point of the mesh every 36 hours, so in our case we can consider constant wind (see Figure 9.2). As for current, it is taken into account through a fileand is update every 1800s so every 10 time steps(see Figure 9.3).

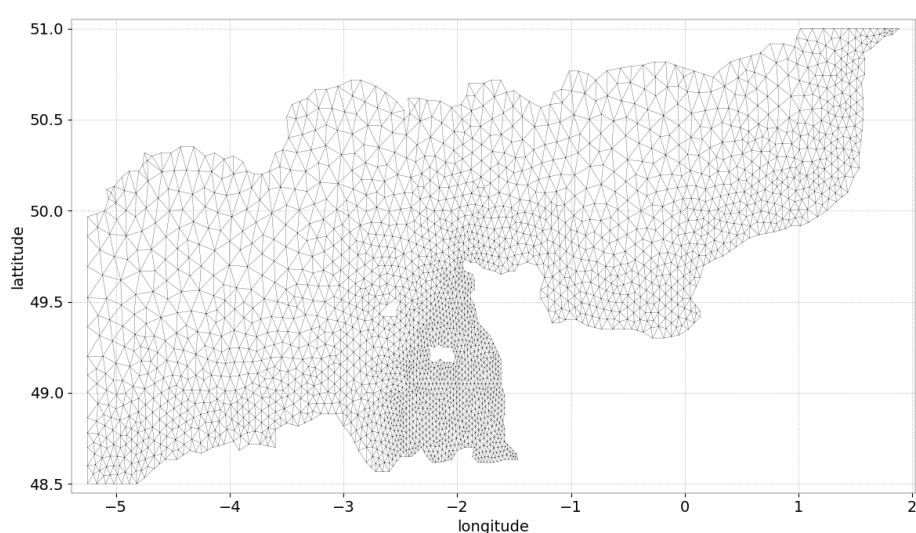


Figure 9.1: Mesh of the domain.

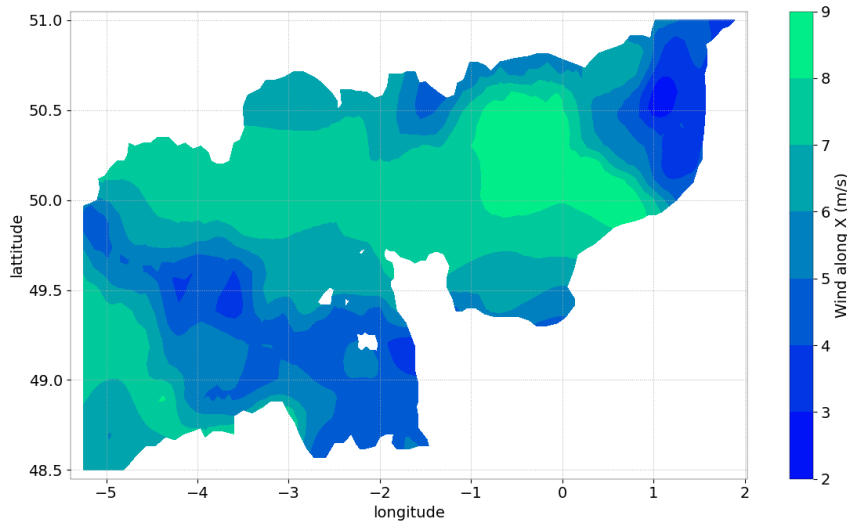


Figure 9.2: Wind.

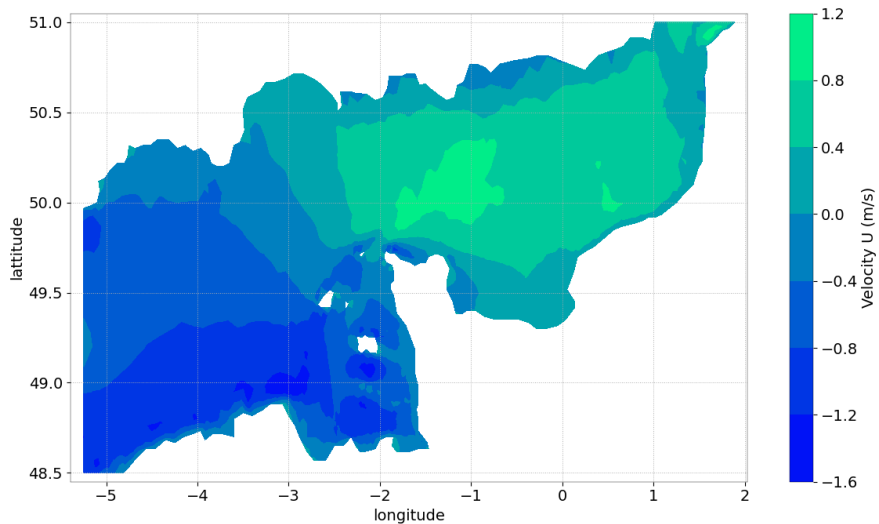


Figure 9.3: Current.

9.3 Results

We present Figure 9.4 the wave height obtained after 50mn.

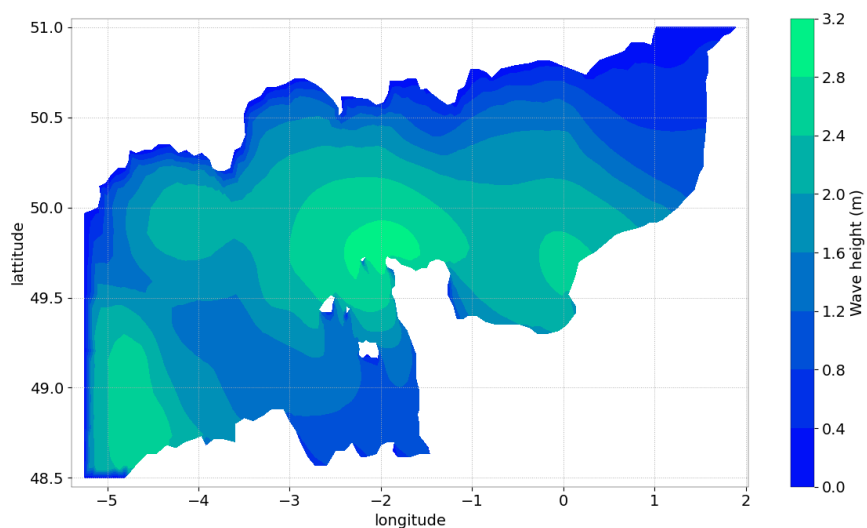


Figure 9.4: Wave height $hm0$.

10. Triplets

10.1 Purpose

This test case has been created to test the extend the covering by using option of triad interactions that were not used in other cases.

10.2 Description of the problem

We simulate non linear transfers between triads. In the first case we use Lumped Triad Approximation model (LTA) and in the second case we use the SPB model

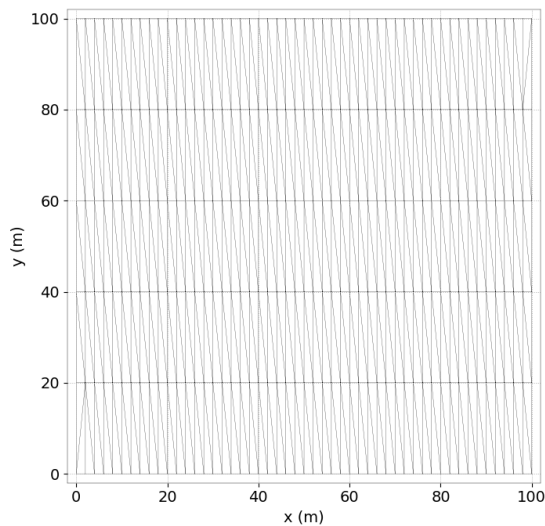


Figure 10.1: Mesh of the domain.

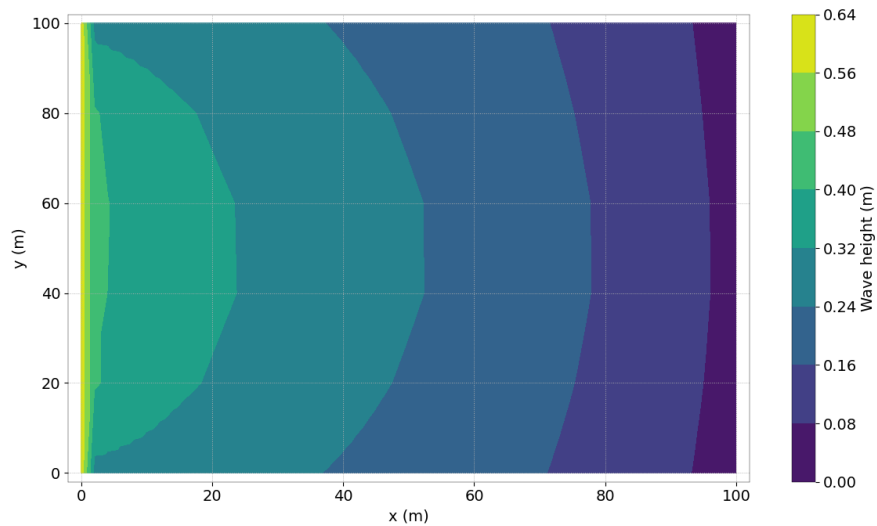


Figure 10.2: Wave height for Lumped Triad Approximation model.

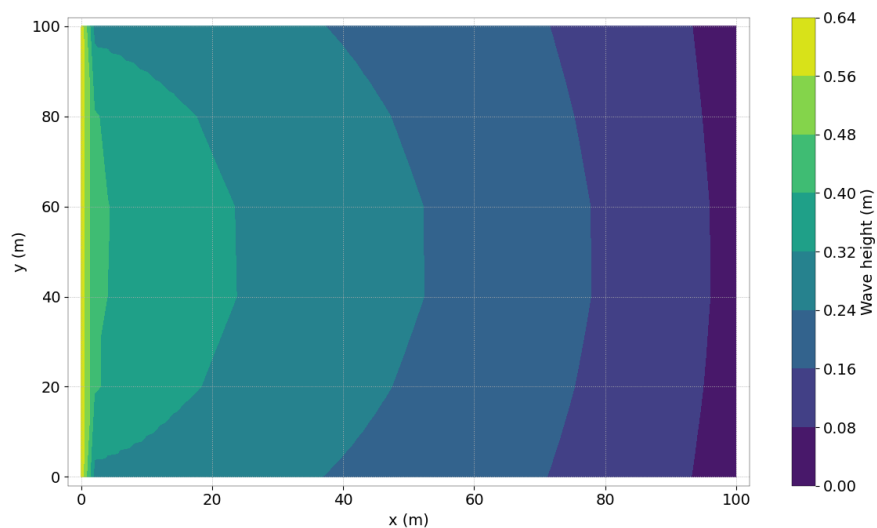


Figure 10.3: Wave height for SPB model.

11. Veget

11.1 Purpose

This test case has been created to test the vegetation dissipation without any fortran user. That is only a test that checks non regression solution. It refers to the model of [28] but since the frequency is not monochromatic the result can not be compared to the results they obtained.

11.2 Description of the problem

We simulate the dissipation due to vegetation in a channel.

The random wave transformation model for a flat bottom by Mendez and Losada (2004) is expressed as follows.

$$H_{rms} = \frac{H_{rms,0}}{1 + \tilde{\beta}x}$$

with

$$\tilde{\beta} = \frac{1}{3\sqrt{\pi}} \tilde{C}_D b_v H_{rms,0} k \frac{\sinh^3 k\alpha h + 3 \sinh k\alpha h}{(\sinh 2kh + 2kh) \sinh kh}$$

where $H_{rms,o}$ is the value of root mean square wave height at the wave boundary $x=0$.

11.3 Physical parameters

Simulations were carried out with a water depth $h = 2.0$ m and root mean square wave height $H_{rms,0}$ (0.4 m) at the incident wave boundary. The vegetation height was taken as equal to the water depth ($\alpha h = 2.0m$), the plant area per unit height was $b_v = 0.04m$, the number of plants per unit area was $N = 10units/m^2$, and the bulk drag coefficient was $\tilde{C}_D = 1.0$. The vegetation was present in the entire computational domain.

11.4 Geometry and Mesh

The computational domain was composed of a flat (slope = 0.0) 2D grid with an aspect ratio of 1 (cross-shore direction):10 (along shore direction). The calculation grid size was set as 2.0 m in the wave propagation direction. There are 906 nodes and 1500 triangles.

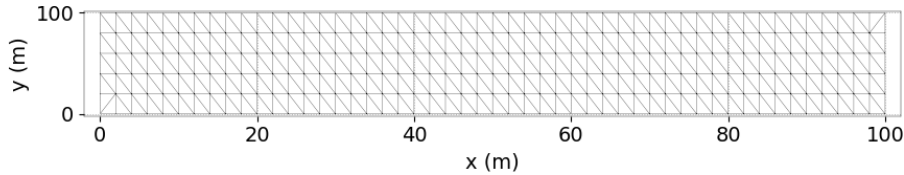


Figure 11.1: Mesh of the domain.

11.5 Initial and Boundary Conditions

The initial significative height is 0.015m with an initial frequency of 1 Hz and an initial peak factor of 3.3 and a mean direction of 90° and a initial directionnal spread of 0. The boundary conditions are given by a jonswap spectrum with a boundary pic factor of 3.3Hz a significative height of 0.5656m and a boundary frequency pic of 1

11.6 Numerical parameters

The time step was of 0.1s and the duration of the computation of 480s. The spectro-angular mesh has 36 directions and 6 frequencies. The frequential ratio was of 1.01 and the minimum frequency of 0.0951Hz.

11.7 Results

We do not compare results with an experiment as the choice of not having any fortran user prevent from being in the same condition but [2] obtained good result agreements when comparing to [28]

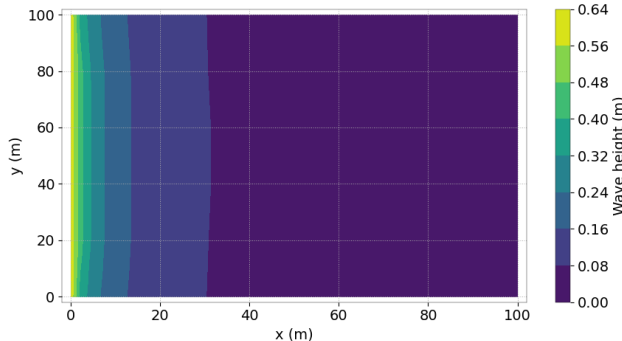


Figure 11.2: Wave height hm0.

12. Angular Spread

12.1 Purpose

This test has been created to check a new functionnality in initial spectrum and boundary spectrum. Classically the function given at the boundary (or initial spectrum) is of the form:

$$S(f, \theta) = J(f)G(\theta) \quad (12.1)$$

with f the frequency, θ the angular dependance, J is often taken as a Jonswap function, and $G(\theta)$ is a function of \cos for example in [29],

$$G(\theta) = G_0 \cos^{2s} \left(\frac{\theta - \theta_0}{2} \right) \quad (12.2)$$

where θ_0 denotes the principal wave direction, G_0 is a constant so that the integration of G over θ is unity. S is the spread parameter that sizes the angle of directions. In the three first option of *BOUNDARY* (or *INITIAL*) *ANGULAR DISTRIBUTION FUNCTION*, s is a constant. Here we check a fourth option proposed by Goda in [15], where s depends on frequency too.

$$s = \begin{cases} s_{max} \left(\frac{f}{f_p} \right)^5 & : f \leq f_p \\ s_{max} \left(\frac{f}{f_p} \right)^{-2.5} & : f > f_p \end{cases} \quad (12.3)$$

Where f_p is the peak frequency, and s_{max} should be 10, 25 and 75 for wind waves, swell with short decay distance, and swell with long decay distance. In our cas we take an intermediary value *GODA COEFFICIENT FOR ANGULAR SPREADING = 35*. The default value is 25.

12.2 Description of the problem

The problem is the same as the test case Shoal.

12.3 Results

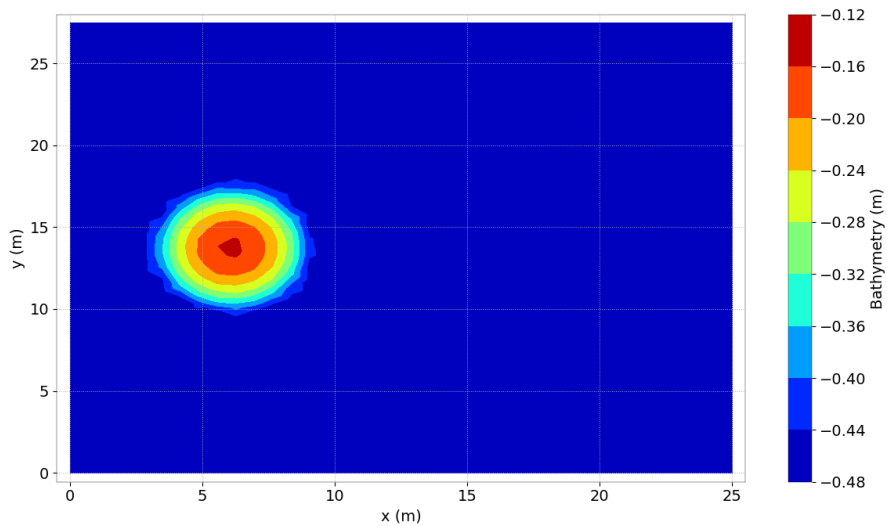


Figure 12.1: Mesh and bathymetry of the domain.

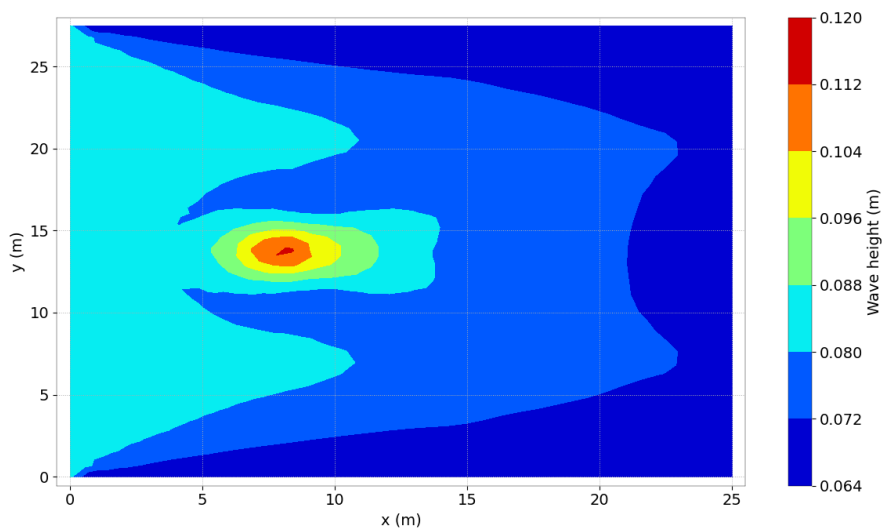


Figure 12.2: Wave heighth $hm0$.

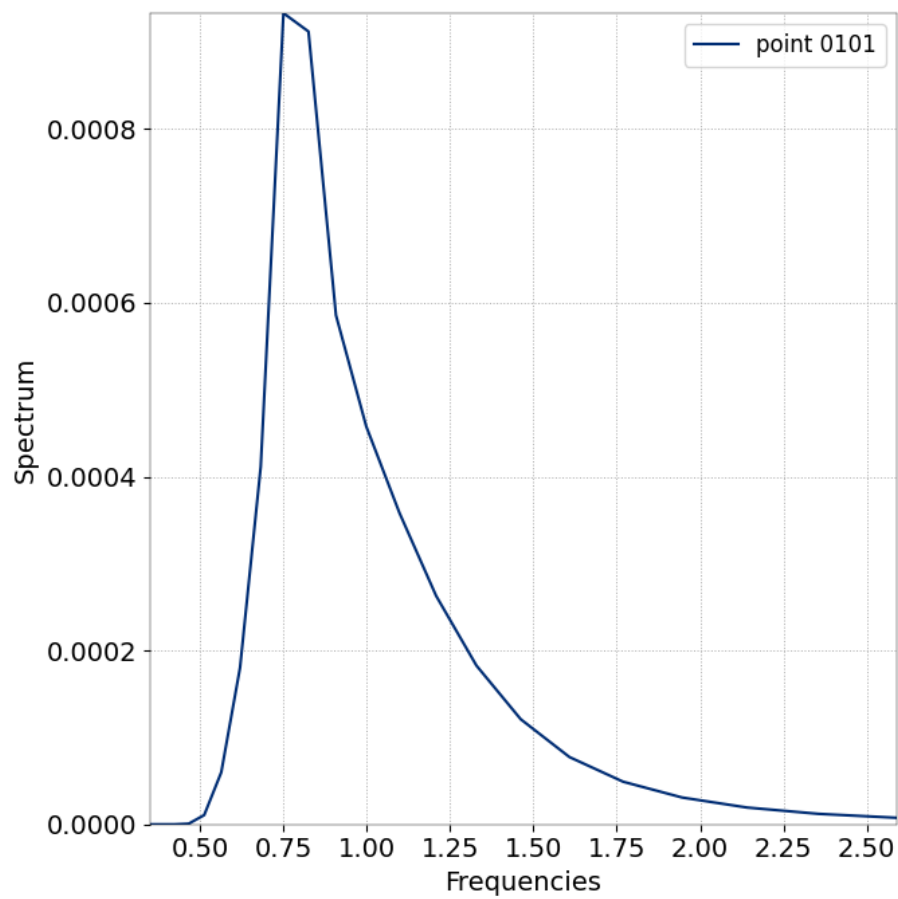


Figure 12.3: Spectrum imposed at the left boundary of the domain.

13. Bottom friction

13.1 Purpose

This test case aims at testing the effect of friction coefficients used in TOMAWAC, one acting upon energy whereas the other one acts upon the mean directional frequency. This test case is an inheritance of a comparison between Cowadis and TOMAWAC. There is no measure to validate the test, it is only a non regression testing.

13.2 Description of the problem

The waves are let freely propagate in a large body of water. The swell should loose some energy and its frequency should change only under the effect of friction bottom (the boundary conditions may be ignored because the domain is very wide).

The expression that is used for computing the friction in TOMAWAC is as follows:

$$Q_{bf}(\theta, \omega) = -\Gamma \left(\frac{\sigma}{g \cdot \sinh(kd)} \right) F(\theta, \omega) \quad (13.1)$$

Where Γ , the BOTTOM FRICTION COEFFICIENT, is taken equal to 0.038, its default value.

13.3 Geometry and mesh

The computational domain is a 100 km by 25 km rectangle and the flat bottom elevation is taken equal to 5m.

The mesh is made with 492 nodes (80 on the boundary) and 902 triangles.

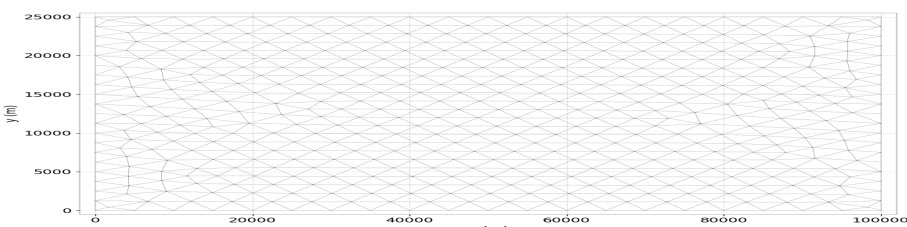


Figure 13.1: Mesh of the domain.

13.4 Numerical parameters

Time duration is 30000 s, time step is equal to 100 s, the spectro-angular mesh has 24 angles and 25 frequencies spread on a geometric progression common ratio 1.1 with a minimum of 0.056447393.

13.5 Initial and Boundary Conditions

For both conditions, we take a Jonswap spectrum with a 1 m significant wave height, a pic frequency of 0.1. The angular distribution function follows a $\cos^2 \theta$ distribution with an angular spreading of 6 and a mean direction of 0.

13.6 Results

In this case we just verify that we still have the same results as the ones obtained during the comparison with Cowadis [26].

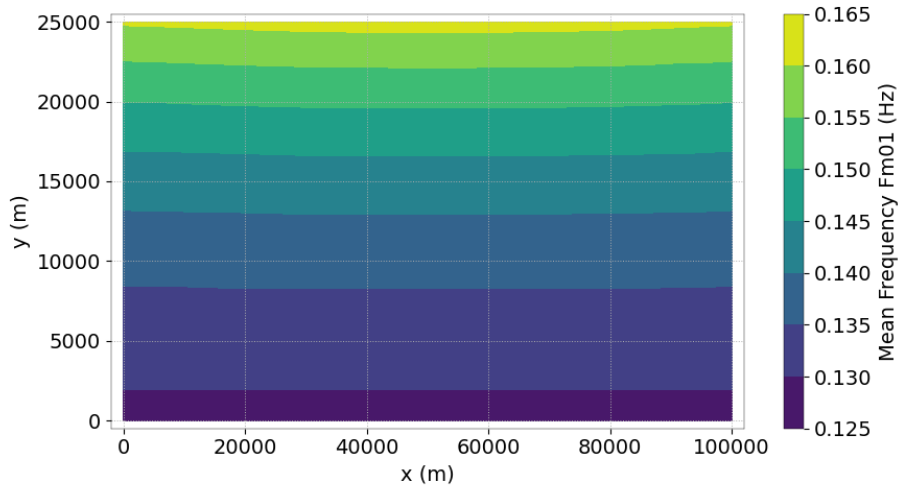


Figure 13.2: MEAN FREQUENCY Fm01

14. Calais

14.1 Purpose

This test case has been exhibited from an old version. It has got mainly one interest, to compare results from version 5P8 to the new version.

14.2 Description of the problem

We simulate waves around the harbour of Calais coming from offshore. At the boundary, the significative height is 4m the frequency peak 0.1 and the direction of 135 degree.

We discretize with 23 frequencies and 24 directions. The mesh is shown on picture 14.1

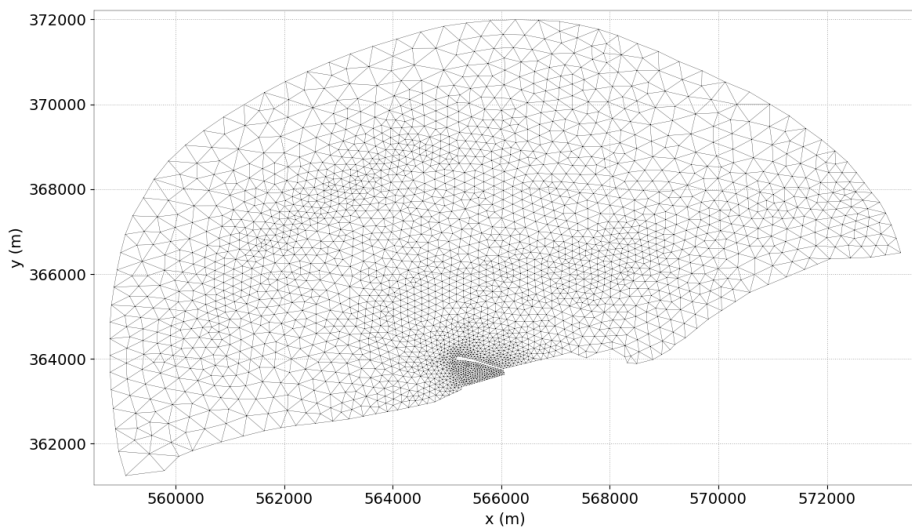


Figure 14.1: Mesh of the neighborhood of Calais.

14.3 Results and Comments

If one run the validation with an old version of the code, one will see a difference of 11 degree on direction in results, 11 Watt on Power and 0.5 m on wave height. But as we can see on figure 14.2, 14.3, 14.4, this is not the case when observing global results. Anyway those differences

come from changes made in the characteristics, so now we take as the reference the results computed with version 7.2.

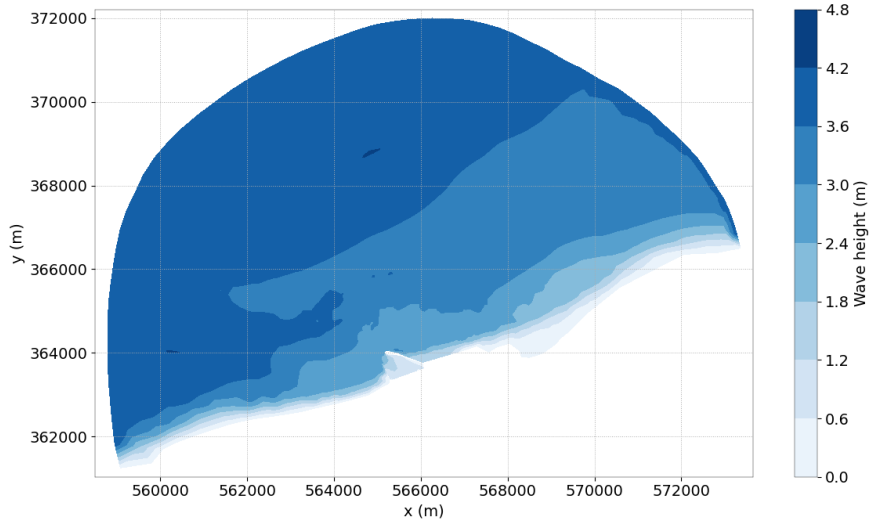


Figure 14.2: Wave height for last version.

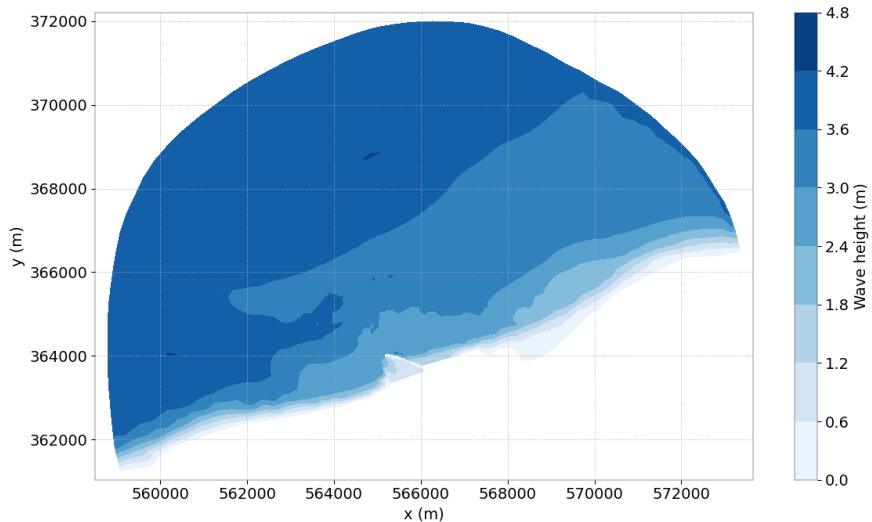


Figure 14.3: Wave height for V6p0 version.

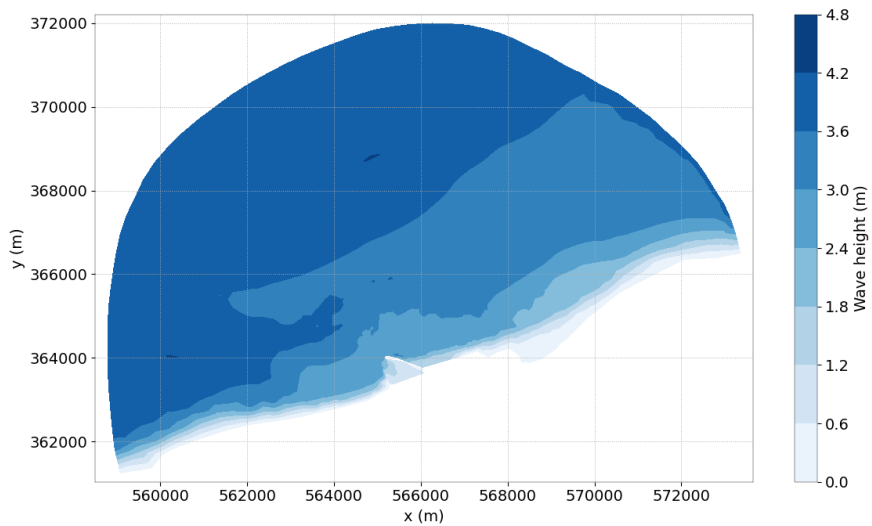


Figure 14.4: Wave height for V5p8 version.

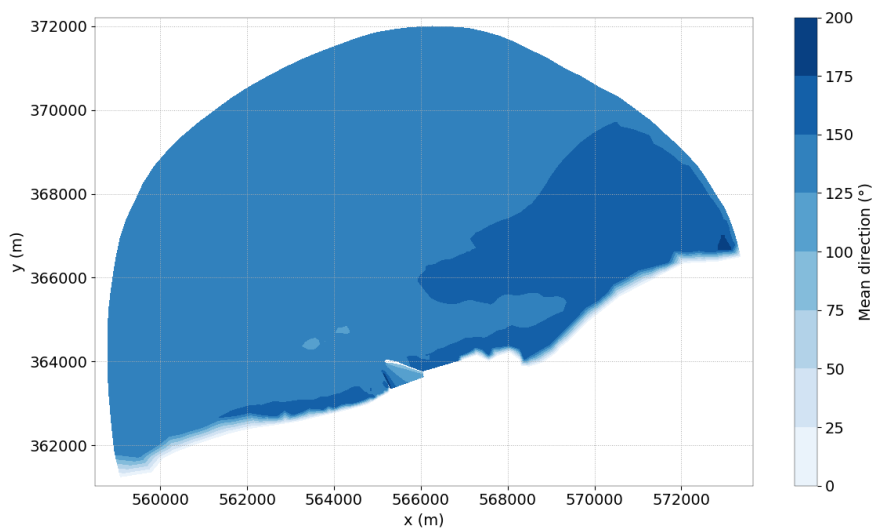


Figure 14.5: Direction for last version.

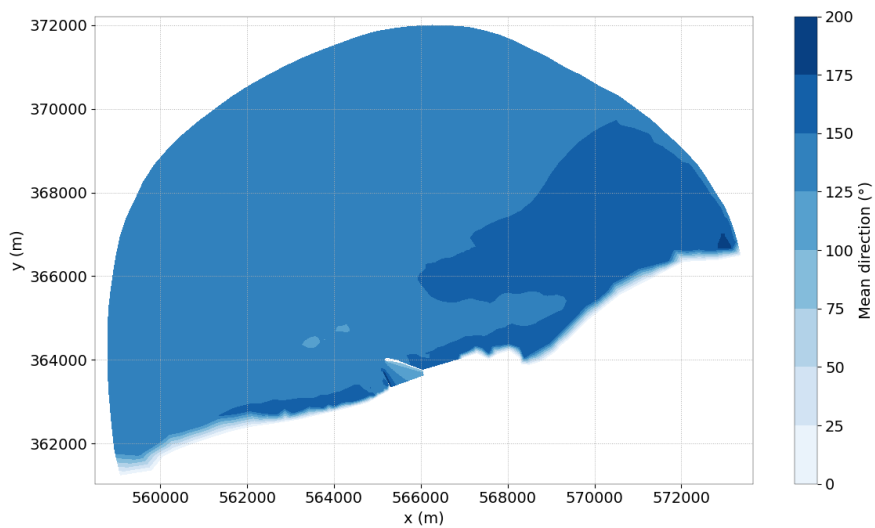


Figure 14.6: Direction for V6P0 version.

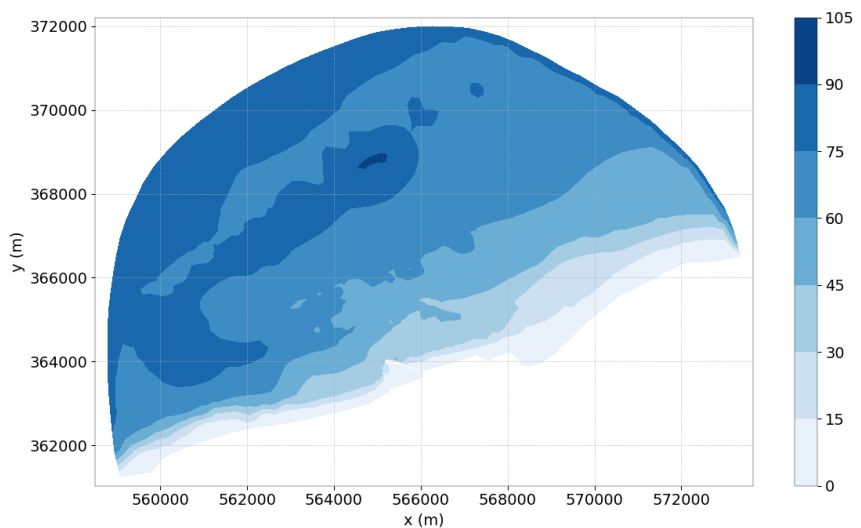


Figure 14.7: Power for last version.

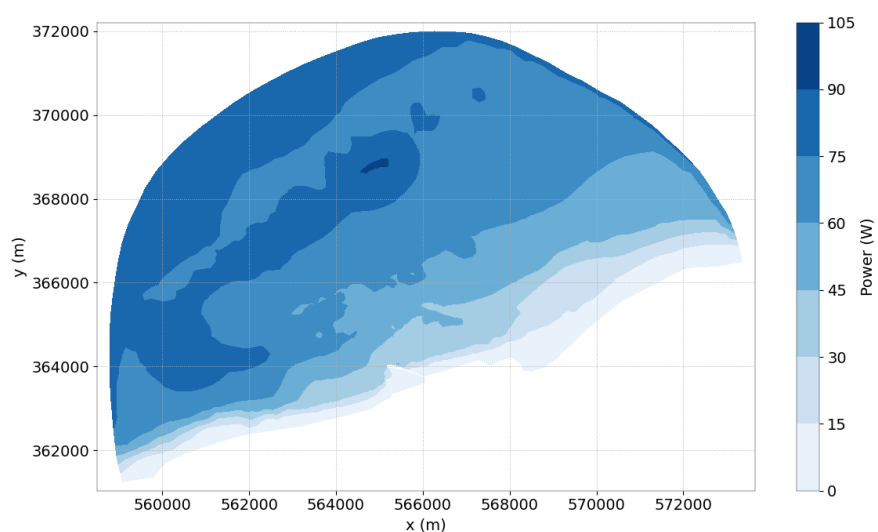


Figure 14.8: Power for V5P8 version.

15. Dean

15.1 Purpose

This test case aims to verify the development made to take into account the wave energy dissipation induced by vegetation. When the ratio between vegetation height and water depth is important, dissipation may become non negligible.

15.2 Description of the problem

In order to carry out an analysis of the influence of plant height, vegetation field width and breaking on waves propagation, Mendez and Losada (2004) analysed the evolution of the wave height over a Dean's shape profile [11] defined as follows:

$$h = 0.25(300 - x)^{\frac{2}{3}}$$

Where h [m] is the water depth, 0.25 the sediment scale parameter, and $x=0$ is the offshore boundary.

15.3 Reference

In this test case the prediction of the effects of vegetation is validated with the original equation and results from Mendez and Losada [28]. The reference file *fom_dean.slf* contains the results that have been compared to [28] in [2].

15.4 Physical parameters

Two vegetation heights, $dv = 1$ m and 3 m and a single 100 m long vegetation field, from 50 to 150 m, are used. The number of plants per square meter is $N = 20 \text{ units/m}^2$ and the plant area per unit height of vegetation is $b_v = 0.25 \text{ m}$. The bulk drag coefficient is 0.2. All these parameters are keywords in the steering file.

15.5 Geometry and Mesh

The computational domain was composed of a flat (slope = 0.0) 2D grid with an aspect ratio of 1 (cross-shore direction):10 (along shore direction). The calculation grid size was set as 2.0 m in the wave propagation direction. Bathymetry and mesh are shown on figure 15.1. There are 906 nodes and 1500 triangles.

The area where vegetation is taken into account is defined by the file *Zone.txt*'

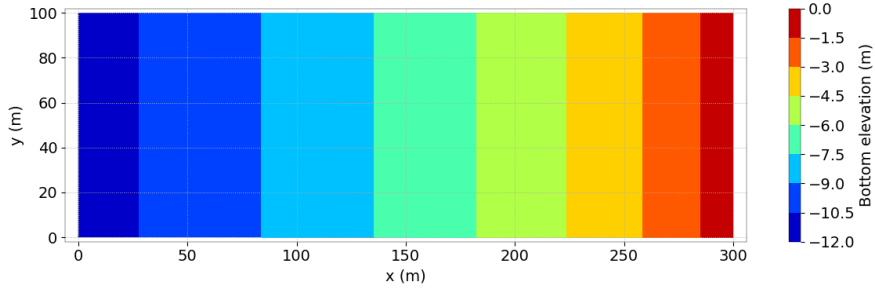


Figure 15.1: Depth evolution.

15.6 Initial and Boundary Conditions

According to the authors, the incident wave conditions imposed to TOMAWAC on the offshore boundary are given by $H_{rms,o} = 2.5 \text{ m}$ (equivalent to significant wave height $H_s = 3.54 \text{ m}$) and $T_p = 10 \text{ s}$. The incident waves are uni-directional random waves as defined in the previous section and the breaking model used is that of Thornton and Guza (1983) with $\gamma = 0.6$ (where the parameter γ is the proportional control factor indicating the maximum water depth “Hm” compatible with water depth “d”:).

The significant initial wave height was taken equal to 3.54 m with a peak frequency of 2.2 Hz. The angular distribution function follows a $\cos^2\theta$ distribution with an angular spreading of 2, and a mean direction of 90.

15.7 Numerical parameters

The time step is of 0.1 s and the duration of the computation of 480 s. The spectro-angular mesh has 36 directions and 6 frequencies. The frequential ratio is of 1.01 and the minimum frequency of 0.0951 Hz. The frequencies are filtered to keep only the fourth one (0.1 Hz) at 90 degrees to respect the $T_p = 10 \text{ s}$ imposed to the boundaries.

The spectrum tail factor was taken at 4.

15.8 Results

The results from Mendez and Losada and TOMAWAC model are compared in Fig. 15.2 below. Even if the test case is made with 1 m of vegetation, we present on Figure 15.2 the results obtained for three different height of vegetation, 0 m, 1 m and 3 m [2]. The results show very good agreement between the Mendez and Losada model [28] and TOMAWAC. We notice that differences seem very small and we can thus conclude that TOMAWAC is able to reproduce the same wave attenuation as with the random wave transformation model for breaking uni-directional random waves.

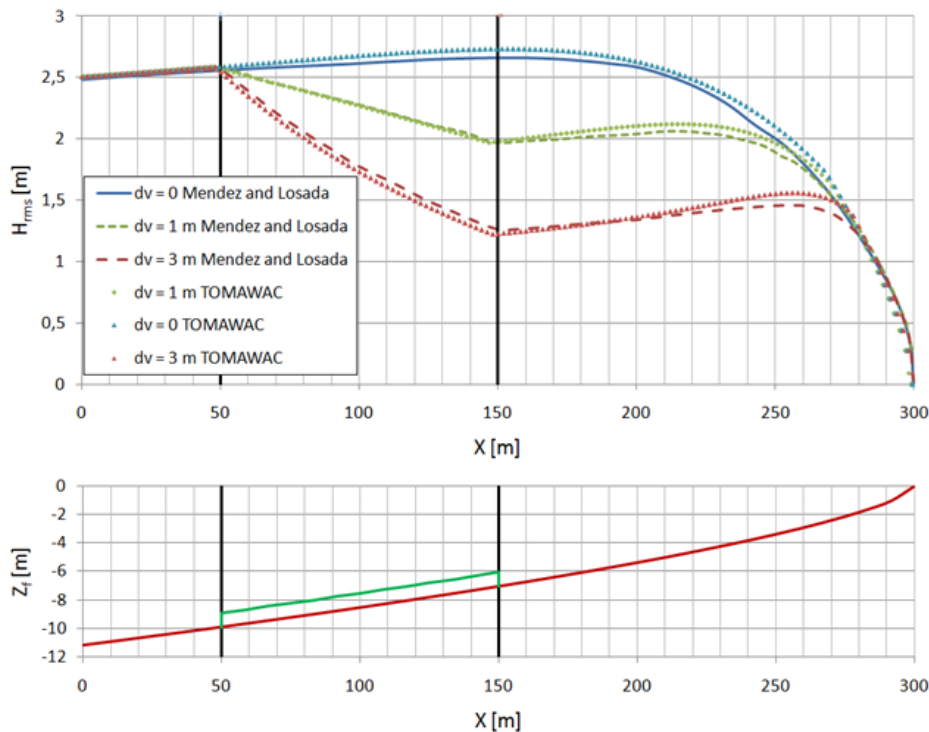


Figure 15.2: Comparison of H_{rms} evolution for numerical wave model (TOMAWAC) and random wave transformation model (Mendez and Losada) over Dean's shape profile.

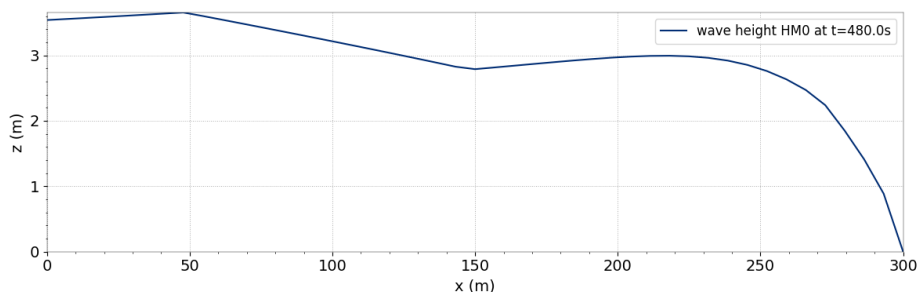


Figure 15.3: Wave height for $dv=1m$.

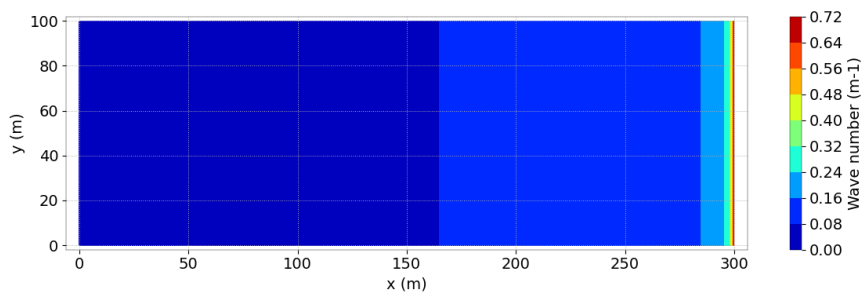


Figure 15.4: Average Wave number for $dv=1m$.

16. Deferl_bj78

16.1 Purpose

The aim of this case is to test the modelisation of depth-induced breaking. The results are compared to laboratory data [3]

16.2 Description of the problem

Our test case corresponds to the “run 15” in Battles and Janssen [3]. It is a rectilinear beach with a bar. The bathymetry of that beach varies as shown on Figure 16.1. The Battle and Janssen’s breaking model is used:

$F_1 = \int_{\theta=0}^{2\pi} F_0(\theta) d\theta$ where $F_0(\theta)$ is the first moment of the action density spectrum over frequency.

$$\frac{dF_1}{dt} = -\alpha_1 Q_b \omega_1 \frac{H_m^2}{8\pi}$$

wherein H_m denotes the maximum wave height. Q_b , the fraction of breaking waves or breaking rate and α_1 a numerical constant of order of 1.

H_m is given by a relationship that is derived from de Miche’s criterion:

$$H_m = \frac{\gamma_1}{k_1} \tanh \left(\frac{\gamma_2 k_1 d}{\gamma_1} \right)$$

wherein k_1 is related to ω_1 by the dispersion relationship.

Q_b is assessed, according to the Battjes and Janssen’s theory as the solution of the implicit equation:

$$\frac{1 - Q_b}{\ln Q_b} = -\frac{8F_1}{H_m^2}$$

The “directionnal” version of that source term is based on the assumption that the breaking does not change the directionnal distribution of energy. The source term writes:

$$Q_{br}(f, \theta) = -\frac{\alpha Q_b f_c H_m^2}{4} \frac{F(f, \theta)}{m_0}$$

The values of numerical constants α_1 , γ_1 et γ_2 as prescribed by Battjes and Janssen are 1, 0.88 and 0.8 respectively. These values, however can and must be matched as a function of the camber of incident waves and bottom slope. To that purpose the following keyword are provided: *DEPTH-INDUCED BREAKING 1 (BJ) COEFFICIENT ALPHA* for α_1 , *DEPTH-INDUCED BREAKING 1 (BJ) COEFFICIENT GAMMA1* for γ_1 and *DEPTH-INDUCED BREAKING 1 (BJ) COEFFICIENT GAMMA2* for γ_2 .

16.3 Physical parameters

The Battjes and Janssen's experiments were conducted in a channel and in signle-direction wave conditions. We have then taken a little directionnal spread($s=32$) in order to set up similar condition.

16.4 Geometry and Mesh

The domain is a 25 m by 12 m rectangle. The depth is constant over y and varrying with x as shown on Figure 16.1 i.e. its value is -0.616 m for x greater than 19 m varies from -0.616 m to -0.121 m for x between 19.02 m and 9.02 m, from -0.121 m to -0.23 m for x between 9.02 m and 4.62 m, from -0.23 m to -0.05 m between 4.62 m and 1 m and -0.05 m after.

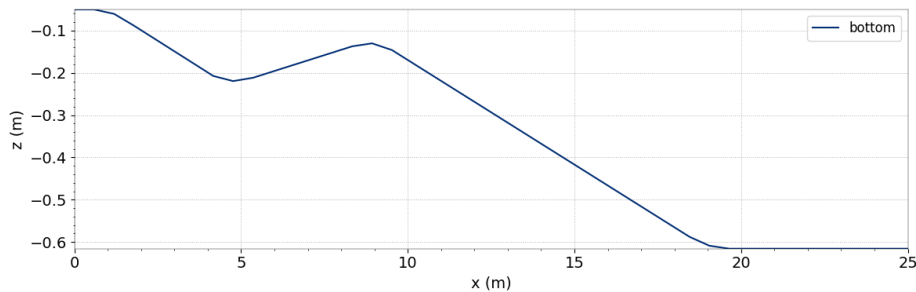


Figure 16.1: Section depth.

The mesh is free, it is made of 648 triangles and 373 points. The boundary has 96 points.

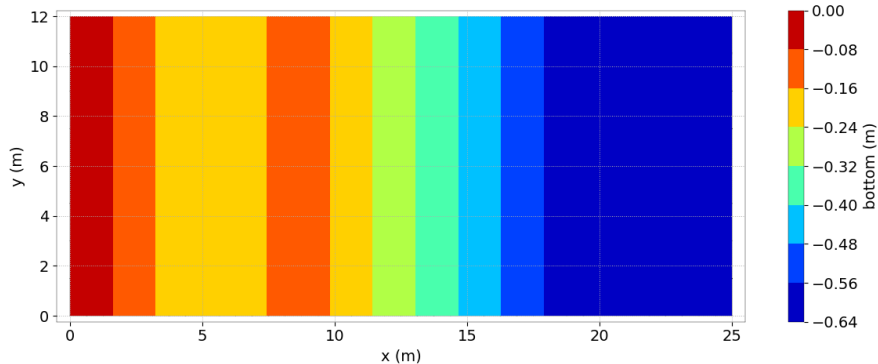


Figure 16.2: Mesh of the domain.

16.4.1 Initial and Boundary Conditions

The initial spectrum is null.

As for the boundary conditions, a Pierson-Moskowitz-typed spectrum is prescribed at the west of the domain with a boundary peak frequency of 0.53Hz, a significative heighth of 0.202 m and a boundary peak factor of 3.3. The boundary principal direction is 270.

16.5 Numerical parameters

The time duration is 35 s with a time step of 0.35 s, the spectro-angular mesh has 24 angles and 25 frequences spread on a geometric progression common ratio 1.1 with a minimum of 0.168874

16.6 Results

Figure 16.3 displays the significant wave heights as computed by TOMAWAC. One can see that TOMAWAC results are quite similar to the laboratory data.

The effect of wave breaking on the mean frequency is not taken into account in this case of TOMAWAC. As we suppose that energy dissipation does not affect the spectro-angular energy spread. The energy transfers of the pre-breaking are not taken into account.

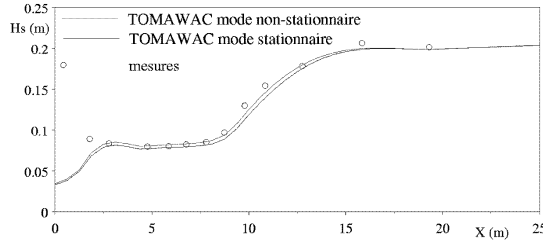


Figure 16.3: Comparison of the significative wave heights.

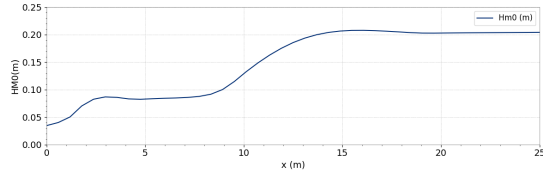


Figure 16.4: Actual wave height.

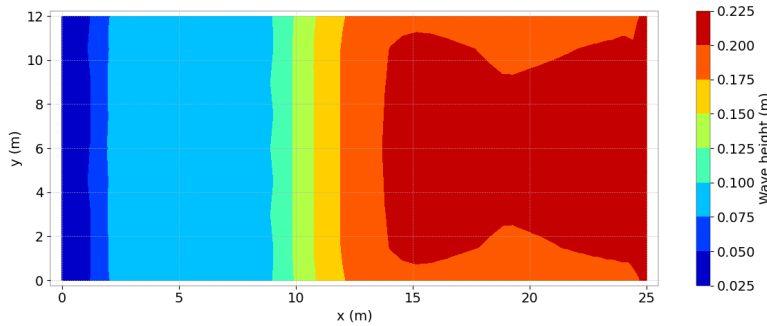


Figure 16.5: Significative wave heights for Battjes and Janssen Model.

16.6.1 Conclusion

The breaking induced dissipation of energy is properly represented in TOMAWAC. The effect on the mean frequency can be neglected.

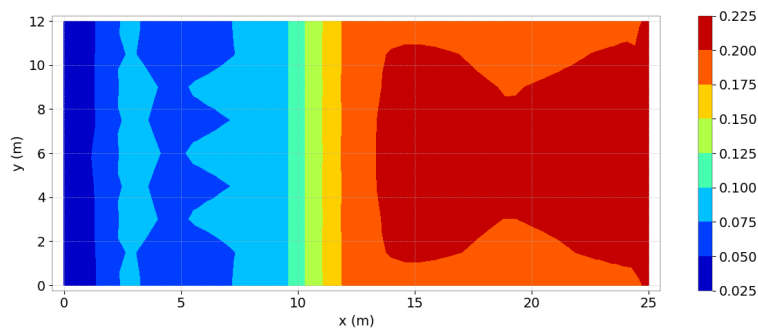


Figure 16.6: Significative wave heigths for Roelvink's model.

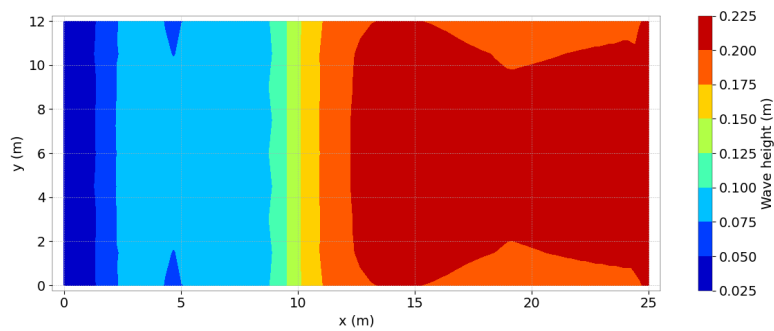


Figure 16.7: Significative wave heigths for Izumiya and Horikawa's turbulence model.

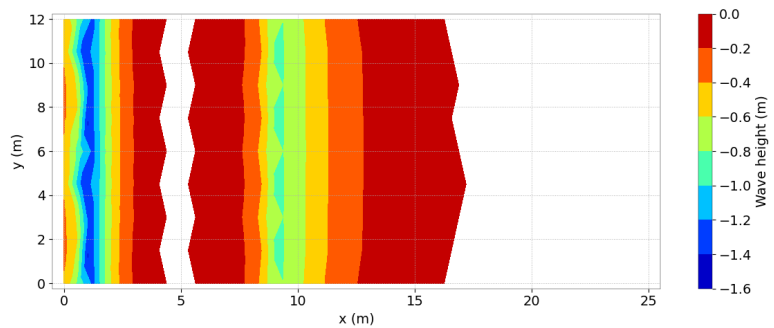


Figure 16.8: Breaking wave ration for Izumiya and Horikawa's turbulence model.

17. Fetch Limited

17.1 Purpose

The goal of this test-case is to validate the generation (Source/sink terms) and the growth of the wave spectrum depending of the length of wind action (fetch) with a constant wind defined at 10 meters from the sea surface. The domain used is simple and we want to observe the evolution of few parameters along its length, as the significant wave height, peak period and variance spectrum. It is supposed that the wind blew long enough to have reached a steady state.

Thus, this benchmark will allow us to compare and validate the different models of wind generation (three models), whitecapping dissipation (two models), non-linear quadruplet interactions (three models but only two are used here). Friction bottom dissipation and eventually depth-induced breaking dissipation (four models) is also included when a finite depth is imposed. The models used are presented in the Table 17.1.

Table 17.1: Different models used for this test-case. In all cases, linear wave growth term from the formula of Cavalieri and Malanotte-Rizzoli (1981) is used.*: *Discrete Interaction Approximation,Hasselmann et al., 1985.* **: *Gaussian Quadrature Method,introduced by Lavrenov [25] and implemented by Benoit and Gagnaire-Renou [14].*

Models	Wind generation model	White capping model	Quadruplet transfers formula	Depth	Bottom friction coeff.	Depth-induced breaking dissipation model
test 1	Janssen [20, 21]	Komen [23] & Janssen [21]	DIA*	inf	–	–
test 2	Snyder [30]	Komen [23] & Janssen [21]	DIA*	inf	–	–
test 3	Snyder [30]	Westhuyzen [13]	DIA*	inf	–	–
test 4	Yan [38]	Westhuyzen [13]	DIA*	inf	–	–
test 5	Snyder [30]	Westhuyzen [13]	Exact GQM** coarse discretization	inf	–	–
test 6	Janssen [20, 21]	Komen [23] & Janssen [21]	Exact GQM** coarse discretization	inf	–	–
test 6b	Janssen [20, 21]	Komen [23] & Janssen [21]	Exact GQM** medium discretization	inf	–	–
test 7a	Snyder [30]	Westhuyzen [13]	DIA*	180	0.038	–
test 7b	Snyder [30]	Westhuyzen [13]	DIA*	60	0.038	–
test 7c	Snyder [30]	Westhuyzen [13]	DIA*	30	0.038	–
test 7d	Snyder [30]	Westhuyzen [13]	DIA*	15	0.038	–
test 7e	Snyder [30]	Westhuyzen [13]	DIA*	5	0.038	Battjes & Janssen (V = 20m/s)

17.2 Reference experiments

In order to validate TOMAWAC results, they will be compared to different empirical formulas:

- Infinite depth:

JONSWAP [16]

CERC (1977) [9]

Wilson and Goda [37]

Kahma and Calkoen [22]

- Finite depth:

CERC (1984)[10]

17.3 Geometry of the domain and bathymetry

Domain dimension: 1000 km * 500 km

	test 7a	180 m
Depth constant along the domain:	test 7b	60 m
	test 7c	30 m
	test 7d	15 m
	test 7e	5 m
	or infinite	

17.3.1 Mesh

Several meshes have been tested. The important point highlighted by the analysis is that at the beginning of the fetch the mesh must be sufficiently fine. At the end, the "free" mesh has been kept because it is the most used in industry and maritime applications (can be adapted to coast).

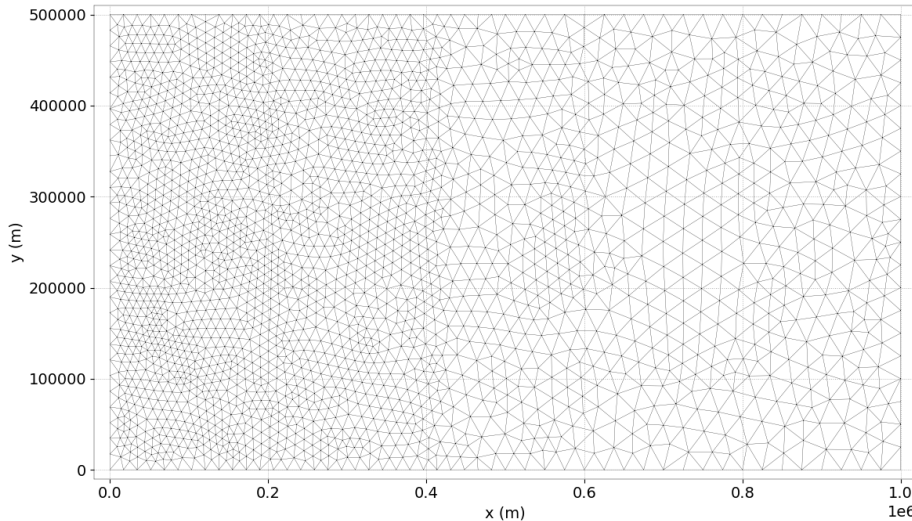


Figure 17.1: Free and refined mesh $\Delta x_{big} \approx 25000m$ - $\Delta x_{med} \approx 20000m$ - $\Delta x_{small} \approx 10000m$.

17.3.2 Spectro-angular discretization

- 50 frequencies ($f_1 = 0.04$ Hz for $U_{10} = 20$ m/s, $f_1 = 0.08$ Hz for $U_{10} = 10$ m/s with geometric spacing $q = 1.05$)
- 36 directions uniformly distributed

17.4 Initial and Boundary conditions

Jonswap spectrum has been set as initial condition.

The domain is a part of a sea. A constant and homogeneous wind blows perpendicular to a long and straight coastline. The boundary conditions are shown in Figure 17.2:

17.4.1 Numerical parameters

- time step: 900 s
- physical time reached: 48 h
- characterization of the computer:

Core: Linux 2.6.32-5-amdb64

Processors: Intel(R) xeon(R) CPU E5620 @ 2.4Ghz

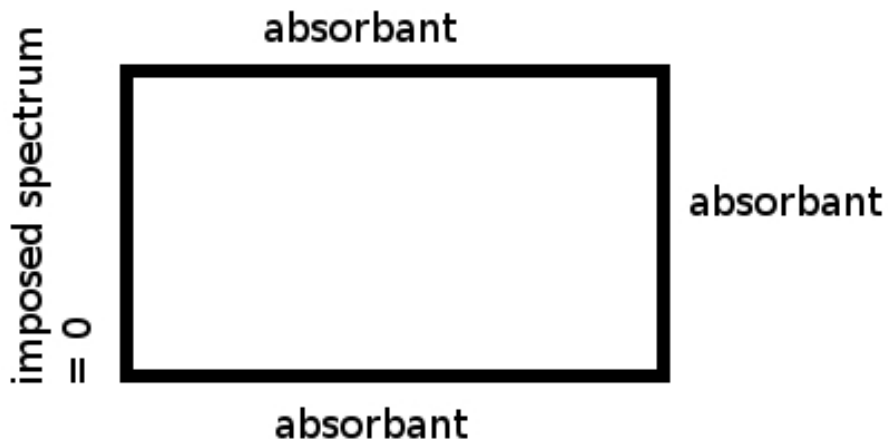


Figure 17.2: Boundary conditions.

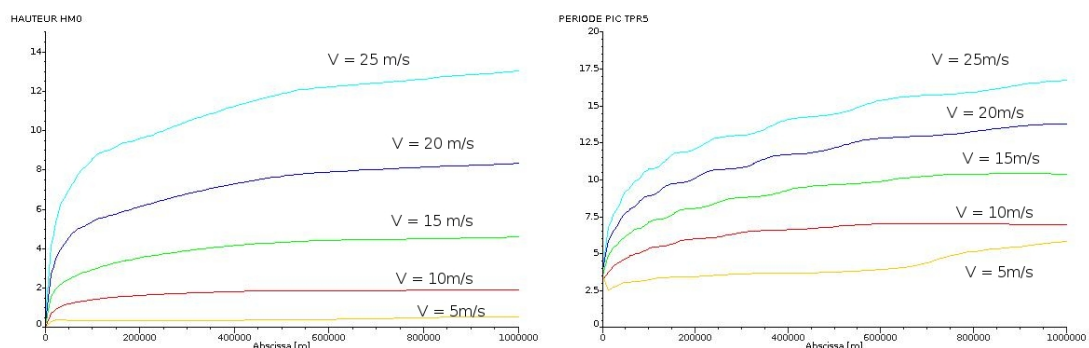
- CPU times:

	tests 1/2/3/4	test 5/6	tests 6b	tests 7
CPU times	3 min	3h25	5h40	25 s

17.5 Results - infinite depth

17.5.1 Wave growth depending on the fetch for different wind velocities.

Figure 17.3 shows the significant wave heights and the peak periods of waves along the fetch (along the axis $y = 250 m$) for the test 1 (the others are not shown because they give the same conclusions). These curves are obtained after 48 hour of wind action for a wind of 5 to 25 m/s. It is clearly seen that the wind has a considerable impact on these values and bigger waves are obtained with stronger wind. Also, stronger is the wind, longer is the fetch needed to reach the steady state. It can be noticed that the significant wave height does not grow linearly but following the squared wind velocity.

Figure 17.3: Significant wave heights and peak periods for the first test, $U_{10} = 5 - 10 - 15 - 20 - 25 \text{ m/s}$.

17.5.2 Non-dimensionnal variances and peak frequencies.

Here all the tests are compared, but only with a 20 m/s and 10 m/s winds. The values obtained with TOMAWAC V6P2 are compared with the empirical formulas: JONSWAP [16], CERC (1977)[9], Wilson [37], Kahma [22]. The non-dimensional variables are:

- Non-dimensional Fetch: $x* = \frac{gx}{U_{10}^2}$
- Non-dimensional variance: $m_0* = \frac{g^2 m_0}{U_{10}^4}$
- Non-dimensional peak frequency: $f_p* = \frac{U_{10} f_p}{g}$

Where U_{10} is the wind velocity at 10 meters from the sea.

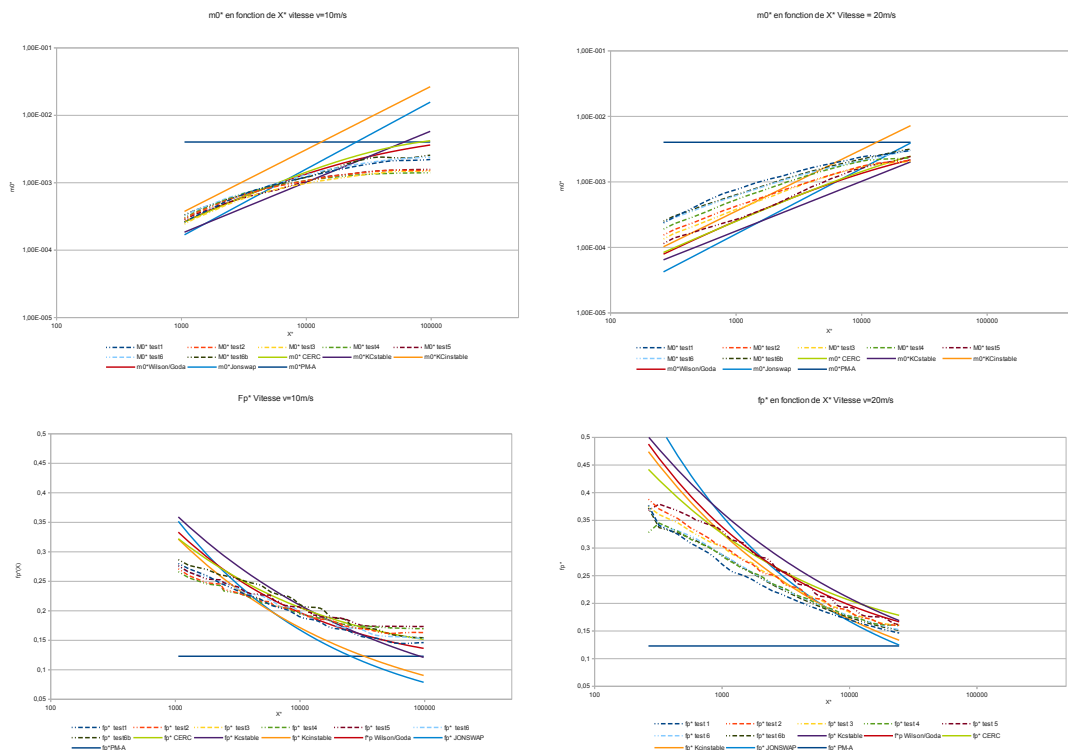


Figure 17.4: Comparison of normalized Variance $M0^*$ and normalized peak frequencies f_p^* for $U_{10} = 10\text{m/s}$ (left) and 20m/s (right), $M0^*$ MP-A and f_p^* PM-A are, respectively, the variance and the peak frequency limits given by the revisited Pierson-Moskowitz formula from Alves [1].

Figure 17.4 shows the different results obtained. Generally, all tests give correct results, and stay close to the CERC, Wilson & Goda and Kahma & Calkoen curves.

The wind impact can be seen by two different behaviours. Indeed, for a 10 m/s wind, the results are really close to the empirical formula at small fetches. As the fetch grows, the differences between the models increase, and the curves began to stray from the empirical formulas. In this case, the models of tests 1, 6 and 6b give the best results. At 20 m/s, a different behaviour is noticed: at small fetch the results are quite different from the empirical curves and it is only when the fetch grows that they match well with the empirical formula. In this case it is the model of test 5 which gives the best results. It can be concluded that there is a range where TOMAWAC results are really correct whatever the models used. For strong winds, an exact

resolution of the quadruplet transfers, Snyder's wind generation model and Westhuyzen white capping model (test 5) give better results at small fetch.

Thus, the analysis of Figure 17.4 shows a good matching between the TOMAWAC wave simulations and the empirical formulas. A comparison was also done with the revisited Pierson-Moskowitz asymptotic limits from Alves and Banner [1] for fully developed wind waves, the U_{10} -scaled asymptotes is added on Figure 17.4. The formula gives:

$$\varepsilon = (4.02 \pm 0.62) * 10^{-3}$$

$$v = (1.23 \pm 0.08) * 10^{-1}$$

It seems that the non-dimensional peak frequency f_p* is a little bit over-estimated and the non-dimensional variance is a bit underestimated. Indeed, the empirical formula given by CERC (1984), which is used as a criterion for fully developed seas, to calculate the minimum fetch during the minimum duration (48h), is $\frac{t_{min}g}{U_{10}} = 68.8 \left(\frac{X_{min}g}{U_{10}^2} \right)^{0.67}$. Applying this formula we found that the fully developed seas are reached around 1117 km for a 10 m/s wind and around 1672km for a 20 m/s wind. Thus, the fully developed sea may not be entirely reached at our last point ($X_{10} = 1000\text{km}$), which may explain the growth of the variance spectrum for some of the tests (see next subsection).

17.5.3 Variance spectrum for a constant wind.

In this subsection, we look at the development of the variance spectrum $E(f)$ along the fetch.

$$E(f) = \int_0^{2\pi} F(f, \theta) d\theta$$

The spectra are worked out for different points of fetch and for two wind speeds (10 m/s and 20 m/s):

Points	fetch
Point 1	25 km
Point 2	50 km
Point 3	100 km
Point 4	150 km
Point 5	200 km
Point 6	300 km
Point 7	400 km
Point 8	800 km
Point 9	750 km
Point 10	1000 km

Dimensional variance spectrum (not shown here) gives correct results with a big growth of the peak value with the wind.

The non-dimensional frequency is defined by: $f_* = \frac{U_{10}*f}{g}$.

and the variance spectra are normalised by the peak value of the Pierson-Moskowitz spectrum, which corresponds to the steady state: $E_{PM}(f_{PM}) = \frac{\alpha g^2}{(2\pi)^4 f_{PM}^5} \exp(-5/4)$ with $f_{PM} = \frac{0.13g}{U_{10}}$ and the Philipp's constant $\alpha = 0.0081$. On Figure 17.5 and 17.6, non-dimensional variance spectra can be observed. We can notice that as the fetch grows, the variance spectrum amplitude grows and the peak frequency declines. Moreover, the variance spectrum tends to the Pierson-Moskowitz spectrum for some cases. The exact quadruplet transfers calculation impact can be seen on the test 5, 6 and 6b, the shape of the curve changes, the spectrum is more peaked and the maximum

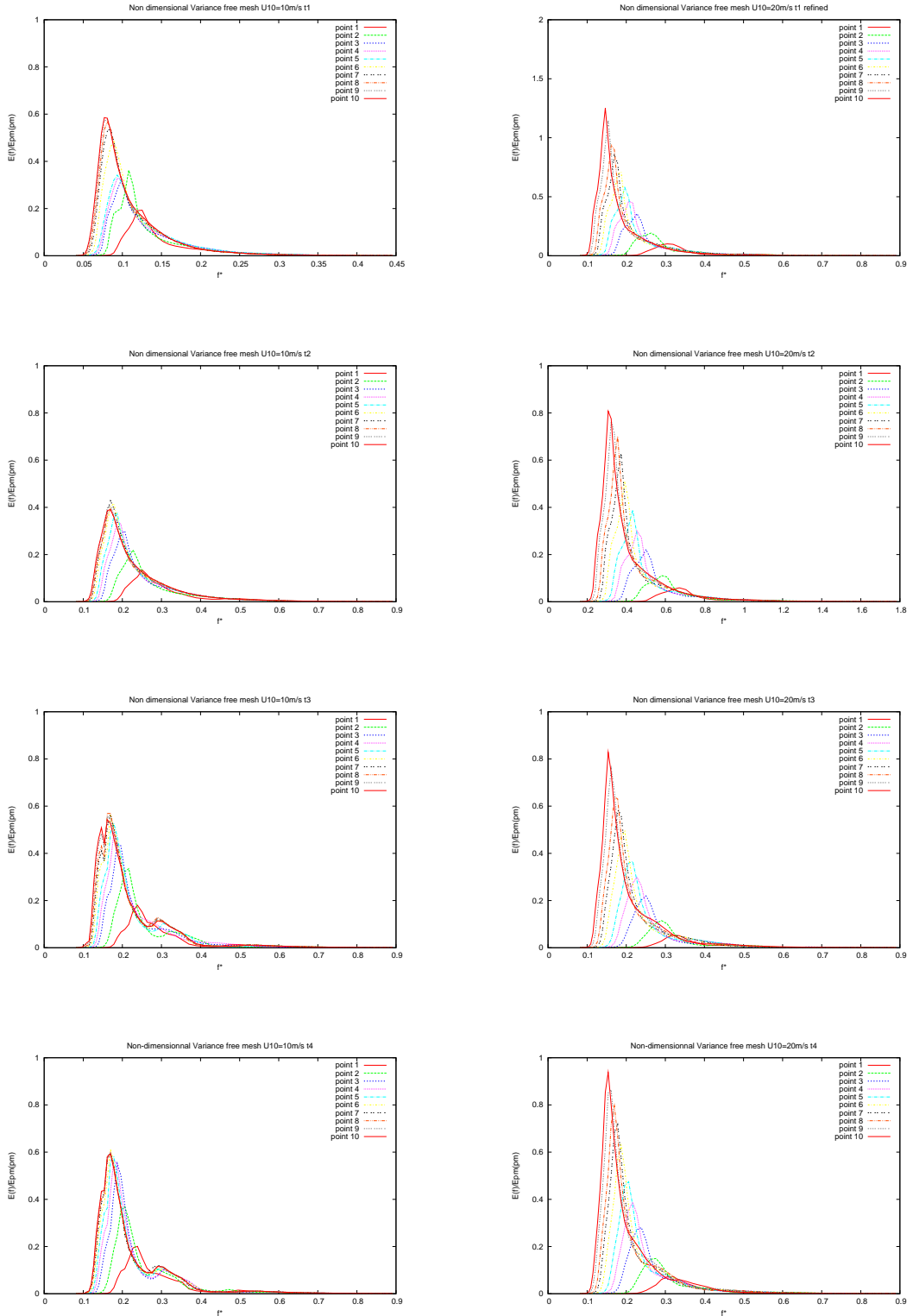


Figure 17.5: Comparison of normalized spectrum variance for part one of the different tests and $U10 = 10\text{m/s}$ (left) and 20m/s (right).

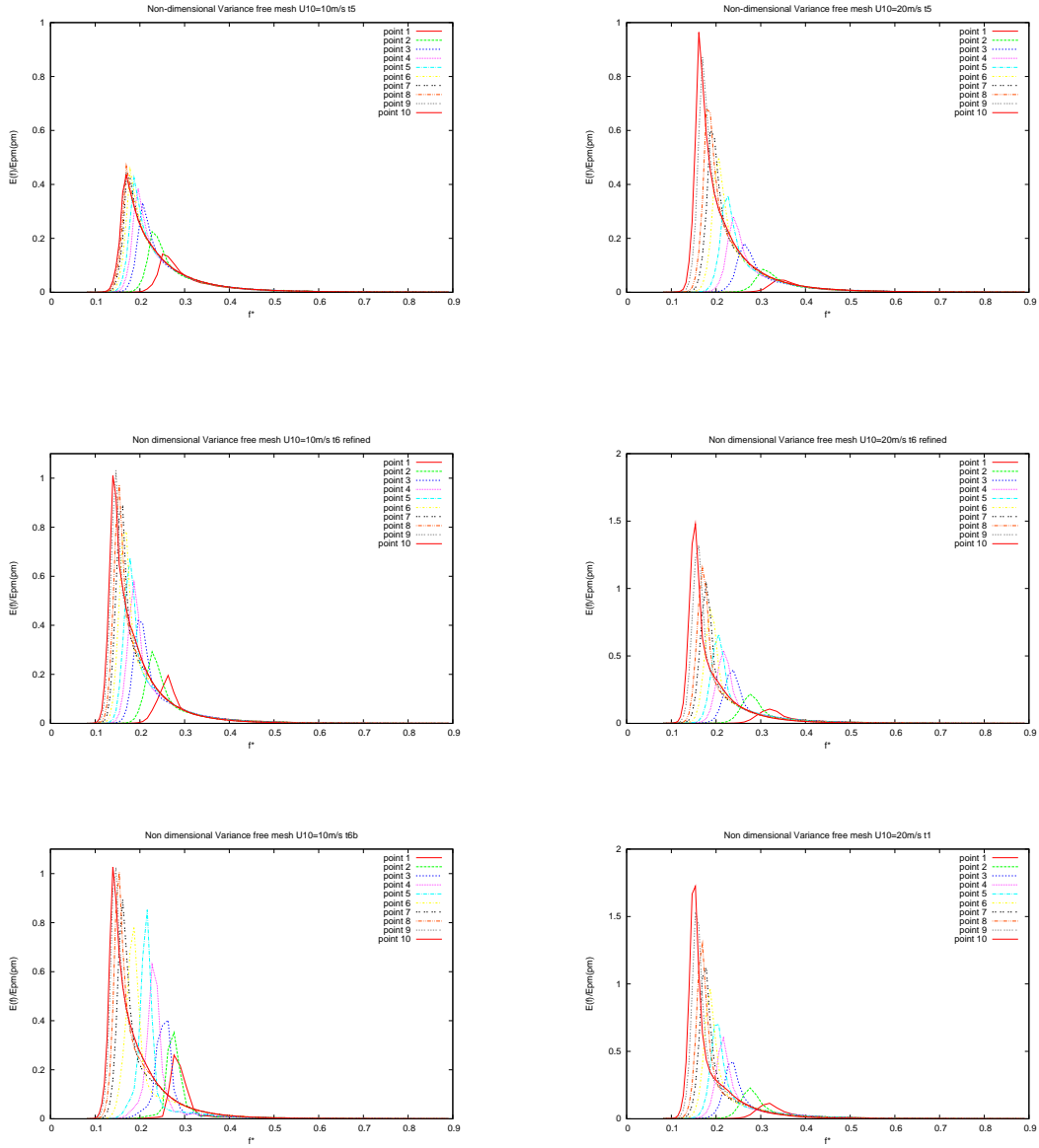


Figure 17.6: Comparaison of normalized spectrum variance for part2 of the different tests and $U10 = 10m/s$ (left) and $20m/s$ (right).

value is higher, and it allows to observe a spectrum peak overstepping the state value predicted by Pierson-Moskowitz formula, it is an overshoot (test 6 for $U10 = 20m/s$ and test 6b).

For $U10 = 10m/s$, the last fetch points (points 7, 8, 9 and 10) get really close spectra. We can conclude that from a certain fetch, the fully developed sea state is reached. Althought, for the case $U10 = 20m/s$, the spectrum continues to grow and the overshoot's presence shows that this balance state is not yet reached. Thus, TOMAWAC gives good results which can be improved with the exact GQM quadruplet transfers model.

17.5.4 Finite depth TOMAWAC results

In this subsection, finite depths are considered: 180 m, 60 m, 30 m, 15 m and 5 m. In regards of Miche's criterion (1994), excepted for a 5 meters depth and $V = 20 m/s$, there is no bathymetric

breaking dissipation. All the tests are done for the same generation (Snyder), white capping (Westhuyzen) and quadruplet transfer (DIA) models. Figure 17.7 shows the evolution of the non-dimensional variance along the fetch for the different tests. In order to compare with the CERC (1984) parametrization, non-dimensional variables are defined as:

- CERC parametrization (1984):

$$X* = \frac{g^2 X}{U_a}$$

$$U_a = 0.71 * U_{10}^{1.23}$$

$$m0* = \frac{g^2 * m0}{U_a^4}$$

It can be noticed that the non-dimensional variance decreases with depth. Indeed, bottom friction effects are more important at small depths. On the contrary, the peak frequency grows when the depth increases because the friction has more impact on small frequency waves, which leads to a growth of the peak frequency.

On Figure 6, we can see that for a 20 m/s wind, TOMAWAC curves are really matching with the CERC (1984) forecasting, particularly for $d = 15 - 30 - 60\text{ m}$. Indeed, it is advised in CERC publication to use their model for a depth between 15 and 90 meters. But the results are still good for $d = 180\text{ m}$ and $d = 5\text{ m}$.

For a 10m/s wind, except for $d = 5\text{ m}$ and $d = 15\text{ m}$, the results are less close to the CERC curves. At small fetches, TOMAWAC results are overvalued, and at large fetches, they are undervalued. In CERC publication (1984), it is advised to use an infinite model for depth over 90m. So the CERC infinite depth model (1977) is added to the graphs and we can see that the results are closer to it for a 10 m/s wind and $d \geq 30\text{m}$. For a 20 m/s wind, at $d = 180\text{m}$ and at large fetches, TOMAWAC results tends to the infinite depth limit. Generally, TOMAWAC gives correct results if you adapt the good model at the application.

17.6 Conclusion

17.6.1 Infinite Depth

This benchmark allows to verify that TOMAWAC results for simultaneous processing of different source terms are correct. A comparison with empirical formulas validates this simulation with generally matching results. The use of the exact GQM quadruplet transfers model allows the visualization of overshoots, but, CPU time are increased, so it is not advisable to use this model for big industrial cases.

17.6.2 Finite depth

Even if a 1000 km fetch with only 5 m depth is hard to study in reality, TOMAWAC results get close to the empirical formula. Bottom friction effect seems to be well represented.

17.6.3 Some Tests

We present Figures 17.10 17.11 and 17.12 some results of other tests. The references for the comparison are made with the version 7.2 of TOMAWAC. Those test cases having non linear terms it can happen that a different compiler gives a different result. Raising the *NUMBER OF ITERATIONS FOR THE SOURCE TERMS* will lower this difference.

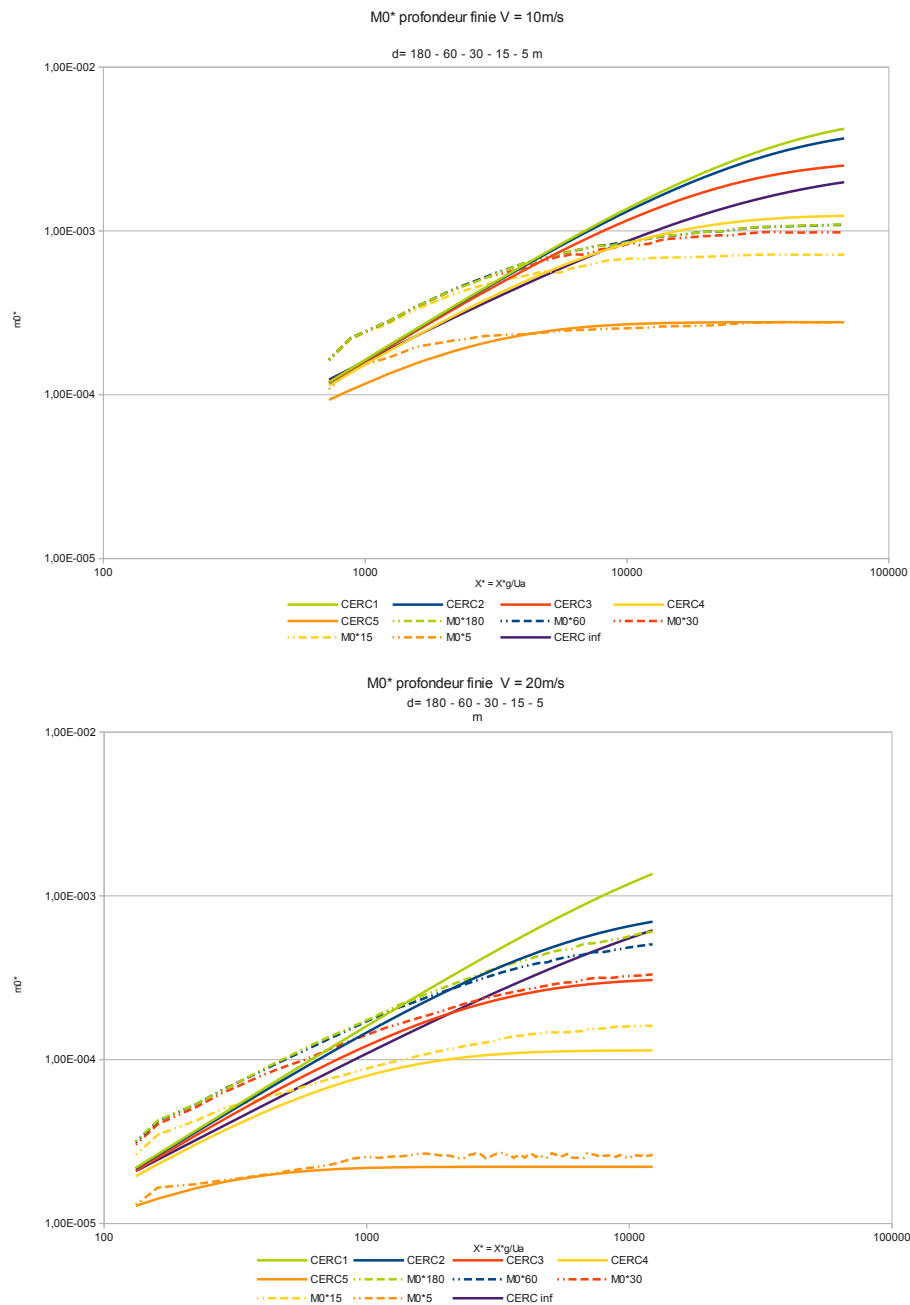


Figure 17.7: Comparaison de la variance normalisée $M0^*$ pour $U_{10} = 10\text{m/s}$ (haut) et 20m/s (bas) pour différentes profondeurs: 5, 15, 30, 60, 180 m.

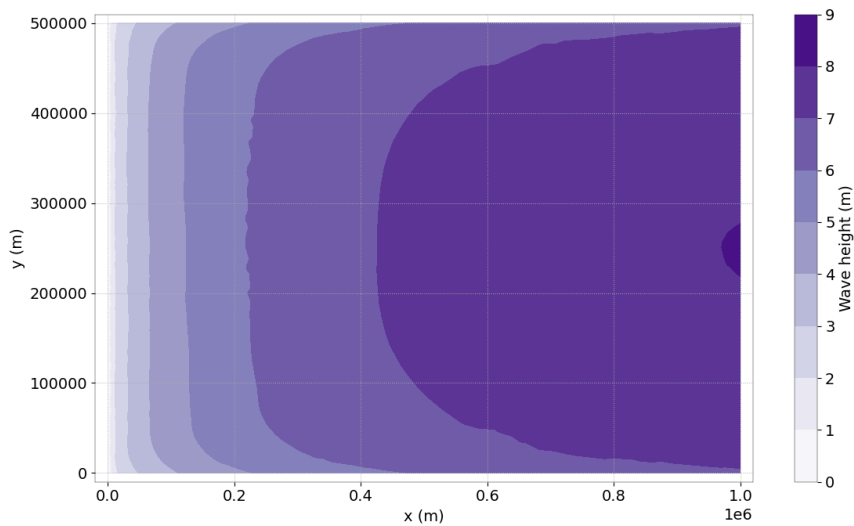


Figure 17.8: Wave height for infinite depth.

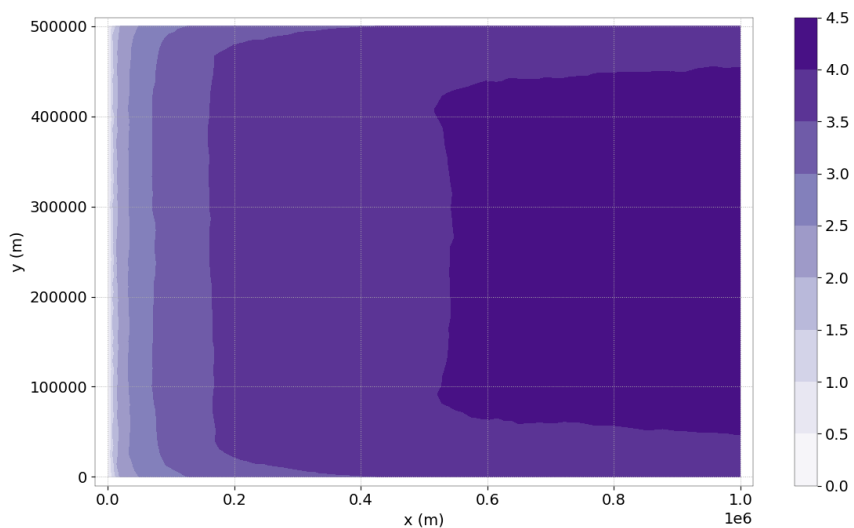


Figure 17.9: Wave height for finite depth.

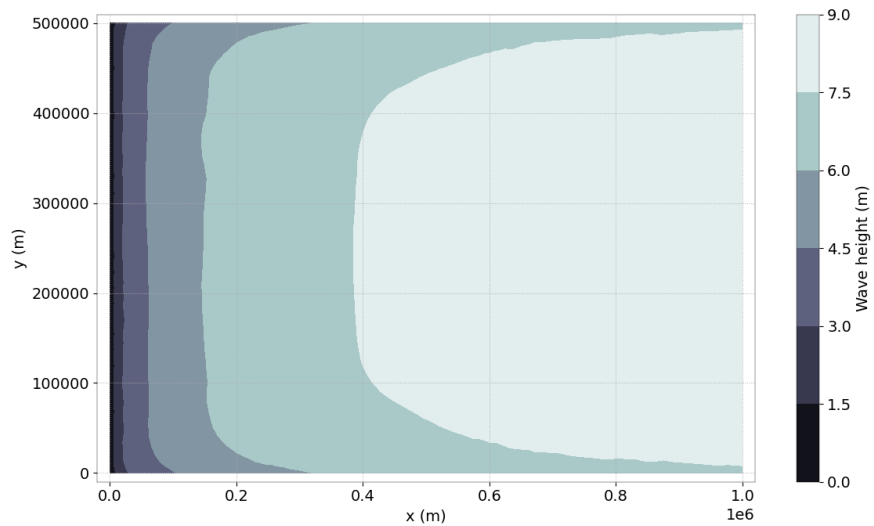


Figure 17.10: Wave heighth for test4.

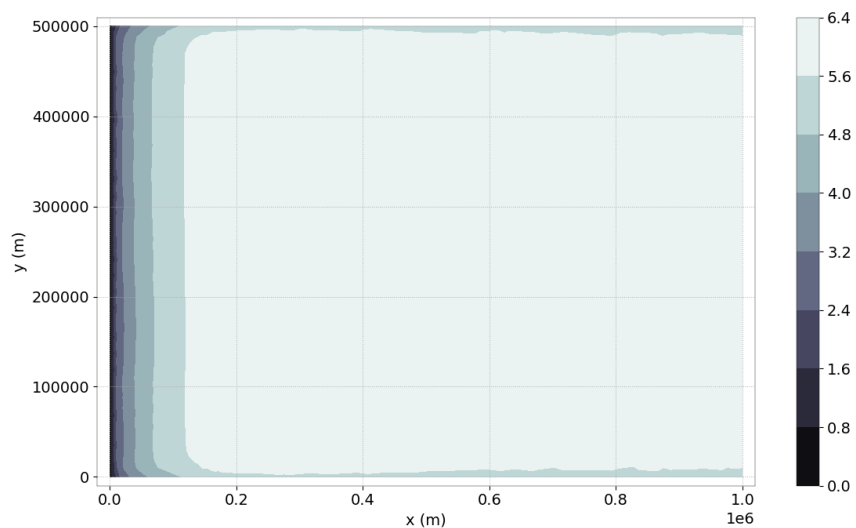


Figure 17.11: Wave heighth for test6.

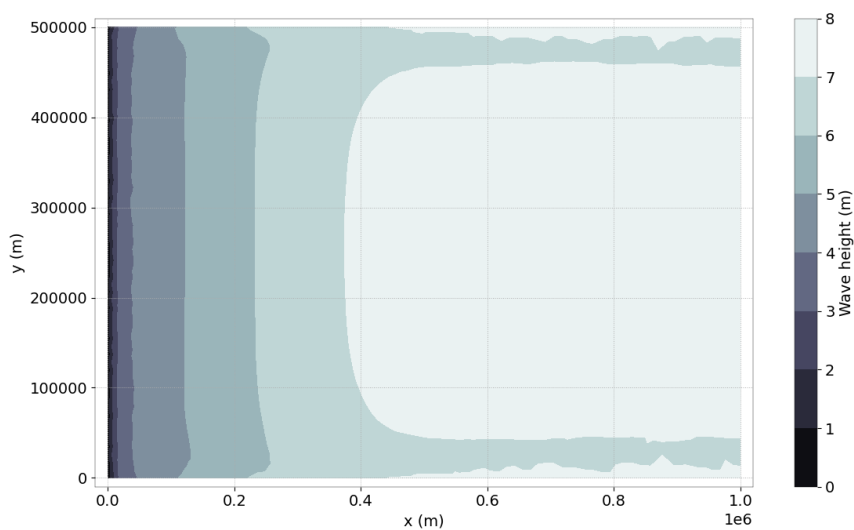


Figure 17.12: Wave height for test6b.

18. Impose spectra

18.1 Description of the problem

This example shows how to impose spectra on the boundary of a nested grid in TOMAWAC. To do so, two simulations are done. One on a larger domain, which we will call the oceanic mesh, and another smaller mesh which fits inside the first mesh. This second mesh will be called the Coastal mesh, and as it is often the case, it will be more refined than the Oceanic mesh. The larger mesh will be used to force the smaller mesh. The only requirement to do this, is that all the points on the open boundary of the smaller mesh need to be present in the larger mesh. This is illustrated in Figure 18.1.

The geometrical parameters of the meshes can be found in Table 18.1.

Table 18.1: Geometrical parameters for the meshes used in this test case.

	Oceanic Mesh	Coastal Mesh
Number of elements	3676	4596
Number of nodes	1899	2460
Maximum edge length (m)	10.0	10.9
Minimum edge length (m)	4.73	0.803

The energy spectrum will be decomposed in 36 directions and 32 frequencies. The minimal frequency is equal to 0.04 Hz and the frequential ratio is 1.055. The initial water depth is 5 m. The modelling time step is equal to 1 s, and the simulation will run for 100 time steps (which is enough to reach a steady state. 3 subiterations will be used to compute the source terms.

Since this is a non-regression test, several modelling options could have been chosen, and the choices made will now be listed for reproducibility. To generate the waves a uniform wind will blow over the whole domain. Its velocity is equal to $(20, 0)$ m/s. The WIND GENERATION is in accordance with WAM cycle 3 [30]. WHITE CAPPING DISSIPATION is in accordance with Van des Westhuysen (2007) [13]. BOTTOM FRICTION DISSIPATION is in accordance with WAM cycle 4 [6, 16]. DEPTH-INDUCED BREAKING DISSIPATION is in accordance with Thornton et Guza (1983) [32]. NON-LINEAR TRANSFERS BETWEEN FREQUENCIES follows WAM cycle 4 (DIA Method) [17]. The LINEAR WAVE GROWTH follows Cavaleri and Malanotte-Rizzoli (1981) [8, 34].

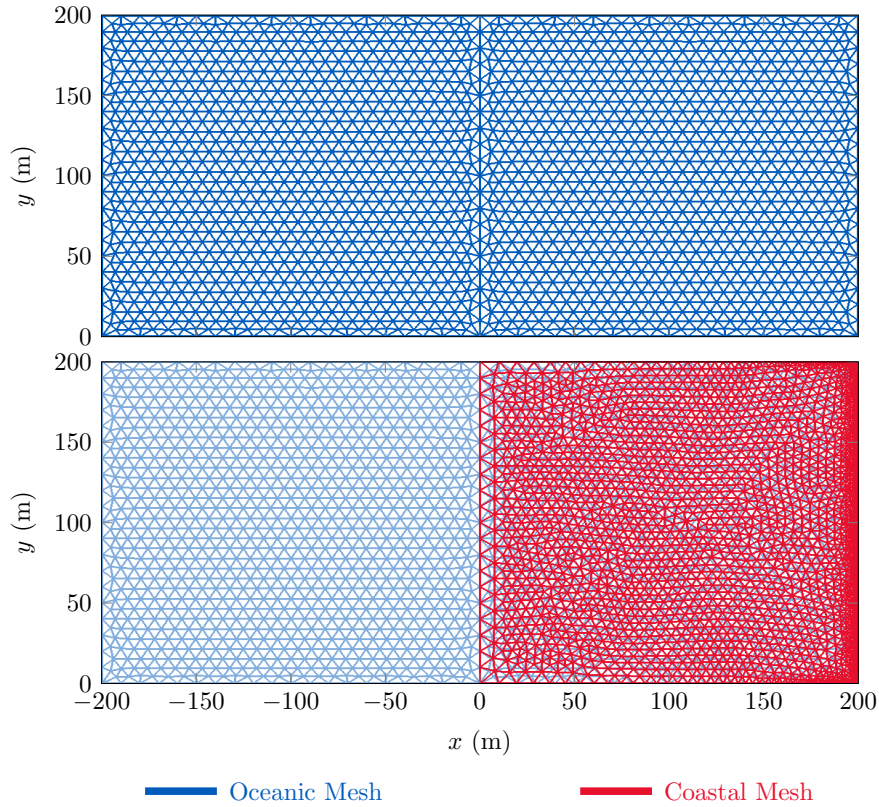


Figure 18.1: Illustration of the meshes of the test case. The mesh in **blue** is the large Oceanic mesh, and the mesh in **red** is the smaller nested Coastal mesh.

18.2 Numerical parameters

To force the Coastal simulation with the Oceanic results, the spectra of the points in the Oceanic mesh that are on the open boundary of the Coastal mesh need to be outputted. This is done most easily using an external text file containing a list of the coordinates of the points to output. In the steering file of the Coastal mesh this is given using the following keyword:

```
/-----/
/ WRITING SPECTRA
/-----/
PUNCTUAL RESULTS FILE = './OceanicResults.spe'
FILE WITH COORDINATES OF SPECTRA TO WRITE =
'./SpectraOutputOceanic.dat'
```

On the Coastal mesh, these spectra are then imposed on the open boundary. To do so, the points along the open boundary need to have the boundary condition 5 4 4 4. The imposed spectra file, and the coordinates of each spectra are given using the following keywords:

```
/-----/
/ IMPOSE SPECTRA ON THE OPEN BOUNDARY
/-----/
IMPOSED SPECTRA FILE = './OceanicResults_dt10.spe'
/IMPOSED SPECTRA FILE FORMAT = 'SERAFIN'
FILE WITH COORDINATES OF SPECTRA TO IMPOSE =
'./SpectraOutputOceanic.dat'
/TIME UNIT OF IMPOSED SPECTRA FILE = 1.
/TIME SHIFT OF IMPOSED SPECTRA FILE = 0.
```

18.3 Results

This test case serves mostly to illustrate how to impose spectra from a large mesh on a smaller nested mesh. Therefore, it will only serve as a non-regression test. The first check is to find the differences on the two-dimensional mesh with the reference file, see Table 18.2.

Table 18.2: Summary of the differences with the reference files for the 2D results. The last column is the maximum accepted difference.

Table not found

The spectra on the nodes along the open boundary of the Coastal mesh will also be checked for non-regression. These spectra are checked with the reference file, and between the Oceanic and Coastal results. This last check is to ensure that what is imposed is the same as what is seen in the code. See Table 18.3.

Table 18.3: Summary of the differences with the reference files for the spectra results. Note, the name of the variables are only true for the Oceanic results. The last column is the maximum accepted difference.

Table not found

Nonetheless, even if the spectra along the open boundary of the Coastal mesh is the same as in the Oceanic mesh, there are differences in the domain (due to the nature of the boundary conditions). This is illustrated with the last columns 6 and 7 of Table 18.2. These differences are minimal, as can be seen in Figures 18.2-18.4, where the values along a cross-section taken at $y = 100$ m are plotted.

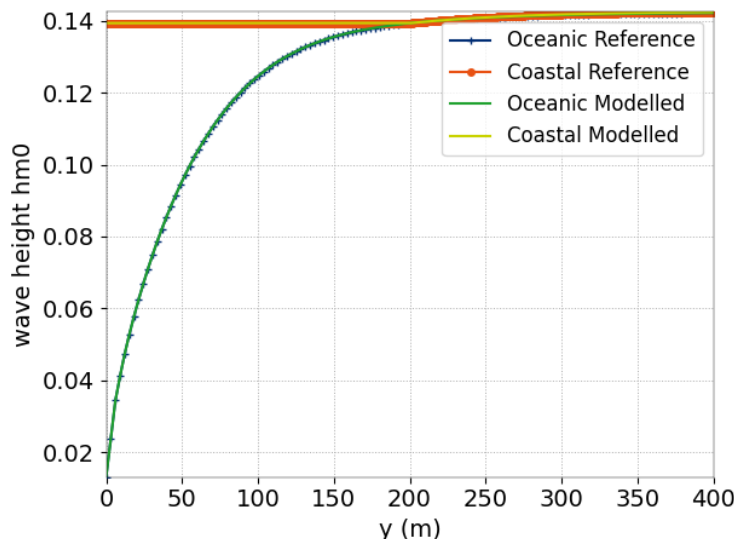


Figure 18.2: Cross-section of the wave height H_{m0} along $y = 100$ m for the Oceanic and Coastal simulations. Note, only the scalar simulations are compared.

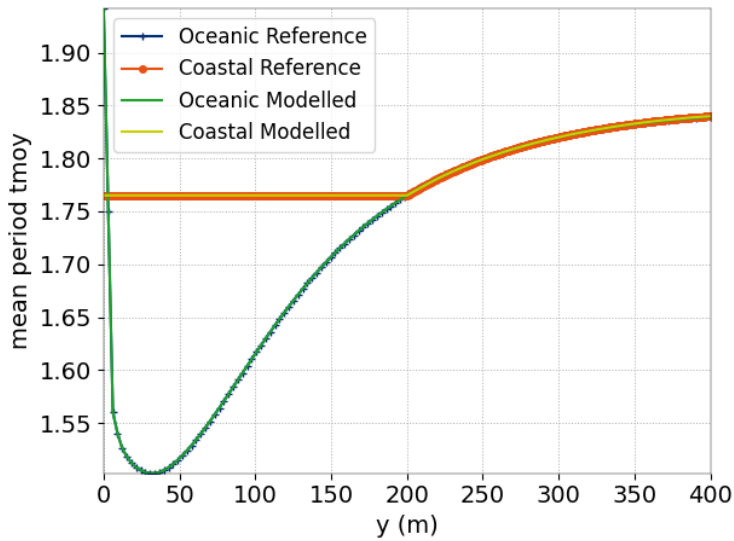


Figure 18.3: Cross-section of the wave period t_{moy} along $y = 100$ m for the Oceanic and Coastal simulations. Note, only the scalar simulations are compared.

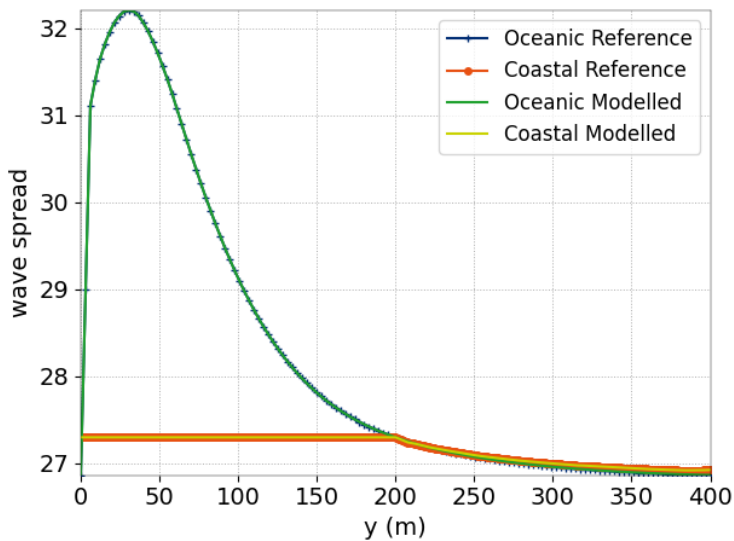


Figure 18.4: Cross-section of the wave spread along $y = 100$ m for the Oceanic and Coastal simulations. Note, only the scalar simulations are compared.

19. Opposing current

19.1 Purpose

The goal of this test-case is to check the behaviour of TOMAWAC in presence of a strong opposing current. When water meets the strong adverse current, with a velocity that approaches the wave group velocity, waves are blocked. Without any option for strong current, the amplitude of waves is overestimated.

19.2 Description of the problem

We present here the simulation of the test case of Lai [24]. We present two different options that prevent from overestimation.

Option 1: consider an equilibrium range spectrum (in the presence of ambient flow) applied as an upper limit for the spectrum Hedges et al ([18])

Option 2: add a dissipative term on the right-hand side of the action balance equation [12]

For more details on formulations, one can refer to TOMAWAC documentation, paragraphs 4.2.3.8.1 and 4.2.3.8.2.

19.3 Reference

The flume experiment of Lai et al [24] investigates the transformation of the wave spectrum on a strong negative current gradient in a flume of 8 m length and 0.75 m depth. An opposing current flow is induced along the flume according to figure 19.1

19.4 Physical parameters

Concerning the modelling of the opposing current with the first option the Phillips's constant in the Pierson-Moskowitz spectrum is equal to 0.0081. For the second option of this modelling, the dissipation coefficient is equal to 0.65, and saturation threshold value is taken to $1.75 \cdot 10^{-3}$. The white-capping dissipation is the model of Westhuyzen 2008. Non linear transfers between frequencies are calculated by the DIA method.

19.5 Geometry and Mesh

The bathymetry is as described on figure 19.2.

The mesh is made of 1701 nodes and 3200 triangles and is shown Figure 19.3.

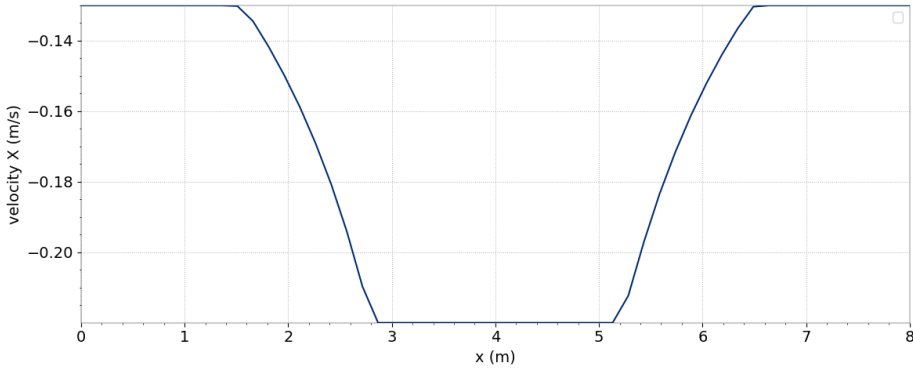


Figure 19.1: Current of the test case.

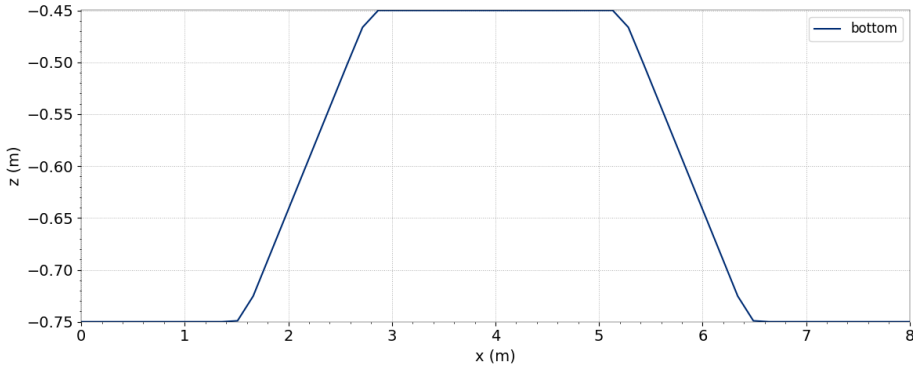


Figure 19.2: Bathymetry of the test case.

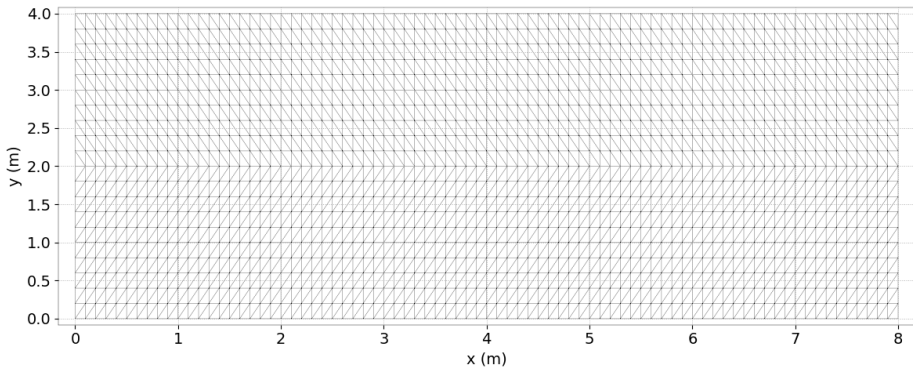


Figure 19.3: Mesh of the domain.

19.6 Initial and Boundary Conditions

For both conditions, we take a Jonswap spectrum with a 1.9 cm significant wave height, a peak frequency of 2.2. The angular distribution function follows a $\cos^{2s} \theta$ distribution with an angular spreading of 65 and a mean direction of 90.

19.7 Numerical parameters

Time duration is 400 s, time step is equal to 0.1 s, the spectro-angular mesh has 72 angles and 36 frequencies spread on a geometric progression common ratio 1.1 with a minimum of 0.25. The option for wave growth limiter is following the Hersbach et Janssen (1999) parameterisation.

19.8 Results

We show the results obtained Figure 19.4. The two options are efficient to reduce the wave height overestimation and lead to a solution closer to measurements. This shows the interest of including these options in the case of a strong opposing current.

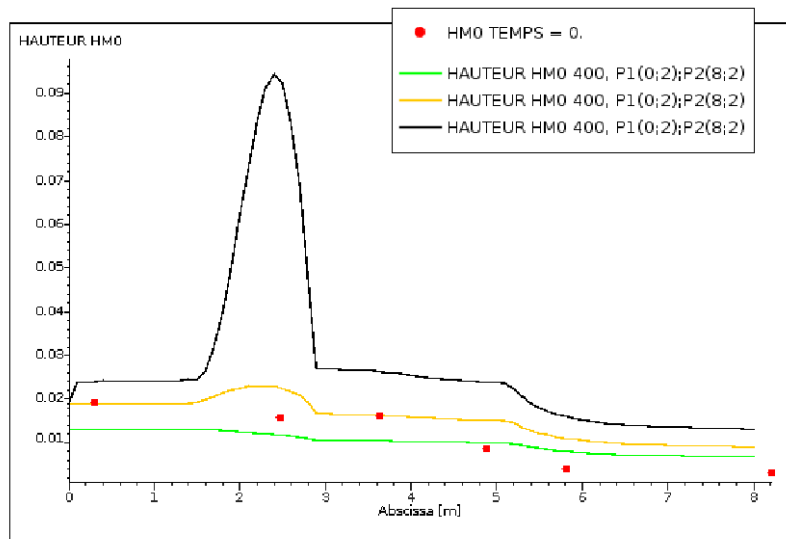


Figure 19.4: Height comparison without wave blocking and with the two options.

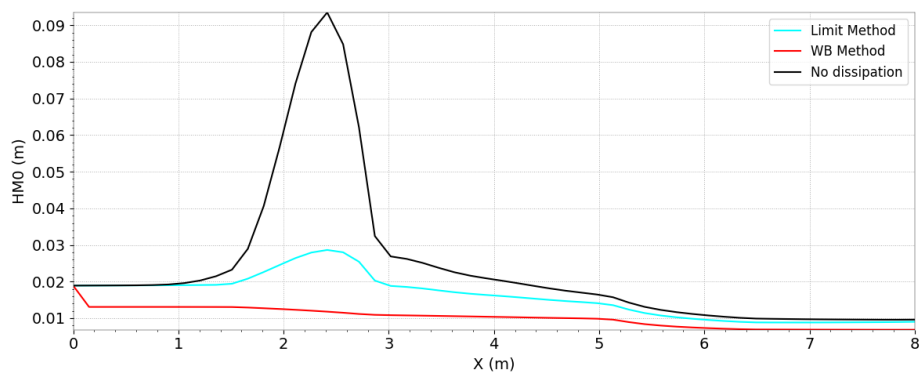


Figure 19.5: Height comparison with the two options for the last validation.

20. Reflection

20.1 Purpose

This test case is an example of reflection effect with TOMAWAC

20.2 Description of the problem

The domain is homogeneous with the upper and the bottom face reflective.

20.3 Geometry and Mesh

The domain is a rectangle of 400 m by 100 m.

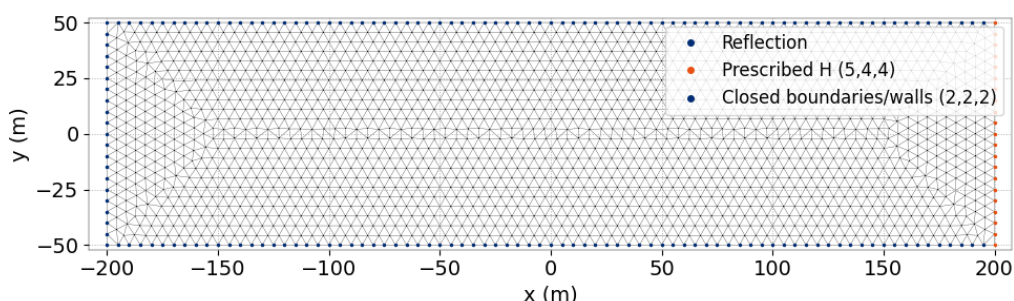


Figure 20.1: Mesh of the domain.

20.4 Initial and Boundary Conditions

The waves are coming from the right boundary with an angle of 300° , a wave height of 0.2 and a peak period of 1.88 s.

20.5 Results

Seeing the result figure 20.2, the reflection seems to work correctly.

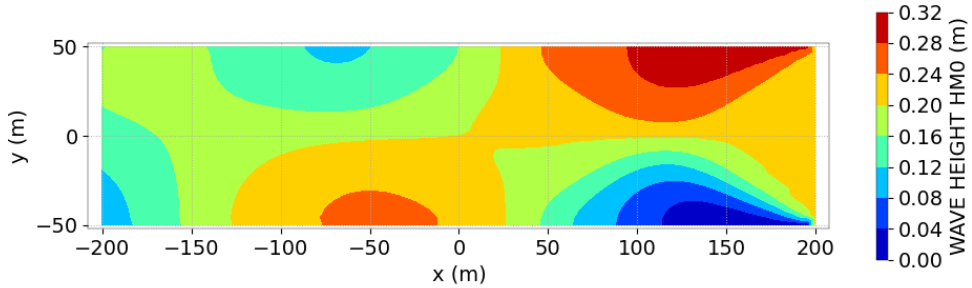


Figure 20.2: Wave height hm0.

20.6 Test of rotated boundary

In order to check that the reflection condition works for any boundary (not parallel with axes like in previous section), we test the same configuration on a rotated geometry of 30° see figure 20.3

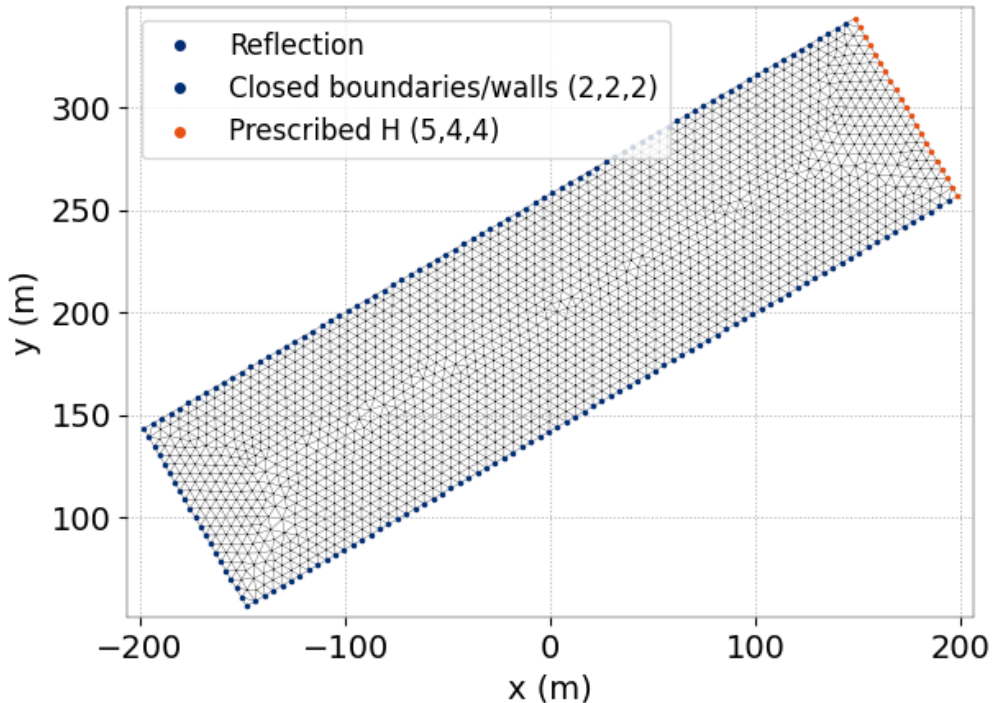


Figure 20.3: Mesh of the domain 2.

We can see on figure 20.4 that the results are simply rotated from those of figure 20.2. Plotting the wave height on point [0,0] of first geometry and [0,0] of second geometry, we can see that it is the same result.

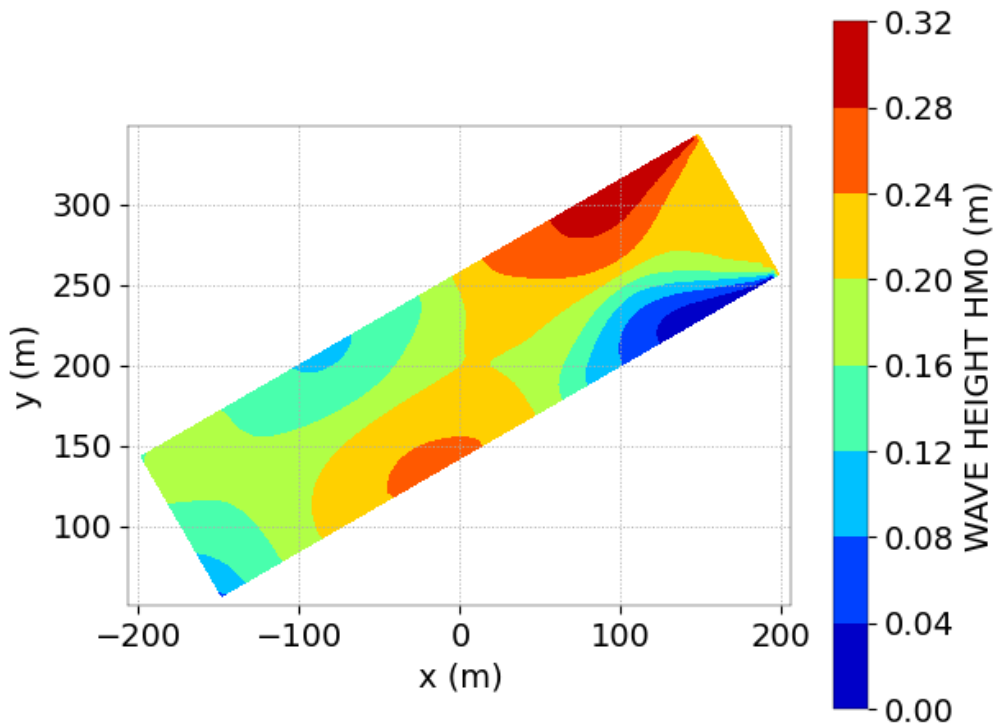


Figure 20.4: Wave height $hm0$.

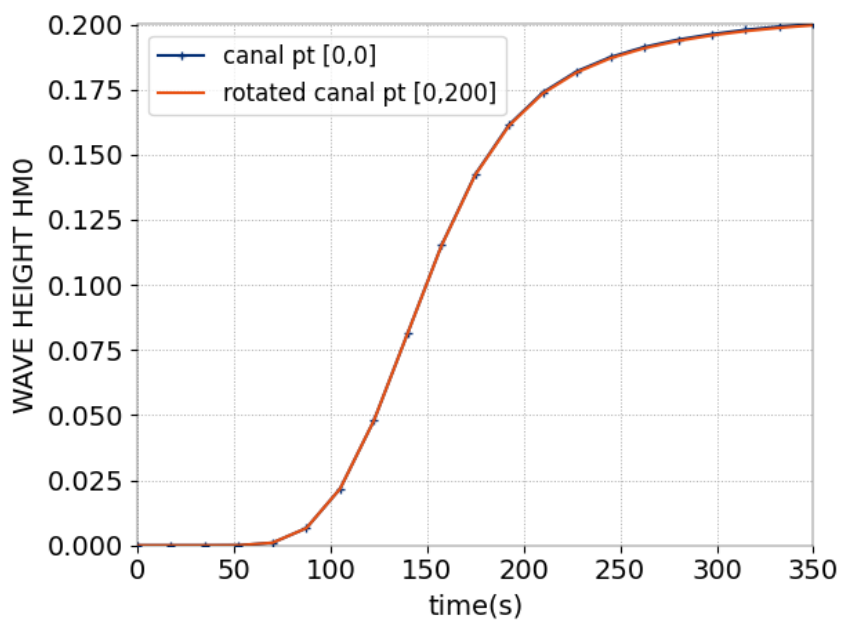


Figure 20.5: Wave height on point $[0,0]$.

21. Shoal: Submerged elliptical mound

21.1 Purpose

The goal of this test-case is to check the behaviour of TOMAWAC in presence of refraction, shoaling and diffraction effects over a shoal.

A shoal causes a concentration area of wave just behind it, what makes fail numerical models of refraction based on the radius theory. This test-case allows to verify simulations from TOMAWAC for refraction, shoaling and diffraction processes.

21.2 Reference experiments

The references of this test-case are the experiments of [35]. They worked on the refraction and the diffraction of irregular waves over a mound using a directional spectral wave generator and they measured the wave's height.

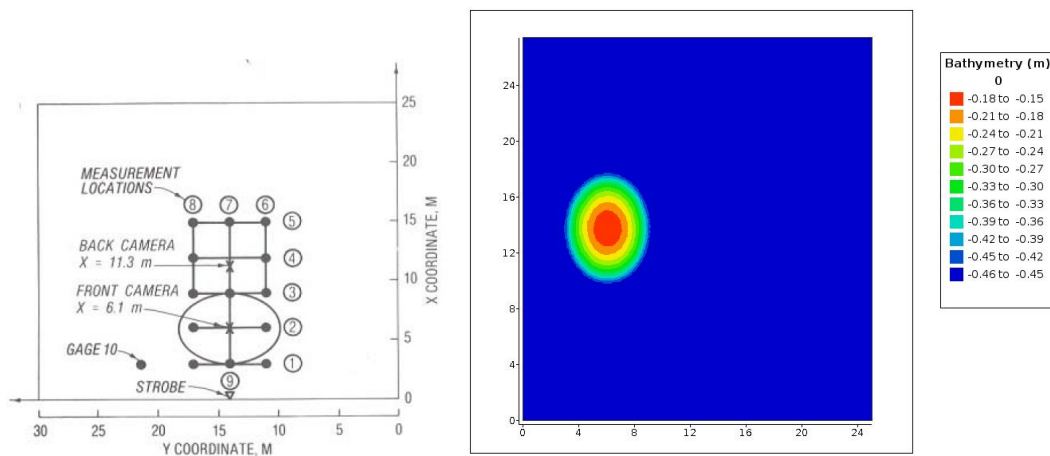


Figure 21.1: Set up of Vincent and Briggs experiments.

Different irregular wave conditions were tested, varying the narrowness and the directional spread of the spectrum. They used a TMA shallow-water spectrum (Bouws et al. 1985) and a wrapped normal spreading function which can be close to a Mitsuyasu directional spreading function.

Table 21.1: Test conditions for shoal test series, Vincent and Briggs experiments.

Test number	Case ID	Type	Period (sec)	Height (cm)	α	γ	σ_m (deg)
(a) Initial Series							
1	M1	Mono	1.30	5.50	—	—	—
2	N1	Spec	1.30	7.75	0.01440	2	10
3	B1	Spec	1.30	7.75	0.01440	2	30
4	N2	Spec	1.30	7.75	0.00440	20	10
5	B2	Spec	1.30	7.75	0.00440	20	30

In this benchmark, only one type of wave condition is tested for the diffraction effects, the N1 one. But B1, B2, N1 and N2 are tested to evaluate the refraction and the shoaling.

21.3 Test-case description

The case is about spectral wave propagation on a submerged elliptical mound. The study will compare the spectral significant wave heights given by TOMAWAC simulations with measurements from [35]'s experiments.

21.3.1 Geometry of the domain and bathymetry

Bassin	dimension:	27.43 m * 18.3 m
	depth constant outside the shoal:	0.4572 m
Elliptical shoal	major radius:	3.96 m
	minor radius:	3.05 m
	maximum height:	0.305 m
	coordinates of the center:	(6.10,13.72)

The elliptical shoal is defined by:

$$a = \left(\frac{x}{3.96} \right) + \left(\frac{y}{3.05} \right) \begin{cases} & \text{if } a \geq 1, Zf = -0.4572 \\ & \text{if } a < 1, Zf = -0.9144 + 0.762\sqrt{1 - 0.64a} \end{cases}$$

21.3.2 Meshes

Spatial discretization

Three meshes are used for the simulation:

- finer: Element size at the shoal 0.2 m $\Delta x/\lambda = 0.09$
- medium: Element size at the shoal 0.4 m $\Delta x/\lambda = 0.18$
- coarser: Element size at the shoal 0.8 m $\Delta x/\lambda = 0.35$

Where λ is the wavelength.

Spectro-angular discretization

- 22 frequencies (0.35 - 2.85 Hz)
- logarithmic scale ($\Delta f/f = 0.1$)
- 36 directions

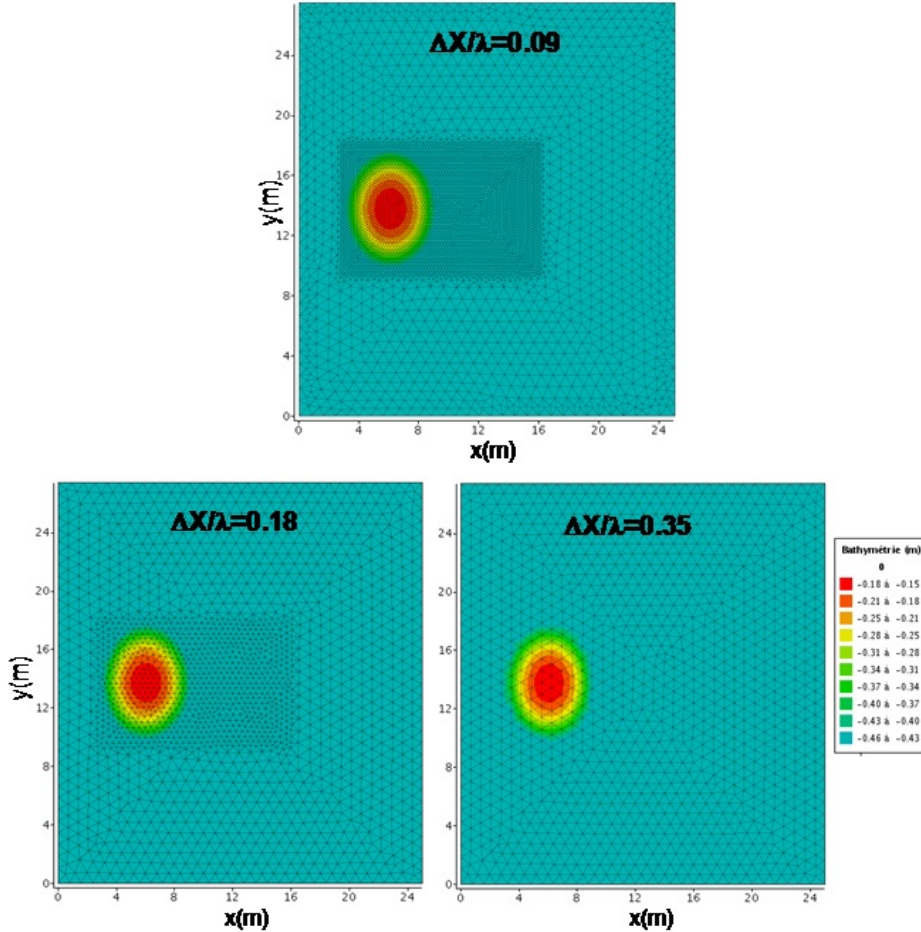


Figure 21.2: The different meshes used.

21.3.3 Initial and Boundary conditions

The domain is initially at rest. The incident wave conditions are the following:

- the incident wave conditions are imposed at the boundary representative of the wave generator. All the others are absorbing boundaries.
- Frequency spectrum: TMA shallow water spectrum

$$S(f, \theta) = E(f) * D(\theta)$$

$$E(f) = \frac{\alpha g^2}{(2\pi)^4} f^{-5} \exp(-1.25(\frac{f_p}{f})^4) * \gamma^{\exp(-0.5(\frac{f-f_p}{\sigma f_p})^2)} * \phi(f, d)$$

- Directional spreading function: gaussian type

$$D(\theta) = \frac{1}{\sqrt{2\pi}\sigma_m} \exp\left[-\frac{(\theta - \theta_m)^2}{2\sigma_m^2}\right]$$

Where:

- α : Phillips constant
- f_p : peak frequency ($f_p = 0.769$ Hz)

- γ : peak factor
- $\sigma = \begin{cases} 0.07 & \text{if } f < f_p \\ 0.09 & \text{if } f > f_p \end{cases}$
- $\phi(f, d)$ is a factor which allows the consideration of depth effects:

$$\phi(f, d) = \begin{cases} 0.5w_p^2 & \text{if } w_d \leq 1 \\ 1 - 0.5(2 - w_d)^2 & \text{if } 1 < w_d < 2 \\ 1 & \text{if } 2 \leq w_d \end{cases}$$
with $w_d = 2\pi f(d/g)^{1/2}$
- θ_m : mean wave direction at frequency f
- σ_m : directional spreading parameter

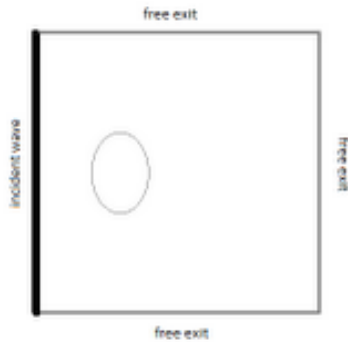


Figure 21.3: The boundary conditions.

21.4 Numerical parameters

- time steps:
 1. $\Delta x/\lambda = 0.09 \rightarrow \Delta t = 0.005$
 2. $\Delta x/\lambda = 0.18 \rightarrow \Delta t = 0.025$
 3. $\Delta x/\lambda = 0.35 \rightarrow \Delta t = 0.1$
- CPU times:
 $\Delta x/\lambda = 0.09 \quad \Delta x/\lambda = 0.18 \quad \Delta x/\lambda = 0.35$

B1	—	1569 s	209 s
B2	—	1387 s	211 s
N2	—	1534 s	239 s
N1	4027 s	1359 s	229 s

21.5 TOMAWAC Results

At first, simulations without diffraction effects are done in order to validate the propagation and refraction of the wave over this complex bathymetry. To compare the simulation results and the measurements of [35], the significant wave heights have been normalized by the incident significant wave height.

- B1 and B2 tests (wide directional spreading):

A good matching can be seen in these tests (see Figure 21.4). After drawing the iso-wave-height compared to the [35]'s measurements, the wave concentration zone is well represented. The amplification factor goes over 1.3 for B1 and 1.4 for B2. As in measurements, this amplification factor is a bit higher for B2 case (higher peak factor) than for B1 case. But simulation factors are a little bit higher than those measured.

Moreover, the computations of normalized wave height along the transect 4 match quite well with the measurements (not shown here).

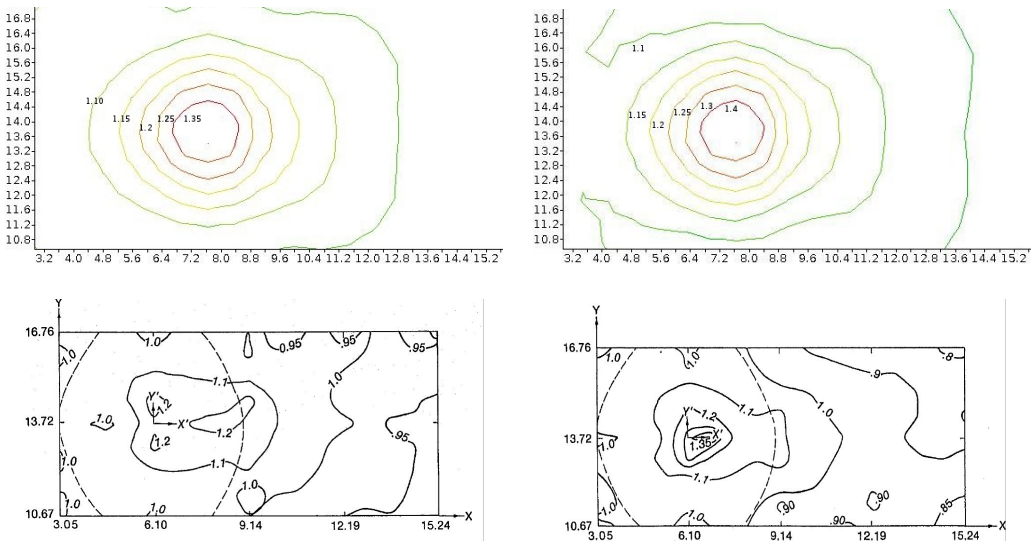


Figure 21.4: Comparison of normalized significant wave height iso-lines for the B1 (left) and B2 (right) tests with the measurements from Vincent and Briggs (coarser mesh).

- N1 and N2 tests (narrow directional spreading):

These tests are not as good as the B ones because only one area of big wave heights is shown while two are highlighted in measurements. Also the amplification factors are bigger than those measured. It can be explained by the lack of representation of the diffraction effects. But again, the results along the transect 4 show a coherence of the simulation and the measurements. (see Figure 21.5 for N2, and Figure 21.7 for N1).

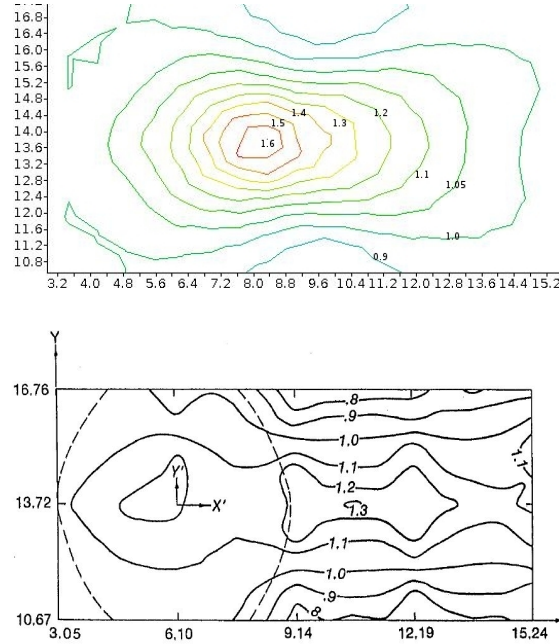


Figure 21.5: Comparaison between normalised iso-line TOMAWAC results and Vincent measurements for the case N2 (coarser mesh).

Subsequently, the computation will include diffraction effects. The diffraction coefficient K_d is defined by the ratio of the spectral significant wave height to the spectral significant incident wave height, $K_d = \frac{H_{m0}}{H_{m0_inc}}$.

Parametrical tests have shown the influence of two non-dimensional parameters: the ratio of the mesh size over the wavelength ($\Delta x/\lambda$) and the current number. The courant number Cr is: $Cr = \frac{C_g(f_p)\Delta t}{\Delta x}$.

where $C_g(f_p)$ is the group velocity associated to the sea-state peak frequency, Δt the simulation time step and Δx the size of the smallest element of the mesh. The diffraction coefficients obtained during the simulations (changing Cr and $\Delta x/\lambda$) are compared with measurements [35] and the iso-Kd curves resulting from TOMAWAC simulations are superposed with the ones measured by Vincent and Briggs. (see Figure 21.8).

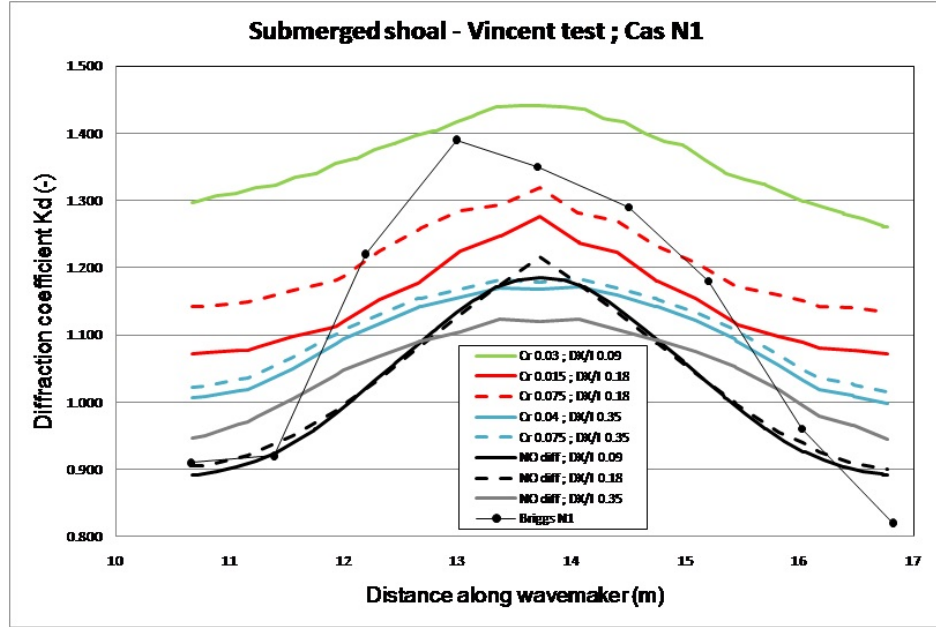


Figure 21.6: Comparison between TOMAWAC results and Vincent measurements: measured and simulated values of the diffraction coefficient along the transect 4 (see Table 21.1) of the model.

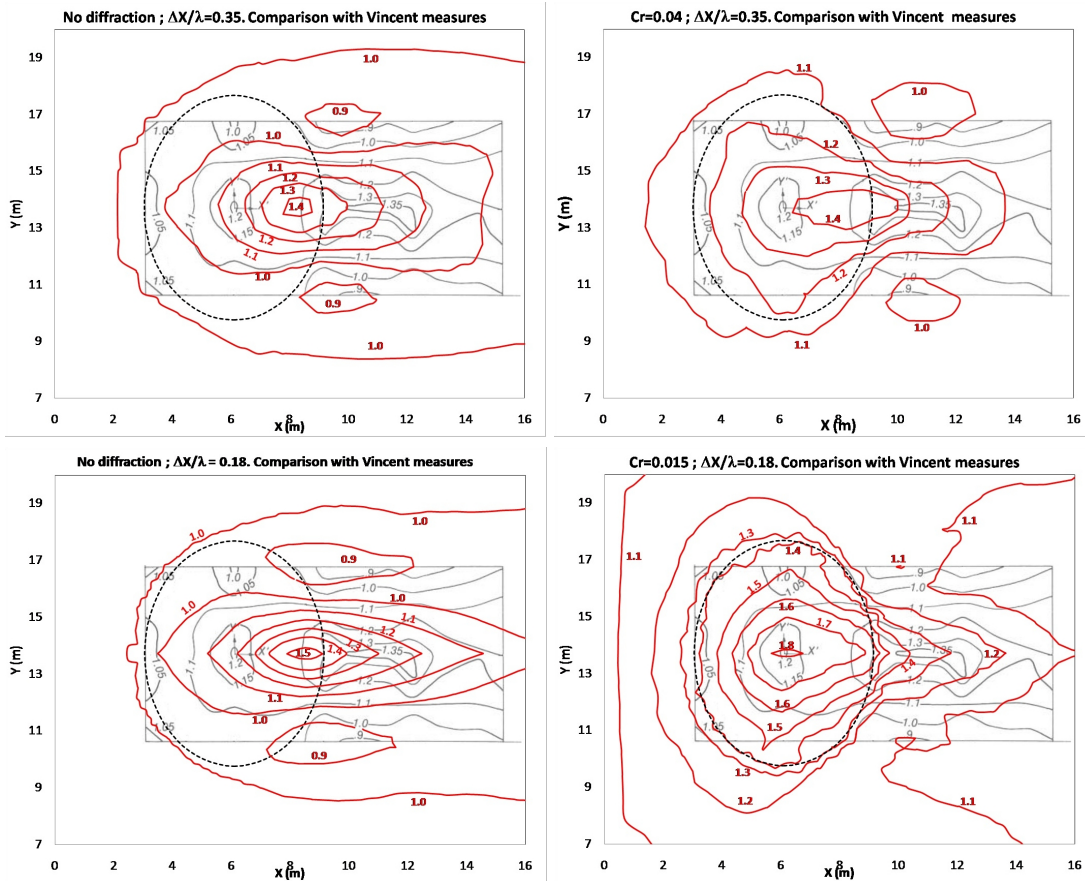


Figure 21.7: Comparison between TOMAWAC results and Vincent measurements: measured and simulated iso-Kd curves over and behind the mound for the case N1.

As one can see in these two graphs (Figures 21.6 & 21.7), the diffraction effects over the shoal are not well simulated by TOMAWAC due to a large build-up of energy. Indeed the larger C_r is and the finer the mesh is, the larger the numerical and the energy build-up are. Moreover with the coarser mesh ($\Delta x/\lambda = 0.35$) TOMAWAC is not able to capture the diffraction effects generated by the submerged shoal. In the Figure 21.7, the simulation's curves are too flattened and the curves that have the shape closest to the measurements are the No diffraction ones. Also in the iso-Kd graph, the curves do not superimpose well when diffraction is taken into account, but for the case with only propagation and refraction the correspondance is correct. Indeed, we can see that the iso-line shapes are closest to the measured ones.

Mainly, the build-up and the numerical noise are generated when a high resolution of the mesh is used and they are due to the meshfree algorithm (used to compute second derivatives during simulation). In order to improve the simulation of the diffraction effects, a spatial filter is built to limit the energy build-up. The effect of this filter can be seen on the diffraction coefficient K_d (see Figure 21.8). The noise and the energy build-up effects are reduced but it does not improve the quality of the results significantly.

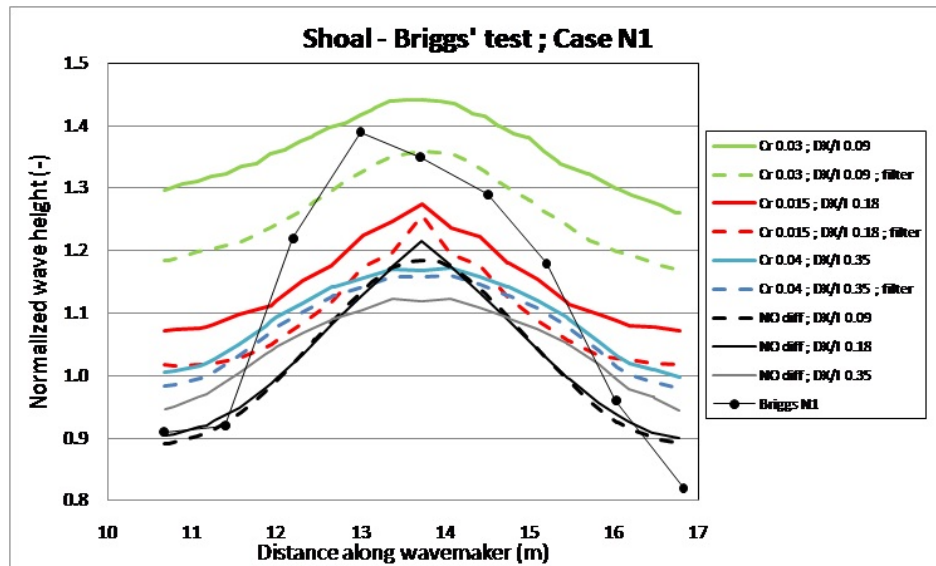


Figure 21.8: Comparaison between TOMAWAC results and Vincent measurements: measured and simulated values using a filter of the diffraction coefficient along the transect 4 of the model.

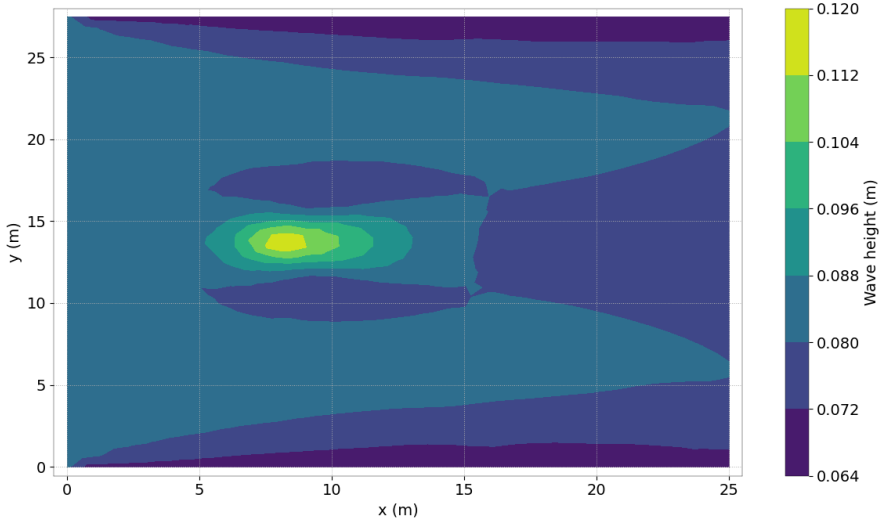


Figure 21.9: Wave height hm_0 for the last calculation.

21.6 Conclusion

This benchmark test allows to compare simulations from TOMAWAC and experimental results. It follows that TOMAWAC provides a correct simulation of the propagation, shoaling and the refraction but the diffraction effects are limited and not really well represented. In order to improve the results, a smoothing filter can be applied on the spatial domain.

22. Turning wind

22.1 Purpose

This test case shows how TOMAWAC calculate the spectrum when there is a wind that is turning. It illustrates the phenomena of white capping and quadruplet interactions.

22.2 Description of the problem

The domain is homogeneous, The depth is infinite, the wind given at 10m is homogeneous propagation step is inhibited and no boundary condition are given. So the domain of computation can be reduced to a few points as the solution is homogeneous and finally we focus on only one of them. The domain is finally very simple (see Figure 22.1)

22.3 Physical parameters

The modulus of the wind is constant, equal to 20 m/s. Initially the direction is set to 90 degrees, (which means that U_Y is null). This is maintained till the peak frequency reaches the double of its equilibrium value (peak frequency of Pierson-Moskowitz). This occurs after 28800 s (8h), at this time we change the direction of wind for 30 degrees (a rotation of 60 degrees). All the values of the wind are read in a file called *wind.slf*.

22.4 Geometry and Mesh

The domain is a square of 2 km. The mesh is very simple as there are 5 nodes and 4 triangles. That also means that this case can not be run in parallel.

22.5 Initial and Boundary Conditions

Initial conditions are imposed homogeneous on the domain with the option 4, with a Phillips constant of 0.024 an initial peak frequency of 0.3 Hz and an initial peak factor of 1. The initial directionnal spread is set to one and the initial main direction to 90 degrees (like the wind). Those value has been set to be identical to the Vledder study [36]

Nothing is imposed at the boundaries.

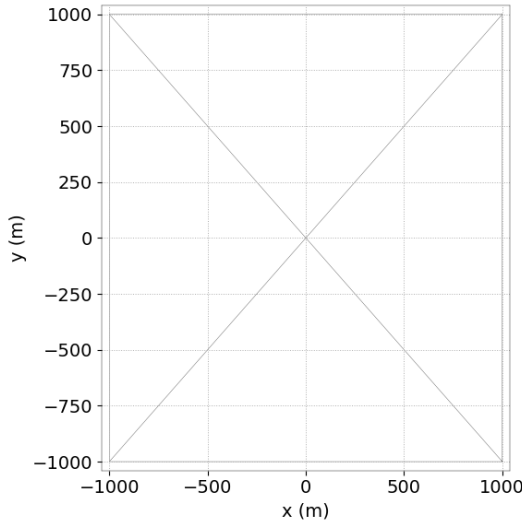


Figure 22.1: Mesh of the domain.

22.6 Numerical parameters

Time duration is set to 115200 s (32 h), time step is equal to 900 s, the spectro-angular mesh has 12 angles and 26 frequencies spread on a geometric progression common ratio 1.1 with a minimum of 0.04177248 Hz.

22.7 Results

We present here the results only for the rotation of 60 degrees as it is the effective rotation that is done in the case. Initially there were 2 more rotations one of 90 degrees and one of 30 degrees. The results for those rotations are described in [4]. Celerity of wind is 20 m/s. During 28790s, the direction is 90 degrees, then it turns to 30 degrees.

At the moment when the direction changes the established swell is going to interact with the wave induced by the new direction of wind. Three phenomena occur in that process.

- Wind contribution to the energy that will raise the new wave,
- Attenuation of the swell part of the spectrum,
- Non linear interactions between swell and wind sea.

The results of TOMAWAC are compared to simulations made by two different codes. EXACT-NL and WAM-cycle 3 (see [36]). Figure 22.2 shows that there are good agreements of TOMAWAC results compared to other simulations. One can denote that the spectrum tail factor can be sensitive. During the first 4 hours a factor 4 is better but after that time a factor 5 is better.

Let us remark that those are old results and a new simulation with new linear terms might give better results.

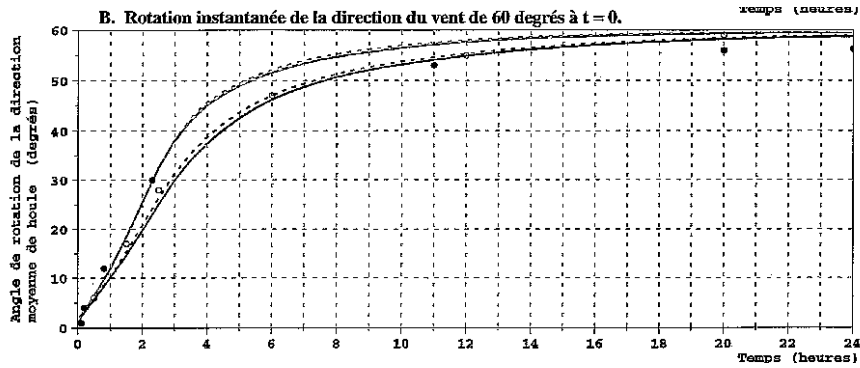


Figure 22.2: Comparison of direction of wave with time after a direction change of 60 degree at $t=0$ s. Simulations are made for different spectrum tail factor and different initial spectrum.

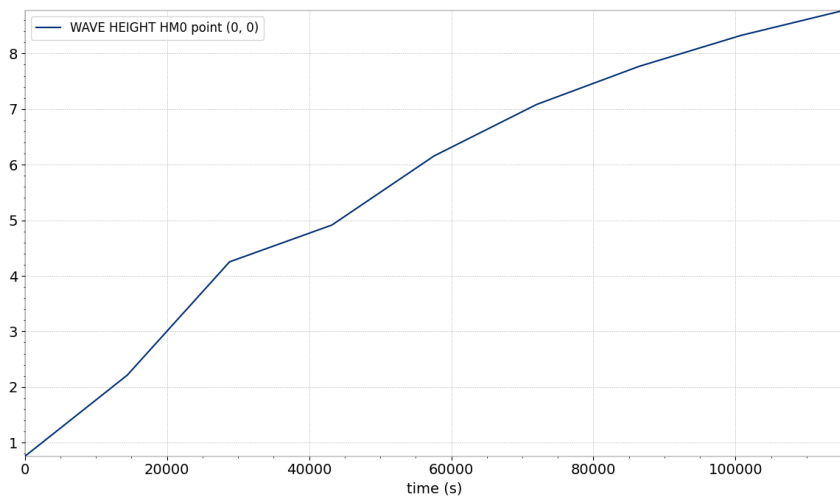


Figure 22.3: Wave height hm_0 when winds changes.

23. Whirl current

23.1 Purpose

This test case should make it possible to check that the effects of refraction by the current are properly taken into account by TOMAWAC 7.0. The distortion of a wave spectrum as it reaches a whirl current zone like those observed along the Norwegian coasts [27]

23.2 Description of the problem

This test case is derived from the Mathiesen's results [27]. Equivalent results can be found in [33] and [19]. The spatial domain is a 80 km-sided square (see Figure 23.1). A circular, origin-centered whirl current is considered ; it is modelled as follows. Is tangential velocity is zero at the origin and linearly increases up to $r = r_l$ as per:

$$u(r) = u_l \frac{r}{r_l} \text{ for } r \leq r_l \leq r_0$$

Then, that velocity follows a Gaussian profile:

$$u(r) = u_{max} \exp \left(- \left(\frac{r - r_0}{br_0} \right)^2 \right) \text{ for } r > r_l$$

Both continuity and derivability for u lead to:

$$\frac{r_l}{r_0} = \frac{1 + \sqrt{1 - 2b^2}}{2}$$

$$\frac{u_l}{u_{max}} = \exp \left(- \left(\frac{r_l - r_0}{br_0} \right)^2 \right)$$

The following values were adopted in the computations: $u_{max} = 1 \text{ m/s}$, $r_0 = 10 \text{ km}$ and $b = 0.3$.

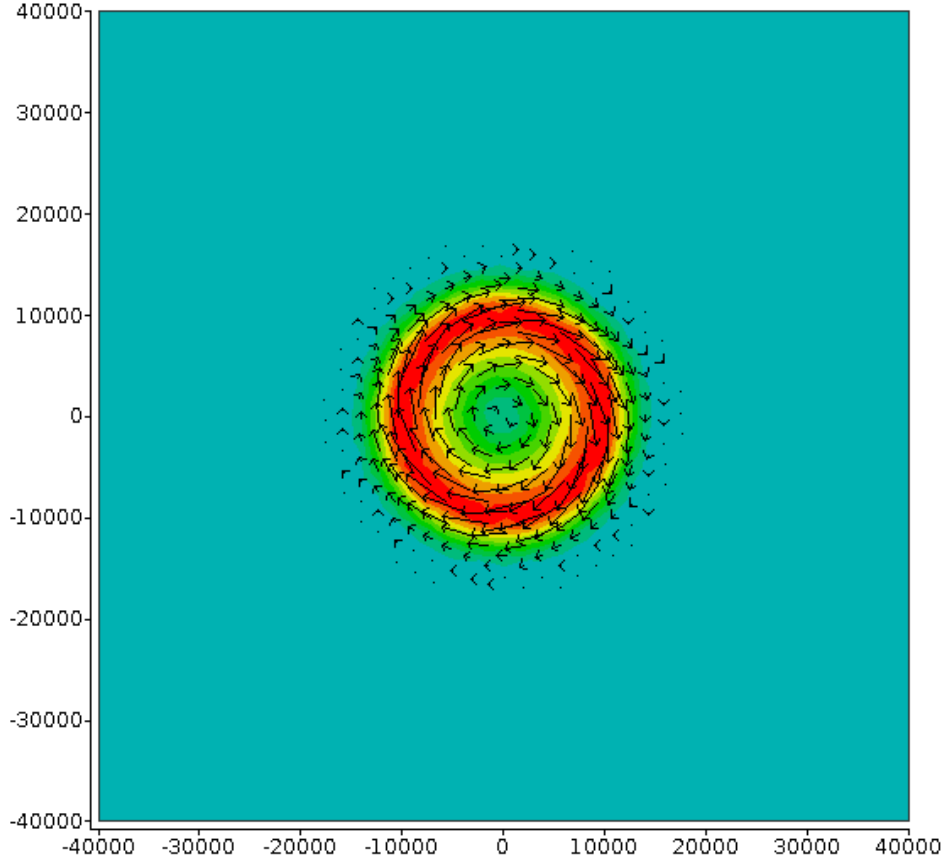


Figure 23.1: Whirl current.

The model as developed by Mathiesen is a refraction model that computes the orthogonal waves through a conventional ray method. The results it provides for the 0.1 Hz frequency are displayed on Figure 23.2. Many orthogonal crossings can be observed.

23.3 Initial and Boundary Conditions

That method of rays can be implemented either forwards (as on Figure 23.2), or backwards, then knowing the arrival point of an orthogonal, it provides the starting point. A whole wave spectrum can be reconstructed by multiplying the computations of this kind. The incident spectrum as prescribed by [27] is as follows:

$$S(f, \theta) = S(f)D(f, \theta)$$

In that expression $S(f)$ is a frequency spectrum of the classical Jonswap type, where the peak frequency f_p is set to 0.1 Hz. $D(f, \theta)$ is a Gaussian distribution:

$$D(f, \theta) = \frac{\exp\left(-\frac{(\theta-\theta_m)^2}{2\sigma_0^2}\right)}{\sqrt{2\pi}\sigma_0}$$

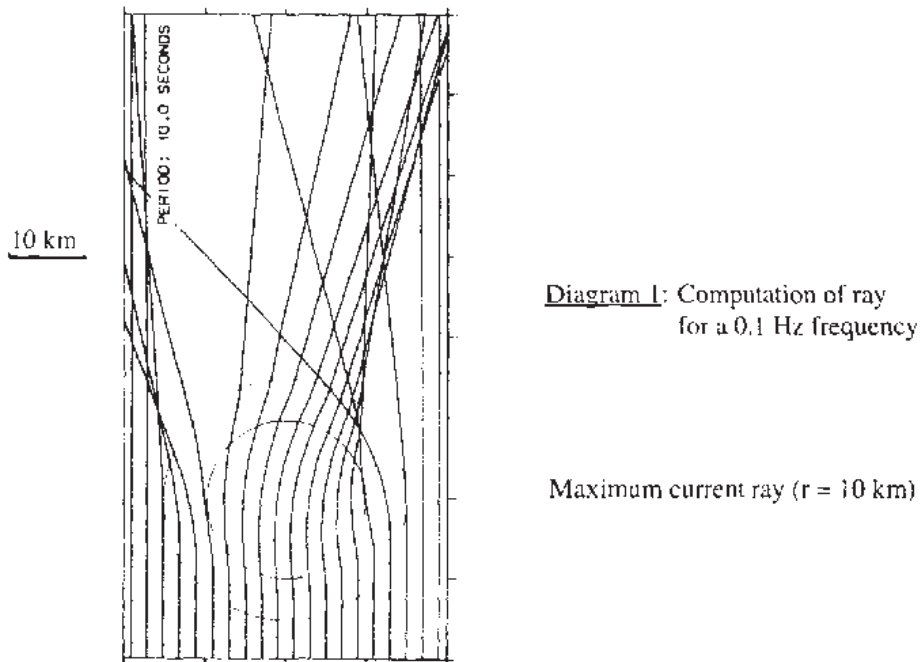


Figure 23.2: Computation of rays.

θ_m is the mean direction of the incident waves (here $\theta_m = 0$) and σ_0 is given by the following relationship.

$$\begin{aligned}\sigma_0 &= \sigma_{0p} \left(\frac{f}{f_p} \right)^{-2.03} \text{ if } f < f_p \\ \sigma_0 &= \sigma_{0p} \left(\frac{f}{f_p} \right)^{1.04} \text{ if } f \geq f_p\end{aligned}$$

where σ_{0p} , the directional spread at the peak, is 25 in our case. This spectrum is imposed on the East South and West boundaries while the North boundary is free.

The initial spectrum is null.

23.4 Geometry and Mesh

The mesh is made of 1876 nodes and 3590 triangles and is shown Figure 23.3

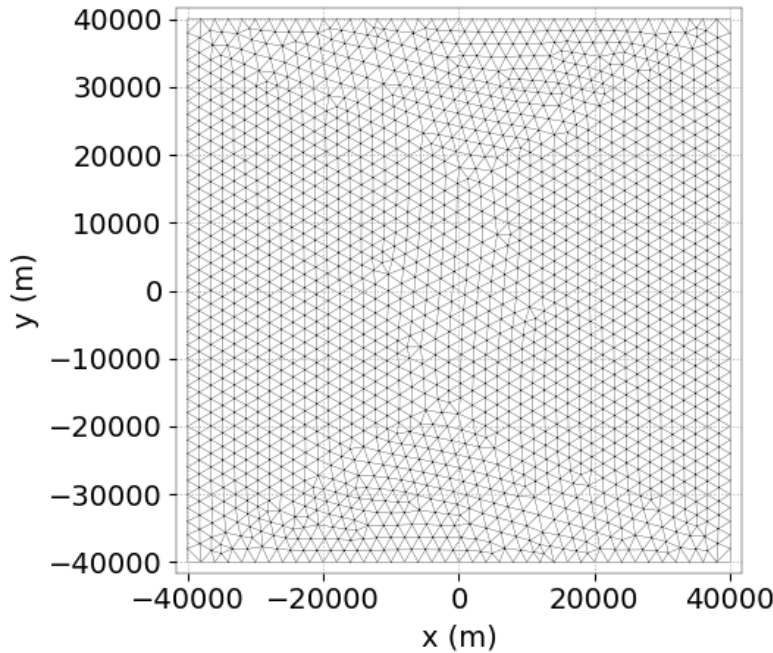


Figure 23.3: Mesh of the domain.

23.5 Numerical parameters

Time duration is 60000 s, time step is equal to 1200 s, the spectro-angular mesh has 48 angles and 25 frequencies spread on a geometric progression common ratio 1.1 with a minimum of 0.04177248.

23.6 Results

On figure 23.4, we present the amplification factor of the height due to the current. We can notice two different zones at the center of the domain where there is a strong modification of the height. One zone where the height is raising (till 35%) when the swell is opposed to the current, and one zone where the height is decreasing (till 20%) where swell and current are in the same direction. On the other parts of the domain, modifications are less than 5%. Those results are coherent with the ray calculus presented on Figure 23.2 since on the two zones we denote orthogonal crossing.

In his paper, Mathiesen [27] defines 8 points shown on Figure 23.4. On these points he gives the energy angular spread at 0.1 Hz (frequency peak of the incident spectrum). We compare this spread to the one obtained by TOMAWAC on Figure 23.5. We can denote that the results are very closed to Mathiesen results especially on points 4 and 7. Notice that Mathiesen took an angular discretisation of 2.5 when ours is of 7.5.

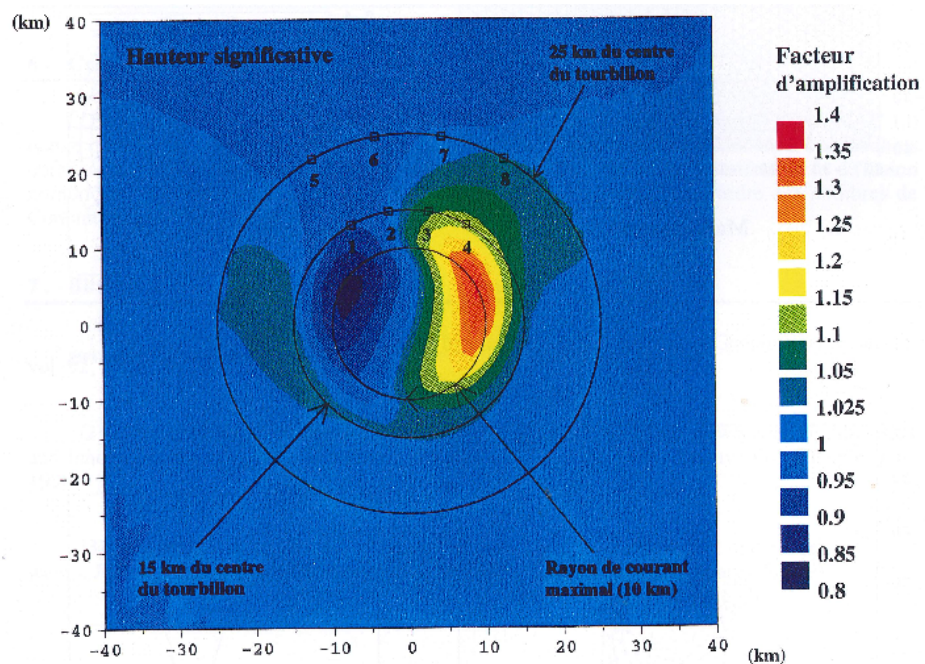


Figure 23.4: Significative heighth and positions of the measurement points.

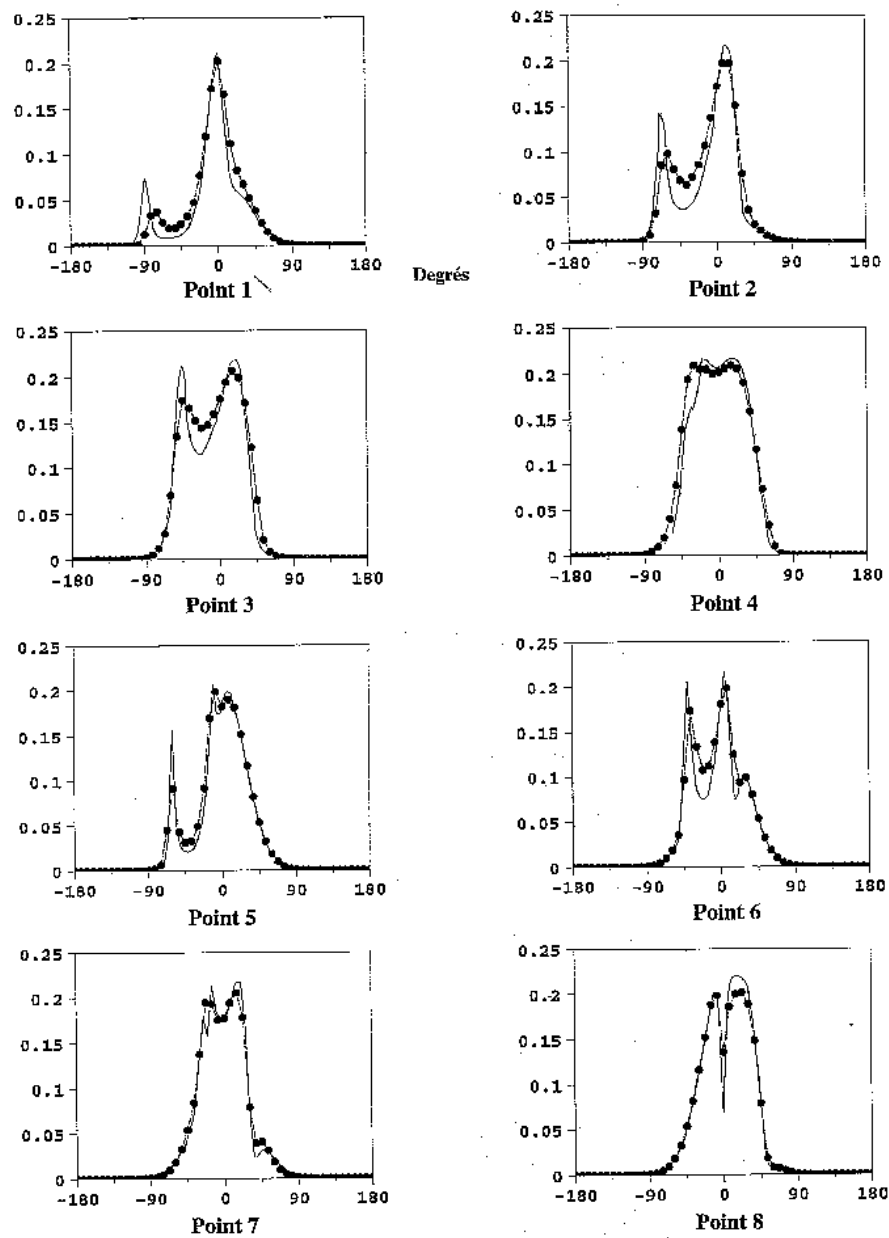


Figure 23.5: Comparison of the angular spread at 0.1 Hz between TOMAWAC and Mathiesen

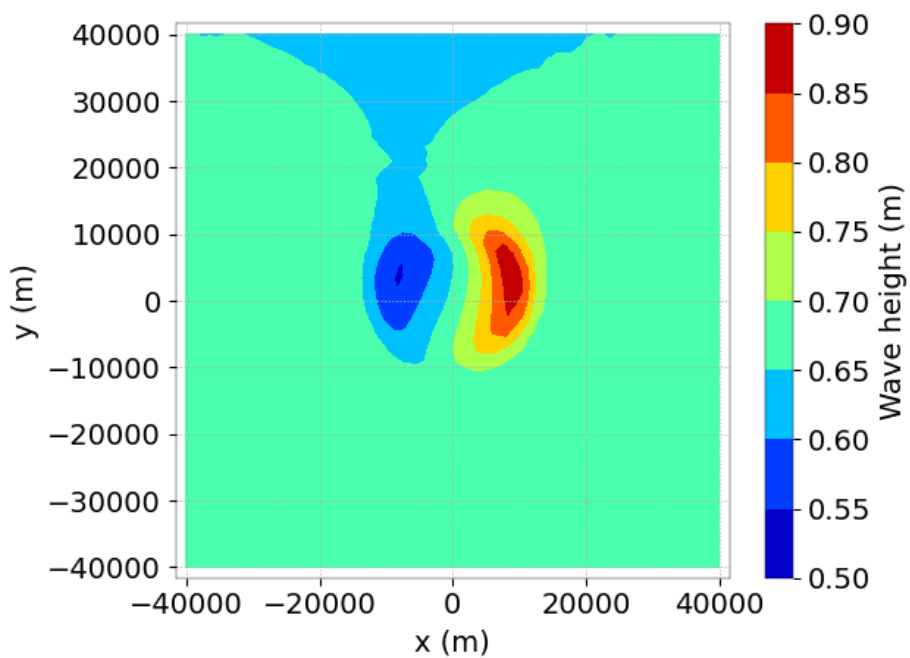


Figure 23.6: significative heighth of the last calculation

23.7 Conclusion

This test case showed on a realistic case of refraction of current that TOMAWAC gives suitable results compared to fine results.

- [1] J.H.G.M. ALVES and M.L. BANNER. Revisiting the pierson-moskowitz asymptotic limits for fully developed wind waves,. *Journal of Physical Oceanography*,, 33:1301 – 1323, 2003.
- [2] V. Bacchi, E. Gagnaire-Renou, N. Durand, and M. Benoit. Wave energy dissipation by vegetation in tomawac. In *21st Telemac- Mascaret User Club Grenoble*. 21st Telemac-Mascaret User Club Grenoble, October 2014.
- [3] J.A. BATTJES and J.P.F.M. JANSSEN. Energy loss and set-up due to breaking of random waves. In *Proc. 16th Int. Conf. Coastal Eng.*, pages 569–587., 1978.
- [4] M. BENOIT. Logiciel tomawac de modélisation des états de mer en éléments finis. dossier de validation de la version 1.0. Technical Report HE-42/96/010/B, EDF-R&D-LNH, 1996. Fiche cas-test : Evolution du spectre directionnel de houle dans un vent tournant.
- [5] M. BENOIT. Logiciel tomawac de modélisation des états de mer en éléments finis. dossier de validation de la version 1.0. Technical Report HE-42/96/010/B, EDF-R&D-LNH, 1996. Fiche cas-test : Simulation des tempêtes observées en Manche début 1990.
- [6] E. BOUWS and G.J. KOMEN. On the balance between growth and dissipation in an extreme depth-limited wind-sea in the southern north-sea. *J. Phys. Oceanogr.*, 13:1653–1658, 1983.
- [7] WA Breugem, E Fonias, L Wang, and A Bolle. Tel2tom: coupling telemac2d and tomawac on arbitrary meshes. In *XXVIthTELEMAC-MASCARET User Conference*. XXVIth TELEMAC-MASCARET User Conference, October 2019.
- [8] L CAVALERI and P. MALANOTTE-RIZZOLI. Wind wave prediction in shallow water : theory and applications. *J. Geophys. Res.*, 86 (C5):10,961–10,975, 1981.
- [9] CERC. *Shore Protection Manual*. USACE, Vicksburg, MS, 1977.
- [10] CERC. *Shore Protection Manual Volume 1*. USACE, Vicksburg, MS, 1984.
- [11] R.G Dean. Equilibrium beach profiles: characteristics and applications. *Journal of Coastal Research*, 7:53–84, 1991.
- [12] A.J. Van der WESTHUYSEN. Spectral modeling of wave dissipation on negative current gradients. *Coastal Eng.*, 58:17–30, 2012.
- [13] A.J. Van der WESTHUYSEN, M. ZIJLEMA, and J.A. BATTJES. Nonlinear saturation-based whitecapping dissipation in swan for deep and shallow water. *Coastal Eng.*, 54: 151–170, 2007.

- [14] E. Gagnaire-Renou, M. Benoit, and Ph. Forget. Ocean wave spectrum properties as derived from quasi-exact computations of nonlinear wave-wave interactions. *J. Geophys. Res. C (Oceans)*, 115, C12, C12058, 2010. doi: 10.1029/2009JC005665.
- [15] Y. Goda and Y. Suzuki. Computation of refraction and diffraction of sea waves with mitsuyasu's directional spectrum. *Port and Harbour Res. Inst.*, pages 1–45, 1975.
- [16] K. HASSELMANN, T.P. BARNETT, E. BOUWS, H. CARLSON, D.E. CARTWRIGHT, K. ENKE, J.A. EWING, H. GIENAPP, D.E. HASSELMANN, P. KRUSEMAN, A. MEERBURG, P. MULLER, D.J. OLBERS, K. RICHTER, W. SELL, and H. WALDEN. Measurements of wind-wave growth and swell decay during the joint north sea wave project (jonswap). *Deutschen Hydrographischen Zeitschrift*, 8 N 12, 1973.
- [17] S. HASSELMANN and K. HASSELMANN. Computations and parameterizations of the nonlinear energy transfer in gravity-wave spectrum. part i: a new method for efficient computations of the exact nonlinear transfer integral. *J. Phys. Oceanogr.*, 15:1369–1377, 1985.
- [18] TS HEDGES, K ANASTASIOU, and D GABRIEL. Interaction of random waves and currents. *Waterway Port Coastal and Ocean Engineering*, 111:275–288, 1985.
- [19] K. P. Hubbert and J. Wolf. Numerical investigation of depth and current refraction of waves. *Journal of Geophysical Research*, 96:2737–2748, 1991.
- [20] P.A.E.M. JANSSEN. Wave-induced stress and the drag of air flow over sea waves. *J. Phys. Oceanogr.*, 19:745–754, 1989.
- [21] P.A.E.M. JANSSEN. Quasi-linear theory of wind-wave generation applied to wave forecasting. *J. Phys. Oceanogr.*, 21:1631–1642, 1991.
- [22] K.K. KAHMA and C J. CALKOEN. Reconciling discrepancies in the observed growth of wind-generated waves. *J. Phys. Oceanogr.*, 22:1389–1405, 1992.
- [23] G.J. KOMEN, S. HASSELMANN, and K. HASSELMANN. On the existence of a fully developed wind-sea spectrum. *J. Phys. Oceanogr.*, 14:1271–1285, 1984.
- [24] R.J. LAI, S.R. LONG, and N.E. HUANG. Laboratory studies of wave-current interaction : kinematics of the strong interaction. *Journal of Geophysical Research*, 94:16201–16214, 1989.
- [25] I.V. LAVRENOV. Effect of wind wave parameter fluctuation on the nonlinear spectrum evolution. *J. Phys. Oceanogr.*, 31:861–873, 2001.
- [26] F. Marcos, M. Benoit, and P. Thellier. Cowadis software for finite element wave propagation in coastal areas : Validation document of release 1.0. Technical report, EDF R&D, 1998.
- [27] M. MATHIESEN. Wave refraction by a current whirl. *Journal of Geophysical Research*, 92:3905–3912, 1987.
- [28] F. M. Mendez and I. J. Losada. An empirical model to estimate the propagation of random breaking and nonbreaking waves over vegetation fields. *Coast. Eng.*, 51:103–118, 2004.
- [29] H. MITSUYASU, F. TASAI, T. SUHARA, S. MIZUNO, M. OHKUSU, T. HONDA, and K. RIKIISHI. Observations of the directional spectrum of ocean wavesusing a cloverleaf buoy. *J. Phys. Oceanogr.*, 5:750–760, 1975.

- [30] R.L. SNYDER., F.W. DOBSON, J.A. ELLIOT, and R.B. LONG. Array measurements of atmospheric pressure fluctuations above surface gravity waves. *J. Fluid Mech.*, 102:1–59, 1981.
- [31] Maria João Teles. *Wave-current modelling at local and regional scales*. PhD thesis, IST Técnico Lisboa, 2013. Phd supervised by António Alberto Pires Silva and Michel Benoit.
- [32] E.B. THORNTON and R.T. GUZA. Transformation of wave height distribution. *J. Geophys. Res.*, 88(10):5925–5938, 1983.
- [33] H.L. TOLMAN. A third-generation model for wind waves on slowly varying unsteady and inhomogeneous depths and currents. *J. Phys. Oceanogr.*, 21:782–797, 1991.
- [34] H.L. TOLMAN. Effects of numerics on the physics in a third-generation wind-wave model. *J. Phys. Oceanogr.*, 22:1095–1111, 1992.
- [35] C.L. VINCENT and M.J. BRIGGS. Refraction-diffraction of irregular waves over a mound. *Journal os Waterway, Port, Coastal and Ocean Engineering*, 115 N2:269–284, 1989.
- [36] G.Ph. VAN VLEDDER. *Directional response of wind waves to turning winds*. PhD thesis, Delft University of Technology, 1990.
- [37] B W. WILSON. Numerical prediction of ocean waves in the north atlantic for december 1959. *Deutsche Hydrographische Zeitschrift*, 18 (3):114–130, 1965.
- [38] L. YAN. An improved wind input source term for third generation ocean wave modelling. Tech. Rep., 8, Royal Dutch Meteor. Inst, 1987.